**The Dissertation Committee for Shawn Catherine McCleskey Certifies that this is the approved version of the following dissertation:**

# OPTICAL SIGNALING STRATEGIES FOR USE IN A MULTI-COMPONENT SENSOR ARRAY

**Committee:**

Eric V. Anslyn, Supervisor

John T. McDevitt, Co-Supervisor

Dean Neikirk

Jason Shear

David Vanden Bout

# OPTICAL SIGNALING STRATEGIES FOR USE IN A MULTI-COMPONENT SENSOR ARRAY

**by**

**SHAWN CATHERINE MCCLESKEY, B.S.**

**DISSERTATION**

Presented to the Faculty of the Graduate School of

The University of Texas at Austin

in Partial Fulfillment

of the Requirements

for the Degree of

**DOCTOR OF PHILOSOPHY**

**The University of Texas at Austin**

**August, 2003**

## Dedication

To family and friends who have faithfully walked alongside me. This journey bears the indelible marks of your love.

## Acknowledgements

There are many people to whom I would like to thank for their help and encouragement during my graduate career at the University of Texas at Austin. First, my advisors, Drs. Eric V. Anslyn and John T. McDevitt, were fundamental to my success. Their guidance and tutelage allowed me to mature and grow as a researcher. Thank you for supporting me and believing in my research abilities even when I may have had my own doubts. Without your help, this work would not have been possible.

I am grateful for the suggestions and contributions of the members of my dissertation committee: Dr. Dean Neikirk, Dr. Jason Shear, and Dr. Vanden Bout. I appreciate the time that you each generously spent with me throughout my studies.

I also wish to extend my gratitude to each of the Anslyn and McDevitt research group members. I am particularly indebted to Dr. Scott Bur, Dr. Mary Jane Gordon, Dr. John J. Lavigne, and Dr. Stephen Schneider. Not only did you help me through the program, you helped me gain a perspective outside of chemistry. Additionally, I would like to acknowledge my good friends and colleagues, Mike Griffin, Brenda Holtzman (Postnikova), and Angie Loving

(Steelman) for your insightful advice and friendship. All of you made Welch Hall a more pleasant environment in which to work.

Finally, I wish to thank my family and friends for being so patient with me these past few years. Mom, Foster, Grandma H., Aunt Karen, and Collin, I thank you for your inspiration and for always being proud of me. I want to thank my close friends Jennifer Fogell, Emma Forsyth, Lee Melhorn (Fisher), and Pei-Ling Wang for extending their friendship to me and keeping me well balanced. To my best friend, Rachael Cobler, I am grateful to you for always believing in me and for lending me a compassionate ear over and over again. And then there is my dear Marco Rimassa. I love you and I will always keep your encouraging words in my heart. Last, I wish to thank my Lord for whom I owe everything and I praise Him through this work.

# OPTICAL SIGNALING STRATEGIES FOR USE IN A MULTI-COMPONENT SENSOR ARRAY

Publication No._____

Shawn Catherine McCleskey, Ph.D.

The University of Texas at Austin, 2003

Supervisor(s): Eric V. Anslyn and John T. McDevitt

This dissertation consists of four chapters that focus on various methods and signaling strategies by which different analytes in solution can be detected within a multi-component sensor array. The first chapter of this dissertation is a review of recent work in the area of chemical sensing. A discussion is provided here of the concepts and basic mechanisms required for a sensing event and different approaches to designing molecular receptors. Next, chemical sensing is described through examples of detection strategies documented in the literature. The introductory chapter concludes by relating different sensory mimics to current methods for vapor and solution phase analyte detection using multicomponent sensor arrays and discussing the importance of pattern recognition protocols for the successful application of sensor arrays.

Chapter 2 discusses competitive indicator-displacement methods for the solution-based UV-Visible analysis of citrate and calcium in beverages. A host compound containing three guanidinium moieties on a triethylbenzene core is employed to bind citrate. Improvements to the sensing scheme via complexometric dyes known to bind calcium ion and the host are described. Application of artificial neural networks to the spectral data also allowed for the evaluation of citrate and calcium concentrations in flavored vodkas.

Chapter 3 describes a new sensing protocol by coupling a combinatorial library of resin-bound receptors to a multi-component sensor array. The anchored receptor includes a rationally designed scaffold with peptide libraries and is used to bind various nucleotide phosphates. Analyte detection is accomplished by a competition assay using fluorescein as the signaling compound. Principal component analysis shows that the sensing ensembles create a fingerprint response for each compound analyzed in the sensor array.

Chapter 4 applies the combinatorial array sensor system described in the previous chapter toward the detection of nerve agent hydrolysis products. First, the synthesis of a control resin-bound peptide library is presented to elucidate the role of the scaffold plays in binding analytes. Studies that lend to an understanding of the sensing protocol mechanism are discussed next in the context of redesigning and optimizing assay conditions. The importance of data processing on the outcome of the principal component analysis is also described. Finally, ideas for expanding the utility of this sensing protocol toward the detection of other classes of analytes via the combinatorial approach are proposed.

# Table of Contents

# List of Tables

# List of Figures

# List of Schemes

# CHAPTER 1: INTRODUCTION

## 1.0 Scope

The various methods and signaling strategies by which multiple analytes in solution can be detected within a multicomponent sensor array define the scope of this dissertation. The aim of this introductory chapter is to summarize developments in the field of chemical sensing and their applications for analyte detection. It reviews the relevant literature through June 2003. The first section describes the basic properties and forces of molecular interactions associated with host-guest chemistry. Also, concepts concerning preorganization, geometric agreement and combinatorial libraries are presented in the context of different approaches available to chemists for designing molecular receptors. The main portion of this chapter is devoted to the development of sensors exploiting the ideas described in Section 1.1 for applications in chemical sensing. This includes several examples of signaling strategies documented in the literature for the detection of various analytes. Several array-based approaches to multi-analyte sensing are discussed next along with the different mathematical techniques used to extract patterns from the large amounts of information generated by these multicomponent sensor arrays. The chapter concludes by detailing how the concepts presented in this chapter pertain to the chemical sensing applications demonstrated throughout this dissertation.

## 1.1 Chemical Sensing

In order to sense the world around us, we rely upon what Nature has provided us so that we can see, hear, touch, smell, and taste experiences present in everyday life. In scientific terms, sensing allows us to evaluate our environment by artificial means through methods and novel materials that mimic gustation, olfaction, vision, and auditory stimulation usable in analyzing complex mixtures. Of the five mammalian senses, gustation and olifaction are known as the chemically derived senses and they provide the foundation from which our response to chemical stimuli emulates. In this respect, many new sensor systems broadly responsive to a large number of analytes have been developed recently modeled in part by the sense of smell (vapor phase) and taste (solution phase). Several examples of these sensory mimic systems are presented in more detail in Section 1.3.3.

The nature of this subject is interdisciplinary, yet the roots of mimic sensing are in chemistry, namely, molecular recognition. Chemical sensing is accomplished by coupling a recognition element to a transduction element in order to signal the presence of the analyte. Since the basis of chemical sensing relies on a sensing element recognizing an analyte, the following section is dedicated to a discussion about molecular recognition and the nature of host/guest interactions. Examples of different methods used to develop molecular receptors for application in chemical sensing are also presented.

### 1.1.1 MOLECULAR RECOGNITION BASICS

Molecular recognition refers to a host or receptor molecule that is capable of associating with a particular guest molecule more strongly than with other molecules. The reason for the tight association between the host and guest molecule can be attributed to the presence of more favorable non-covalent interactions between the two molecules. Non-covalent interactions typically seen with the association between two molecules includes electrostatics, Van der Waals forces, and hydrophobic interactions. Therefore, understanding molecular recognition requires studying these types of interactions and how these interactions in concert with each other help achieve host-guest complexes.

The most prevalent of the non-covalent interactions are the electrostatic forces between two charged entities. In Nature, there are many examples that scientists have learned from such as DNA base pairing, antibody-antigen interactions, and substrate-enzyme complexes. These types of interactions include charge pairing, hydrogen bonding, and ionic interactions. Some common pairs of charged functional groups found in Nature and synthetic systems are listed in Table 1.1.

| Anions | Structure | Cation Partners | Structure |
|---|---|---|---|
| carboxylate | 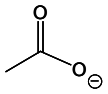 | ammoniums | 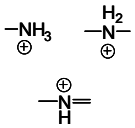 |
| phosphate | 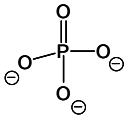 | guanidinium | 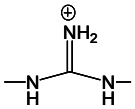 |
| sulfate | 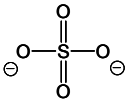 | metals | Ca(II), Zn(II), Mg(II), etc |
| phenoxide | 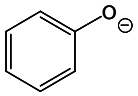 | | |

**Table 1.1:** Examples of electrostatic functional groups and their potential counterions found in Nature and synthetic systems.

An important aspect of these types of interactions is their dependence on pH and their solvation sphere. Since the enthalpic energies associated with electrostatic interactions are calculated through Coulomb's law (Eq 1.1), the energy decreases inversely with the distance between the two entities.[1] This means that the interaction is stronger in a hydrophobic environment which forces the two molecules in closer proximity and is weaker in an environment that completely solvates the ionizable functionality. For instance, Nature will often place the charged binding site of an enzyme in a hydrophobic pocket in order to minimize its exposure to water and increase the electrostatic effect. However, the opposite is observed when sodium chloride is placed in a polar protic solvent like water. The two ions completely dissociate in water destroying the presence of an electrostatic bonds.

$$E(r) = \frac{-Ze^2}{(4\pi\varepsilon_0)r} \qquad \text{Eq. 1.1}$$

Other electrostatic interactions concerning aromatic compounds include π-π and cation-π stacking.[2] Sometimes referred to as a type of ionic interaction, the basic concept of aromatic compounds aggregating to each other or coordinating to cations can be explained by considering the electrostatic potential associated with benzene (Figure 1.1). Here, areas of negative charge are seen above and below the plane of the benzene molecule with a ring of positive potential in the plane. Simple cations have been observed interacting strongly with the negatively polarized face of benzene.[3] Similarly, the attraction of the negative face on one aromatic ring to the positive edge of another aromatic ring has contributed to stabilizing DNA structures and the behavior observed with some liquid crystals.[4]

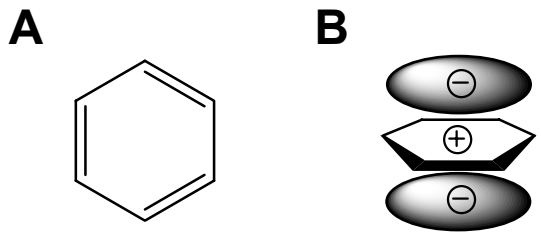


**Figure 1.1:** Benzene used as an example for π-interactions. (A) General molecular structure of benzene. (B) Electrostatic potential of benzene with areas of negative charge above and below the plane with a positive charge in the plane of the molecule.

Van der Waals interactions (or London dispersion forces) are much weaker forces than electrostatic interactions and account for a much smaller portion in the energy of binding (1%).[1] However, they are important when

considering the interactions of molecules that do not contain charged groups. Consider a nonpolar molecule like methane. Despite the fact that methane does not have a permanent dipole moment, electrons are dynamic and are capable of generating an instantaneous dipole that temporarily induces an opposite dipole in a neighboring molecule (Figure 1.2). Even though these temporarily induced dipoles are small, they do produce attractive forces between nonpolar molecules.

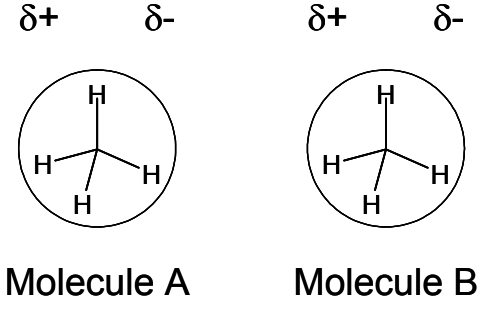


**Figure 1.2:** Temporary and induced dipoles in nonpolar molecules due to the nonuniform distribution of electrons at any given moment.

Another important non-covalent interaction to consider is the hydrophobic effect that refers to the low solubility of hydrocarbons in water. The ability of two hydrophobic molecules to aggregate in water is the result of two factors. First, the presence of a hydrocarbon in water breaks up the hydrogen bonding network, creating an unfavorable entropic situation. However, when two hydrocarbon molecules approach one another, the water molecules surrounding each hydrocarbon are "liberated" back into bulk water, increasing the entropy of the system due to the two hydrocarbons aggregating. Second, stability for the two hydrocarbons is increased due to Van der Waals forces. For instance, computer calculations predict that the binding energy of two approaching methylene groups

increases by 0.7 kcal/mole in water compared to other nonpolar aprotic solvents.[3,5]

Despite the fact that molecular recognition has been the focus of study for decades, there is still much to learn about the role that non-covalent interactions play in the attraction between two molecules. Chemists continue to investigate molecular recognition phenomena due to its importance in biological systems and relevance in understanding the world around us.

### 1.1.2 APPROACHES TO MOLECULAR RECEPTORS

The term "molecular recognition" refers to entities interacting with each other selectively and reversibly. Since the aggregation of two or more molecules is not entropically favored due to losses of rotational and translational entropy,[6] the design of the receptor or host molecule must be carefully rationalized. Integrating the necessary functional groups into the design of the host can utilize the short-range non-covalent interactions described above to our benefit, creating a more rigid host backbone capable of overcoming some of the entropic barriers associated with a binding event.

The use of a host to selectively bind a guest can be guided by many different factors. Several of these factors include the relative size and shape of the host to the guest, the placement and geometry of functional groups on the host, the choice of which binding moieties will be used in order to create a binding pocket, and the type of solvent used for the study. Below are some examples of different approaches investigators have taken to develop various host-guest systems.

The selectivity of synthetic host-guest systems is often enhanced by constructing a host with a binding pocket anchored to a backbone structure or scaffold. This predetermines the geometry of the functional groups on the receptor and helps facilitate the binding of small organic guests.[7] Many examples of supramolecular host systems utilizing backbones such as crown ethers,[8] cryptands,[9] calixpyrroles,[10] calixarenes,[11] porphyrins,[12] and cyclodextrins[13,14] have been developed for the selective complexation of anions, cations, dissolved metals, and other neutral species.

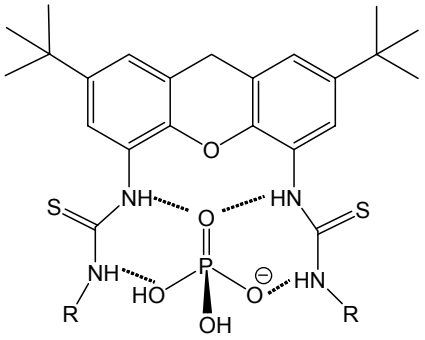


**1.1**

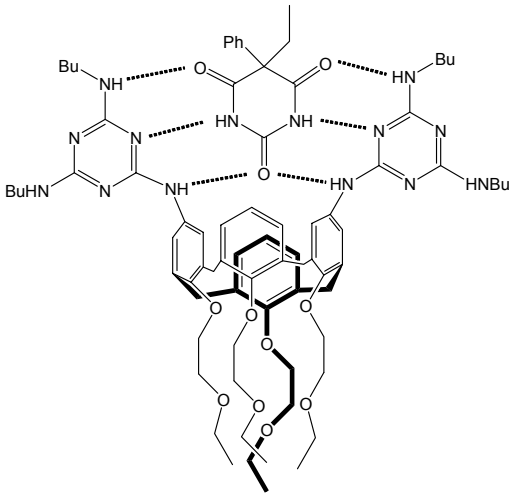


**1.2**

**Scheme 1.1:** Molecular receptors containing a rationally designed scaffold. General molecular structure of an anion recognition receptor (**1.1**) using a xanthenene spacer produced by Umezawa.[15] General molecular structure of a modified calyx[4]arene (**1.2**) used to complex neutral guests created by Reinhoudt.[16]

In Scheme 1.1, example hosts utilizing two different backbones in concert with correct placement of hydrogen bonding groups were found to be selective for their analyte due to the complementarity between the receptor and the analyte.

For instance, compound **1.1** consists of a xanthenene spacer with thiourea cleft moieties and was found to bind anions like phosphate with high association constants in DMSO.[15] Receptor **1.2** was designed such that the cavity would not be used for recognition, but as a platform for spacing to allow for two triazine units to successfully bind barbiturates in chloroform.[16]

There are many more molecular receptors designed with more elaborate motifs reported than those presented here. Even though there has been much progress in the design of molecular receptors, chemists continue to get their inspiration from Nature's example and through trial and error make their way towards the invention of new systems and better methods.

An emerging technique used to develop artificial receptors is the use of molecularly imprinted polymers (MIPs). This technique involves the polymerization of functional monomers and cross-linkers in the presence of a template molecule (target) where the removal of the template molecule from the polymer network leaves a matrix composed of cavities complimentary to the chemical functionality of the target molecule.

Several MIPs have been developed for binding guests like amino acids,[17] pesticides,[18] steroids,[19] and sugars.[20] MIPs are not just limited to these examples, but they can be tailored for a diverse range of analytes. Also, there have been reports using MIPs for the detection of chemical warfare degradation products,[21] and improvements on the synthesis of MIPs have been suggested that utilize automated procedures to produce combinatorial libraries of MIPs.[22] A few shortcomings have been reported, but the study of MIPs as synthetic receptors is

still in progress.[23] In short, MIPs provide a different strategy for the creation of selective artificial receptors and show promise for use in chemical sensing applications.

Many effective host compounds have been generated using combinatorial approaches. Usually, these combinatorial receptors are produced by successively attaching subunits like peptides, nucleotides, and other oligomeric structures.[24-26] The technique employed to produce these libraries is called the "split-and-pool" method and it is an established method used to generate one-bead, one-compound combinatorial libraries.[27] This rapidly creates a large number of host compounds and imparts molecular diversity to each member in the library. With the application of screening processes, a successful candidate that binds the target compound can rapidly be discovered, decoded, and resynthesized in mass for other studies.

Combinatorial methods are also being applied towards the creation of libraries made up of resin-bound unnatural oligomers such as peptoids (**1.3**)[28,29] and guanidiniums (**1.4**).[30,31] These examples demonstrate feasibility that this approach can be used to generate synthetic host systems capable of selectively binding target guests (Scheme 1.2). They also hold promise for incorporation into microarrays due to their potential capacity of binding more analytes with different members of the same library of receptors.[32]

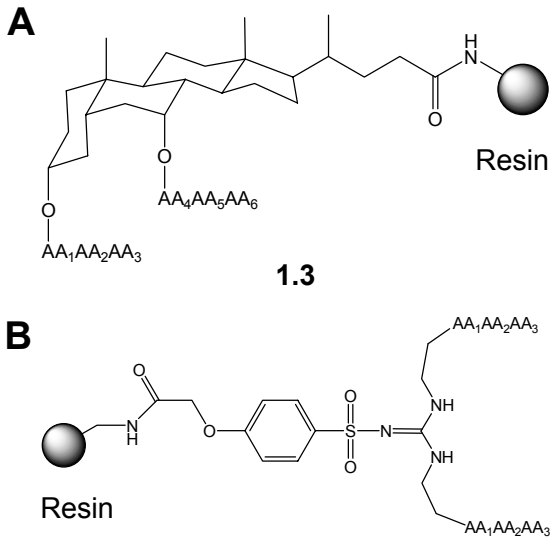


**Scheme 1.2:** Molecular receptors derived from the combinatorial approach. The molecular structure of the receptor consisting of a peptidosteroidal backbone and tripeptide arms (**1.3**) made by Still.[28] The molecular structure of the "tweezer receptor" using a guanadinium binding site and two tripeptide arms (**1.**4) created by Kilburn and Bradley.[30]

New concepts in molecular recognition are still being explored. Exciting advances like directed self-assembly, ion-pair recognition, and the creation of new materials will give chemists a larger variety of tools to choose from when approaching the quandary of how to selectively bind a guest molecule with a synthetic host.

## 1.2 Signaling Strategies

There have been numerous reports describing advances in the rational design of synthetic receptors for selective complexation of neutral and ionic species such as sugars,[33-35] metal ions,[36-38] and anions.[39] Selectivity is achieved

through recognition of the analyte at a receptor site that is preorganized by an appropriate scaffold, and by a combination of effects such as ion-pairing, hydrogen-bonding, π-interactions, and solvophobic interactions. This means that the approach the chemist utilizes to design a host is critical to the success of the sensing application. With this in mind, the rational design of host molecules for the binding of small organic guests is refined to the point that their use as selective sensors is very realistic.

Many analytes we seek to sense are difficult to detect because they do not contain chromophoric groups that would allow for their direct detection via simple spectroscopic methods. In fact, there are some examples of chemical sensors utilizing detection modes like nuclear magnetic resonance (NMR),[40] isothermal calorimetry (ICP),[41] and cyclic voltametry (CV).[42] However, there are many more optical sensing strategies reported and some interesting examples are provided in more detail below.

For optically-based applications, sensing involves the detection of a signal from a reporter molecule (either a colorimetric or fluorimetric probe) that is produced by a binding event (Figure 1.3). When the receptor molecule interacts with an analyte, the microenvironment of a reporter molecule is perturbed sufficiently to modulate the signal from the reporter, thereby detecting the presence of the analyte. This approach allows for the spectroscopic monitoring of chemical interactions. Changes in signal can result from adjustments in pH or polarity of the solvent, and energy transfer or communication between probes.

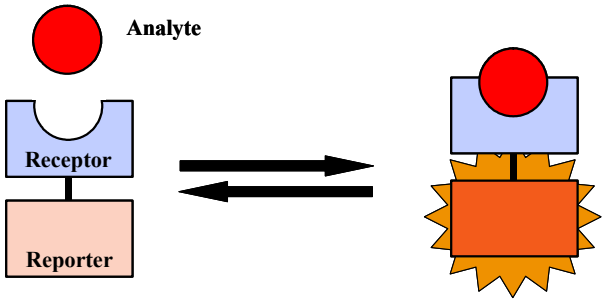


**Figure 1.3:** Optical signaling mechanism: Upon binding of the analyte, a sensing element will have a detectable response.[43]

As of yet, only the elements of molecular recognition and approaches used to develop receptors have been described. Even though the recognition process is an important first step in chemical sensing applications, the different transduction elements available are also important toward the application of these molecular receptors as chemical sensors. In this regard, the following sections discuss various optical signaling strategies reported in the literature that can be used as different transduction mechanisms in chemical sensing applications.

### 1.2.1 COMPETITION ASSAYS

A tool that has been exploited in the field of biochemistry is the use of a competition assay.[44] With this technique, an antibody is anchored to a support, which is subjected to a tagged antigen. When this sensing ensemble is exposed to a complex fluid containing the analyte of interest, the number of tagged antigens displaced can be correlated to the amount of analyte present in the sample.

Similarly, competition assays can be used as a relatively simple transducer for sensing applications (Figure 1.4).[45-49] Introduction of a surrogate substrate, or indicator, to the receptor will establish equilibrium of binding between the

indicator and the receptor and a receptor-indicator complex, resulting in a particular optical response. Addition of the analyte of interest to the indicator-receptor ensemble perturbs the equilibrium. The change in the established equilibrium between the indicator and the receptor is dependent on the relative degree of association between the analyte and the receptor.

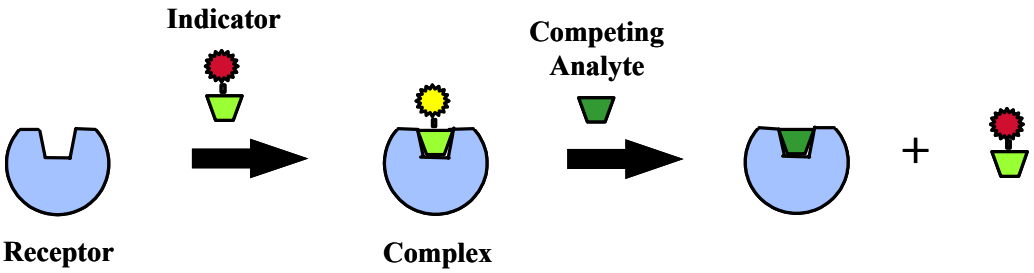


**Figure 1.4:** A competition assay allows for the presence on an analyte to be detected upon displacement of an indicator molecule.

A popular method of developing an optical sensor uses the theme of covalently attaching a transduction element to a receptor.[50-53] A disadvantage to this approach is that it introduces additional covalent architecture so that the receptor can be converted into a sensor. This often requires more synthetic steps which can be time-consuming and expensive, so utilizing competition assays allows synthetic receptors to act as sensors without introducing additional covalent architecture.

### 1.2.2 MICROENVIRONMENTAL CHANGE

One of the most common signaling strategies used in chemical sensing involves using pH sensitive probes. There is a wide variety of pH indicators available, but one of the first pH indicators to be used as a pH sensor was

fluorescein and it is often used to this day in studying biological systems.[54,55] Fluorescein has a complex pH-dependent equilibrium (Figure 1.5) that undergoes measurable colorimetric and fluorescent changes in the visible spectrum. These optical changes are the result in the change of the protonation state of the phenols and the carboxylate moieties on the xanthenene ring. As the pH of the solution approaches the p$K_a$ of one of the phenols, there is an increase in the energy gap between the excited state and the ground state that leads to an increase in the quantum yield making fluorescein a very sensitive pH sensor.

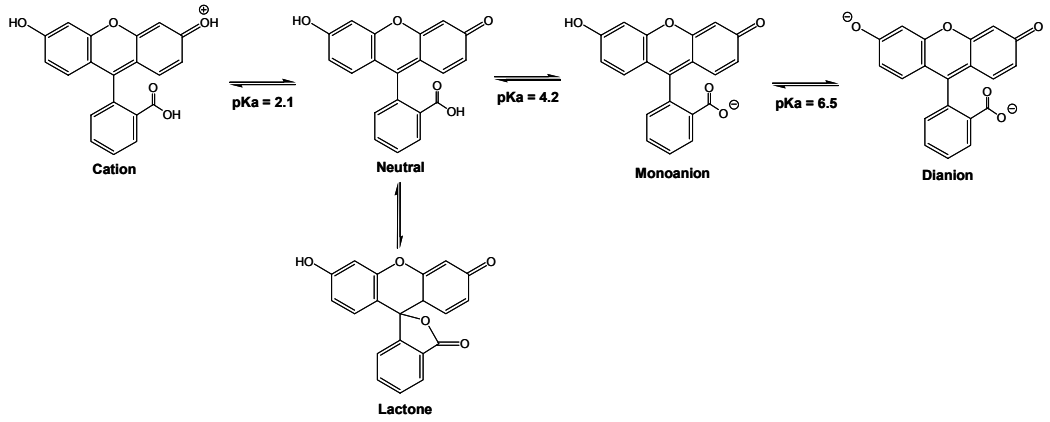


**Figure 1.5:** The ionization state of the pH sensitive probe carboxyfluorescein.[56]

Setbacks to using fluorescein include susceptibility to photobleaching, a p$K_a$ that is close to some biological systems where a probe with a higher p$K_a$ would be preferable, and the fact that the cationic and neutral form are not fluorescent, preventing use in low pH solutions or organic solvents.[56] However, like many of the molecular receptors mentioned earlier, chemists have modified fluorescein to overcome some of these issues have created new probes with chelating arms (chromoionophores) that allow for ion-selective pH sensors.

Another possible signaling motif exploits the hydrophobic effect. Ueno and coworkers at the Tokyo Institute of Technology demonstrated that fluorescently labeled cyclodextrins (CDs) could be used for chemical sensing.[57-59] CDs are a group of torus-shaped cyclic D-glucose oligomers with the primary hydroxyl groups of the sugar rings on the narrow rim of the CD cone (Figure 1.6). These molecules are soluble in water and have shown the ability to shape-selectively complex a variety of organic compounds including naphthalene and pyrene in their hydrophobic cavity in aqueous solution.[46,60,61]

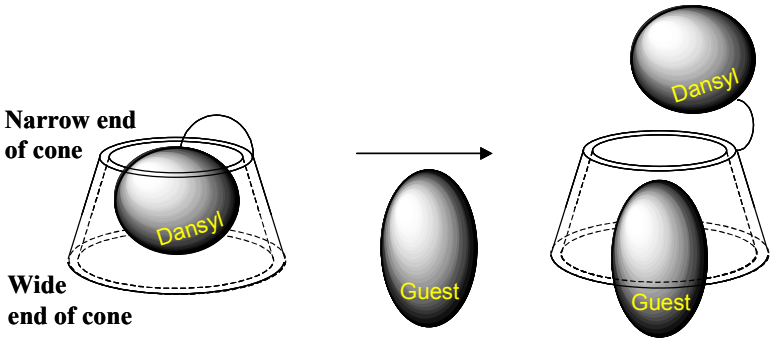


**Figure 1.6:** Schematic representation of the proposed sensor mechanism for dansyl modified CDs upon addition of guests.[43]

Sensing of these different guests by Ueno and coworkers was done by competition assays.[62] The CD molecules by themselves are silent in the UV-Visible region, and detection of organic guests was accomplished using dansyl-modified CDs.[57] Dansyl is a solvatochromic dye that is sensitive to the hydrophobicity of its microenvironment. As the guest binds to the CD, a noticeable fluorescence signal modulation was detected. This fluorescence change was rationalized as being the result of displacement of the dye from the CD cavity as shown in Figure 1.6. Different guests resulted in variable decreases of the

dansyl fluorescence demonstrating that dansyl-modified CDs are sensitive chemosensors.

### 1.2.3 ENERGY TRANSFER

Energy transfer (ET) offers many opportunities for chemical sensing. Specifically, fluorescence resonance energy transfer (FRET) has been described as the radiationless transmission of energy from the initially excited donor molecule to an acceptor molecule by resonance interaction of the oscillating dipoles between the two chromophores.[63] The efficiency of energy transfer is dependent on the extent of spectral overlap of the emission spectrum of the donor with the absorption spectrum of the acceptor (Figure 1.7), the quantum yield of fluorescence of the donor, the relative orientation of the donor and acceptor transition dipoles, and the distance between the two chromophores.[63]

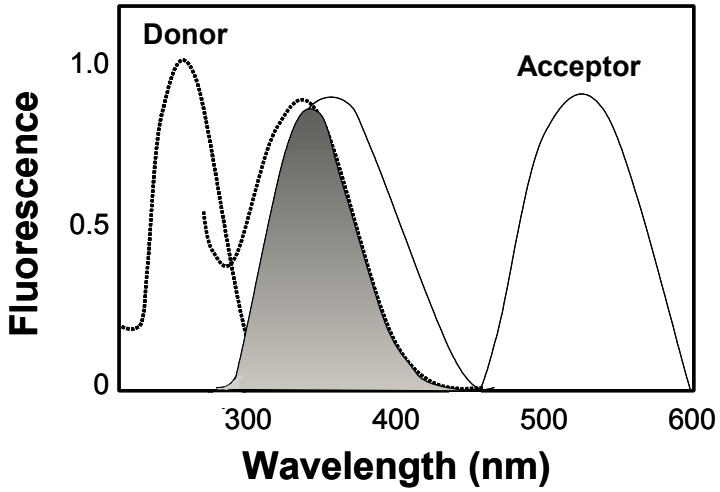


**Figure 1.7:** Overlap integral (shaded area) for energy transfer from a donor molecule (dashed line) to an acceptor molecule (solid line).

The FRET method is frequently used to measure the distances between two sites on a biological macromolecule.[63] Utilizing energy-transfer in a sensing scheme allows for the monitoring of the emission spectra of the probes upon introduction of the analyte. This creates two modes of detection since one can monitor emission intensities at two wavelengths (donor and acceptor). A correlation could also be made between the ratio of the donor and acceptor emission intensities and the analyte concentration, allowing the chemist to take measurements that are independent of the inherent fluorophore concentration.

Other mechanisms for sensing include photoinduced electron-transfer (PET). Generally, PET is used to quench the fluorescence of a fluorophore attached to an amine on a cyclam or azocrown molecule capable of complexing cations. The lone pair on the amine in the macrocycle is involved in the quenching of the fluorophore while the macrocycle remains empty (no cation present). However, when a cation is introduced into the host, the lone pair on the amine participates in the binding of the analyte leaving the fluorophore to generate a fluorescent signal.[56] A significant advantage to this approach compared to other signaling strategies is that the dynamic range of signal with PET is larger due to the reduction of background signal (switching the probe from "off" to "on").

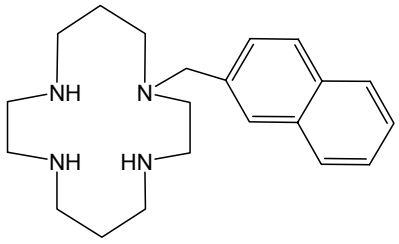


**1.5**

**Scheme 1.3:** Molecular structure of molecular thermometer created by Fabbrizzi utilizing PET as the sensing strategy.[64]

There are many examples of sensors using this signaling strategy for complexing metal ions.[65] In one case, a PET sensor was used to sense for the physical property temperature. Fabbrizzi and coworkers constructed a molecular thermometer (Scheme 1.3) using a naphthalene fluorophore segment covalently linked to a tetraazamacrocycle.[64] In acetonitrile (20°C), they found that the Ni(II) complex **1.5** was present in 30% as a low spin species, while the high spin species was present in 70%. The interconversion of **1.5** was found to be temperature dependent, so the temperature was measured indirectly by calculating the ratio of the two nickel spin state species. Fabbrizzi was able to record an increase in the fluorescence emission for **1.5** over a temperature range of 27˚C to 65˚C, creating a useful sensor capable of sensing the presence of Ni(II) and temperature.

## 1.3 Multi-Analyte Sensing

The development of compact array-based sensors has been largely motivated by the demand for time-efficient and cost-effective analysis of complex mixtures. As described in earlier sections of this chapter, chemical sensing has

been achieved through the rational design of a receptor that has a high binding affinity for a specific molecule (Figure 1.8A). This type of approach is impractical for analyzing complex mixtures because it requires the synthesis of a unique, highly selective sensor for each type of analyte to be detected.[66] As a result, trends in chemical sensing have shifted to the design of new materials and devices that rely on a series of chemo- or biosensors such that recognition can be achieved by the distinct pattern of responses produced from the combined effect of all the sensors in the array (Figure 1.8B).

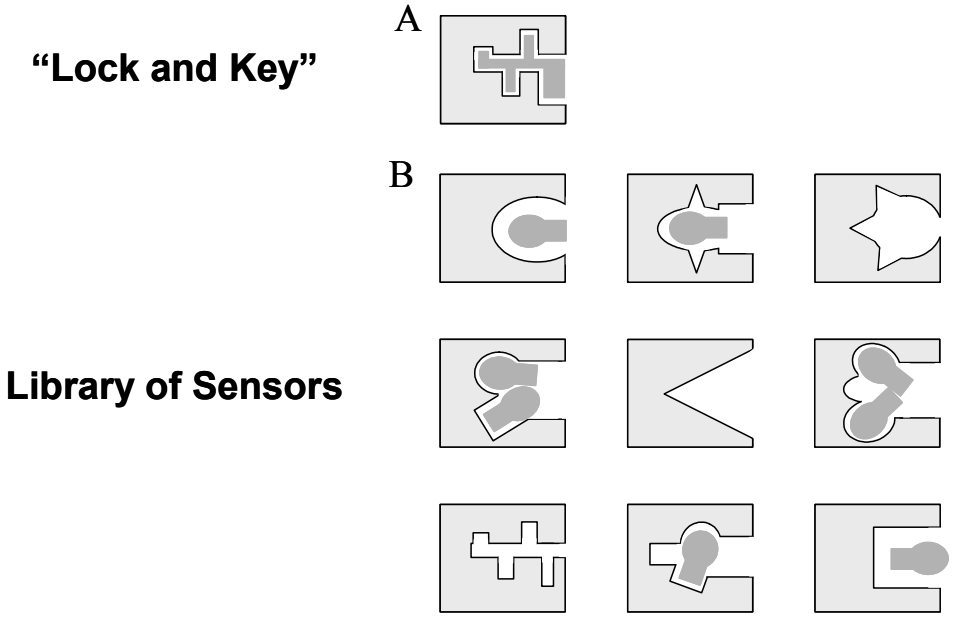


**Figure 1.8:** Shift in approaches taken for chemical sensing**.** (A) "Lock and Key" approach to host-guest systems. (B) Library of receptors approach.[43]

These approaches are advantageous because these devices can be calibrated or "taught" to recognize a certain class of analytes with the help of pattern recognition techniques[67,68] For instance, if a similar analyte is introduced

to the array that it was not originally designed to recognize, the device could result in an individualized response, thus signaling the presence of a new species. Hence, the following section is dedicated to the discussion of sensor arrays designed to analyze complex mixtures in vapor and solution phases inspired by Nature's approach to smell and taste.

### 1.3.1 SENSORY MIMICS

Many array-based sensors that are capable of sensing and identifying multiple analytes in the vapor phase have been reported. These vapor sensors use a variety of transduction schemes such as Surface Acoustic Wave (SAW),[69-71] carbon black-polymer resistors,[72,73] and conductive polymer[74] transducers. These structure sensors (referred to as "electronic noses") mimic the mammalian sense of smell and have demonstrated the ability to differentiate components within a complex vapor mixture.[75] The components of the mixture are classified based upon the distinct pattern of responses detected over a collection of sensors in the array.

A significant drawback of these types of devices is that they only apply to analytes in the vapor phase. The need to develop sensors for applications involving fluid analysis for areas such as environmental monitoring of waterways or analyses of biologically relevant systems has spurred researchers into developing sensing devices that mimic the mammalian sense of taste. The array-based methodologies capable of fluid analysis that have emerged lately utilize a range of detection schemes including microelectrodes,[67,76] conducting polymers,[77-79] and fiber optic sensors.[80]

Likewise, at the University of Texas at Austin, the Anslyn and McDevitt groups in collaboration with professors Jason Shear and Dean Neikirk, have developed a device that allows for the simultaneous identification of multiple analytes in solution.[81,82] This device termed the "electronic tongue" consists of an array of cross-linked copolymer microspheres ("taste buds") that are chemically modified with receptors or chemical indicators, and placed into a micromachined platform as schematically represented in Figure 1.9. The detection platform consists of a stereomicroscope fitted with a charged coupled device (CCD) that yields red, green, and blue (RGB) signals for each sensor (bead) placed in spatially addressable positions on the chip. The signaling mechanism used in the "electronic tongue" is an observed color change by the CCD camera of the sensing ensemble on the resin bead once it has been exposed to the analyte. Analysis of the red, green, and blue light intensities from each of the sensors in the array generates a pattern that can be used for analyte identification.

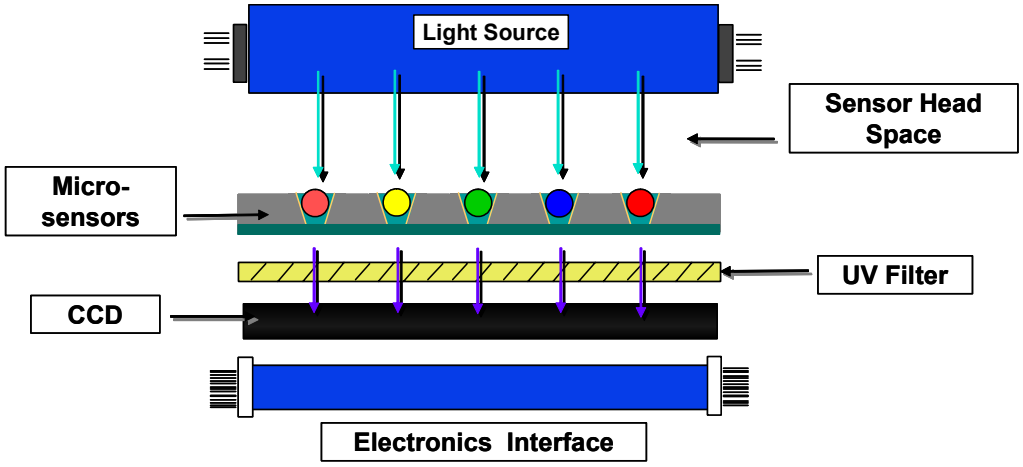


**Figure 1.9:** Schematic of micromachined chemosensor array ("electronic tongue").[43]

An example of how RGB analysis is used to extract out information from the sensors is shown in Figure 1.10. Figure 1.10A shows a digital picture taken by the CCD camera of two resin beads composed of the same matrix that have been chemically modified with acetic anhydride (top) which is used as a reference sensor or "blank" and 5-carboxyfluorescein (bottom) which may be used to indicate the pH of the solution. In the "blank" sensor case, the histograms of the RGB intensities indicate that most of the light in each channel is passing through the bead to be detected by the CCD camera (Figure 1.10B). However, in the fluorescein sensor example, the RGB histogram shows a significant decrease in the amount of light detected by the CCD camera in the blue channel relative to the other two channels. This means that the 'electronic tongue' platform can be used in the same fashion as a double-beam spectrophotometer where the 'effective absorbance' of the fluorescein sensor can be calculated relative to the blank sensor using Beer's Law for the determination of hydronium ion concentration in the solution being analyzed.

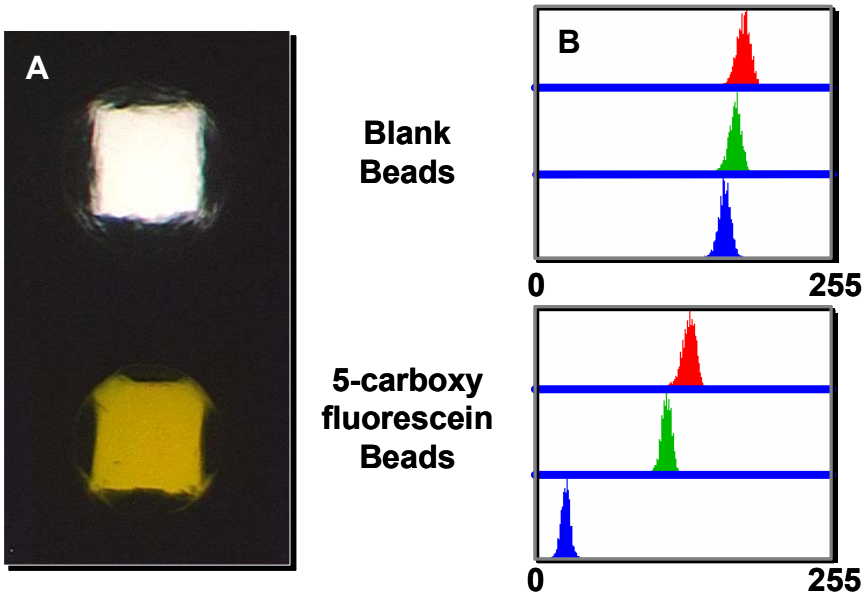


**Figure 1.10:** RGB Analysis of data generated by the multicomponent sensor array. (A) Color digital picture of a blank bead and a fluorescein anchored bead in the array. (B) Color histogram of each RGB channel for each bead in the array.

Sample delivery to the sensors is accomplished by a computer controlled high-pressure liquid chromatography system that is connected to a flow cell. A schematic of the flow cell is shown in Figure 1.11A. The silicon chip is situated between two layers of Plexiglass which is clamped into an aluminum housing. PEEK tubing is inserted into the Plexiglass layer which allows for fluid delivery to enter from the top of the sensors and exit the flow cell from beneath the array. The coupling of the fluid delivery system to the flow cell allows for specific amounts of solutions to pass through the array of sensors for analysis.

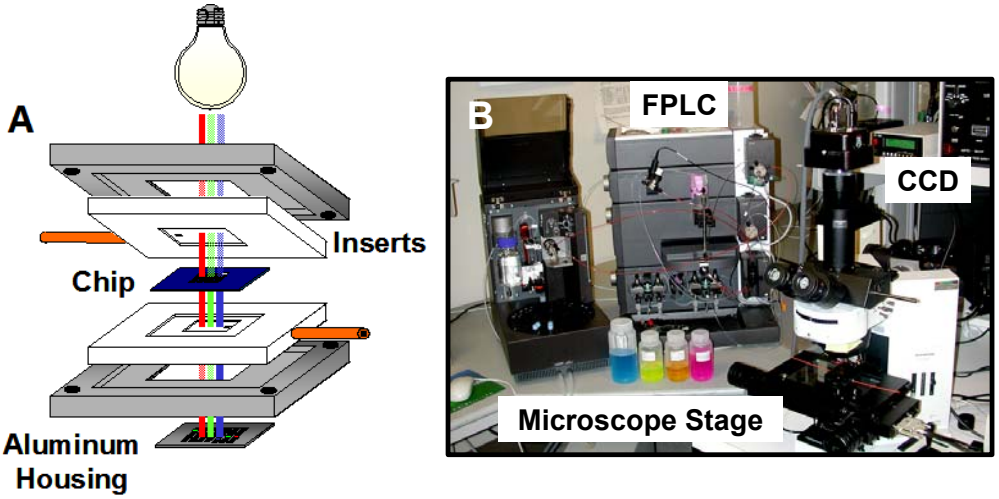


**Figure 1.11:** Diagram of the fluid delivery system. (A) Schematic of flow cell. (B) Picture of instrument used for experiments composed of a FPLC fluid delivery system, CCD camera, flow cell, and a stereomicroscope.

With this arrangement of components, a very versatile instrument has emerged that is capable of detecting cations, anions, solvents, sugars, and protein structures such as biological cofactors and antibodies.[83-85] The main components -the resin beads, a silicon microchip, a flow cell, and a CCD camera- allow for this analytical sensing device (Figure 1.11B) to be adapted for a range of applications including environmental testing, liquid process control, and human medicine. Specifically, the CCD detection affords highly sensitive and simultaneous measurements of all the sensors in the array. Also, new sensors can be readily synthesized incorporating a range of molecular building blocks (including combinatorial libraries) using established solid phase synthesis protocols. Finally, pattern recognition techniques can be applied to the

information generated by this platform so that the power of statistics can enable this analytical detection device to solve more complex problems.

### 1.3.2 PATTERN RECOGNITION

Despite the recent attention that pattern recognition (PR) techniques have received in the literature, the use of mathematical statistics in the handling and interpretation of chemical data has been in practice long before the fieldname, chemometrics, was coined in the early 1970's.[86] The methods applied to data sets where measurements are recorded on many variables over a number of samples are regularly called multivariate analysis (MVA) methods. The most common methods used in chemical data handling are principle component analysis (PCA), statistical discriminate analysis (SCA), soft independent modeling of class analogy (SIMCA), cluster analysis through the k-nearest neighbor (k-NN), and artificial neural networks (ANN).[68]

There are many detailed texts written describing the different MVA methods available in chemistry.[87-90] Since this dissertation only concerns the application of just two PR methods, the discussion here is limited to PCA and ANNs. Even though the basis for each approach to be discussed here has been previously published, a more qualitative summary will be provided so that the reader may appreciate the basic issues related to pattern recognition that will be applied in later chapters in this dissertation.

PCA methods are commonly used to investigate variable (sensor) interrelationships (correlations) among different samples. The main objective of PCA is to simplify the dimensionality of a multivariate data set to a few

components so that the structure of the data may be interpreted more readily.[89] For instance, consider a data set where *n* variables (sensors) give responses to *m* samples as seen in Table 1.2. Here, the rows represent the responses of each sensor for each sample and the columns signify the response of a single sensor across all the samples.

| | | Sensors | | | | | |
|---|---|---|---|---|---|---|---|
| | | $S_1$ | $S_2$ | . | . | . | $S_n$ |
| Samples | ATP | $s_{ATP1}$ | $s_{ATP2}$ | . | . | . | $s_{ATPn}$ |
| | AMP | $s_{AMP1}$ | $s_{AMP2}$ | . | . | . | $s_{AMPn}$ |
| | . | . | . | . | . | . | . |
| | . | . | . | . | . | . | . |
| | *m* | $s_{m1}$ | $s_{m2}$ | . | . | . | $s_{mn}$ |

**Table 1.2:** Example data for PCA where *m* is the number of samples tested, *s* represents a measurement response, and *n* is the number of sensors used in the study. [The sample examples are adenosine 5'-triphosphate (ATP) and adenosine 5'-triphosphate (ATP).]

In PCA, the sample responses obtained from a series of sensors are placed into a matrix (n × m) where upon they are transformed into eigenvectors and associated eigenvalues. In other words, PCA takes the correlated responses (measured data) from each sensor ($S_1$, $S_2$,..$S_n$) and replaces them with linear combinations of the measured responses ($s_{ATP1}$, $s_{AMP1}$…$s_{mn}$) to generate derived variables (eigenvectors) that are uncorrelated (unrelated functions of the responses). This is done in order to generate a different dimension in the data set which can be used to explain patterns in the data. These uncorrelated derived variables are referred to as principal components (PCs).

If there are *n* response variables in the data set, then *n* components can be derived, though, it is expected that most of the variability from the measured data set can be accounted for within the first few PCs derived from the response variables (sensors). Hence, the magnitude of the eigenvalue associated with the eigenvector describes the importance (variability) of the newly derived variable. Each PC is orthogonal (perpendicular) to the one that precedes it so that the variance is maximized in each new component being generated: the first PC accounts for the largest portion of variance in the data set and the second PC is responsible for the second largest portion of variability and so forth. This allows for these uncorrelated components to represent crucial features in the original data set with minimal loss of information.[88]

Consider the following example illustrated in Figure 1.12 using two variables (sensors) measuring two different samples (adenosine 5'-monophosphate, AMP, and guanosine 5'-triphosphate, GTP) to create a two-dimensional plot. Here, the distances between the responses of each sensor can be used to describe the similarities and differences inherent within the data set (Figure 1.12A). The first component axis (PC1) is drawn in the direction of the maximum spread (variance) of data points (Figure 1.12B) and the second component axis (PC2), perpendicular to PC1, is drawn in the direction of the remaining variance not accounted for by PC1 (Figure 1.12C).

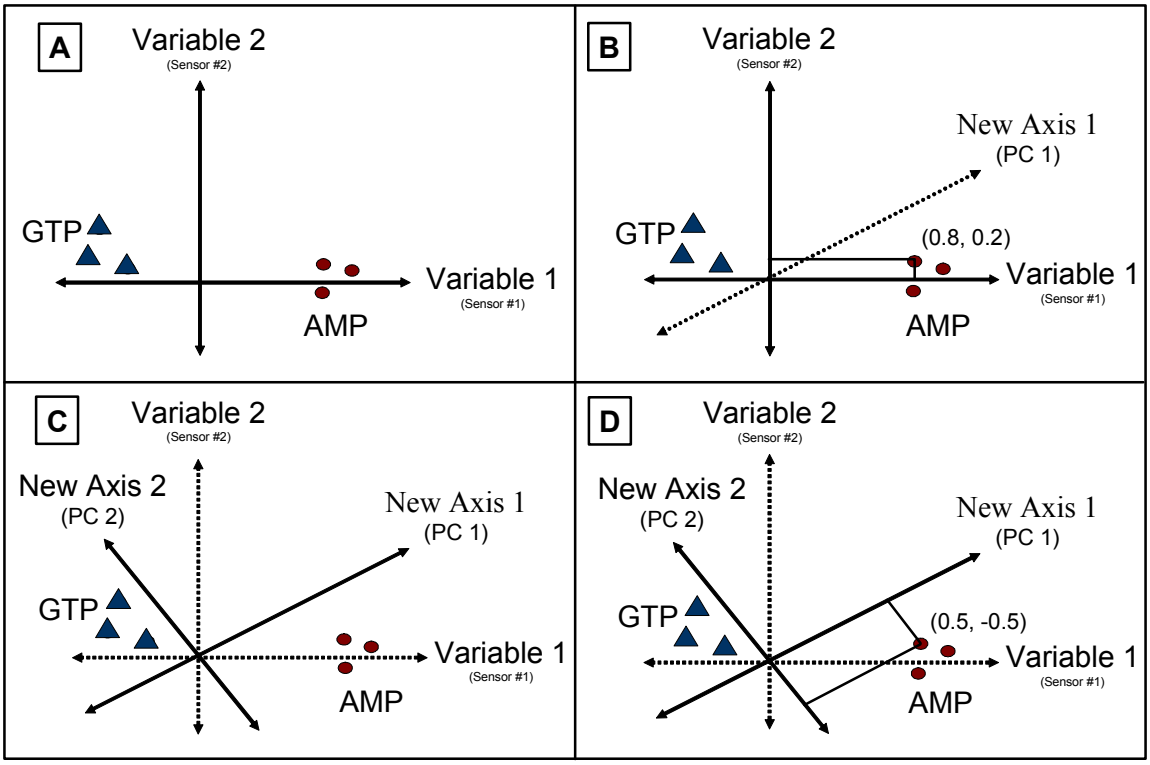


**Figure 1.12:** Principle component analysis of two variables upon exposure to two different samples. (A) The individual sensor response of two different sensors to three AMP and GTP samples. (B) A plot of the raw data with the first PC axis drawn in a dashed line. The coordinates of one sample relative to the original variable axes is shown in parenthesis. (C) The first two PC axes drawn in bold while the variable axes are shown in dashed lines. (D) The coordinates (or scores) of the same sample relative to the new PC axes is shown in parenthesis.

Now that a new dimensional space has been created by PC1 and PC2 (shown in solid lines in Figure 1.12C), coordinates of the samples (AMP and GTP) relative to the new axis can be determined and are given "scores." For instance, the coordinate of one AMP sample relative to the variable axes is (0.8, 0.2) as shown in Figure 1.12B. However, the coordinates of this same sample

relative to the new PC axes is (0.5, -0.5) as shown in Figure 1.12D. These new coordinates (scores) can then be plotted with respect to the PCs and used to describe the correlation between samples. An example of this kind of plot, termed a score plot, is shown in Figure 1.13. A score plot allows for the trends in the data to be visualized in a simple way. Samples with similar PC scores indicate that they may have comparable characteristics. For example, in Figure 1.13 the clustering of the ATP and GTP samples can be explained by the fact that they are triphosphates and more similar in structure than the monophosphate samples, AMP and pyrophosphate, that cluster in a different region on the score plot.

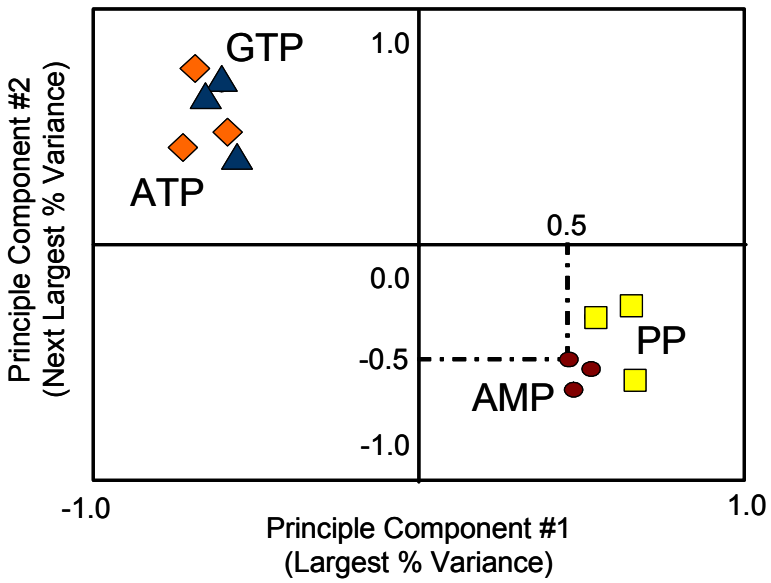


**Figure 1.13:** PCA score plot showing clustering of different types of phosphates (♦ATP, ▲GTP, ●AMP, ■Pyrophosphate or PP) with one of the AMP samples coordinates drawn in dashed lines to each PC axis.

Each PC is derived from the linear combination of the measured response variables (sensors) and can be examined to determine which sensors contribute most significantly to that PC. Thus, PC1 can be written as the following equation:

$$PC1 = \alpha_{11}S_1 + \alpha_{12}S_2 + ...\alpha_{1n}S_n \quad \text{(Eq. 1.2)}$$

where the α term refers to the weight (or factor loading value) for each sensor ($S_n$) in this principal component. Each factor loading value measures the relative importance of that sensor to a particular feature in the data and is determined by the cosine of the angle between the variable axis and the principal component axis.[88] A large α value indicates that the sensor it describes contributes significantly towards the formation of that PC and plays a larger role in the determination of how that PC explains the data structure. Where as, a small α value signifies a minor contribution in the formation of the PC and imparts a weak influence on how the PC describes patterns in the data. These values allow the variables (sensors) that contribute most significantly to the discrimination between samples to be assesed.[89]

In Figure 1.12B, PC1 is more aligned with Variable 1 axis than the Variable 2 axis. This indicates that the response of variable 1 (sensor #1) contributed more to the directionality of PC1 than the response of variable 2 (sensor #2) and also signifies that sensor #1 is more important in the discrimination between samples than sensor #2. If the PC points in the same direction as a variable axis, the angle between them is zero and the cosine is 1. Therefore, the PC drawn in this instance describes all of the variation in that variable axis. The same argument holds for a PC drawn at $90^o$ to the variable

axis. The cosine of $90^{o}$ is zero, indicating that none of the response variation is contained in the PC axis. To summarize, similar factor loading values indicate that the variables (sensors) responded in a similar fashion to the samples and may indicate important relationships among the sensors.

The example given above only represents the basic idea of PCA and how it can be applied in a two-variable case. PCA can be extended to multiple variables where the computations are more involved and require the use of a statistical analysis software program. This makes PCA a powerful tool for chemical applications where the basic principle of data reduction allows chemists to explore their own data in a more simplified form.

Another frequently mentioned pattern recognition technique used for applications in chemistry is an ANN. The ANNs considered here are the feed-forward multilayer perceptron (FF-MLP) ANNs that have often proven to be useful for the analysis of data from sensor arrays.[68] The objective for ANN analysis is to generate a model from multivariate data sets and create criterion from which a successful network response will reveal the "best fit" answer to any input.

The basic architecture of a FF-MLP neural network consists of several layers containing a number of units, or neurons, where the data is processed and passed onto subsequent units located in the next layer. A general schematic of a single neuron is shown in Figure 1.14. In a FF-MLP, each neuron produces an output as a function of its input which may be data from the sensor array or the output of a previous neuron. The information that is received in each unit is

compiled by first applying a series of weights ($w_{ij}$) and biases to each input value ($I_i$) and then subjecting each value to a transfer function that is ultimately presented as the output value ($Out_j$).[87] The application of weights and biases to each input value allows for the network to adjust or learn its training data.

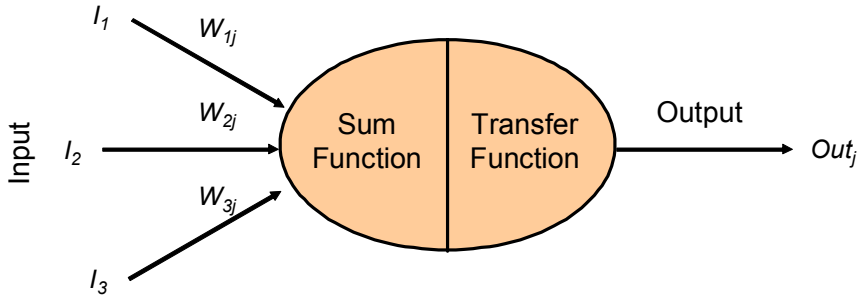


**Figure 1.14:** Operation of a single "neuron" or input unit in an FF-MLP ANN. A summation of all input signals are subjected to a weight ($W_{nj}$) and transfer function before sent on as an output ($Out_j$) to the next "neuron."

The network is often organized into three layers as shown in the diagram below (Figure 1.15). The input layer usually contains a number of neurons (often equal to the number of sensors) that accept the external data and perform no calculations on the data but only represent input values.[90] The output layer typically contains neurons for each value to be predicted by the network. The intermediate (hidden) layers are situated between the input layer and the output layer where the number of hidden layers can be varied and are determined experimentally. The neurons in each layer are all connected to each other (as shown in Figure 1.15) and this allows the network to solve nonlinear problems.

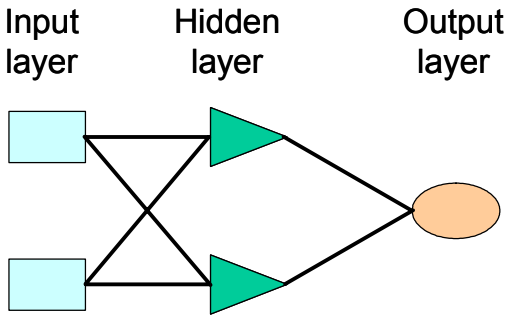


**Figure 1.15:** A diagram of a three layered FF-MLP ANN. The ANN is composed of an input layer, a variable number of hidden layers, and an output layer.

In order to generate an answer from the network, the network must be trained by iteratively changing the weights and biases using a back propagation algorithm. Individual data streams with known output values are entered into the network and the weights and biases are changed so that the error between the true value and the predicted (network) value are minimized. The training errors reported by the network need to be evaluated carefully since the network is capable of being overtrained (the network memorizes the data and has no predictive behavior).[68] If high errors persist, changing parameters like the number of layers, neurons, or data formats initially imputed into the input layer may improve the performance of the network.

Once the network has been trained, validating the networks ability to predict values based on the relationships learned from the data is done by omitting a single data point from the training data set. Training of the network is carried out again, and then the left out point is imputed as an unknown sample. If the error associated with this removed data point is close to the training error, the

network model is said to be valid. Ultimately, the error associated with a "real" unknown sample is the best way to gage the networks ability.

A common attribute for PCA and ANN analysis is that they are both used to understand relationships between data sets. Yet, the significant difference lies in the approach with which the data is inputted for each analysis. PCA is considered an unsupervised learning technique meaning that the relationship between the data will evolve from the calculations without using membership classification beforehand. On the other hand, ANN analysis is used to create a model based on data sets with known output values for classifying or quantifying future unknown samples. These methods sometimes experience limitations with their sensitivity to analyzing samples outside their training set or sample volume giving erroneous results.[68,90] However, both of these methods possess distinctive advantages for analyzing multivariate data sets in various settings and ultimately provide a chemist with the means to quickly extract distinctive patterns from large volumes of data found in real-world problems.

## 1.4 Outlook

The field of chemical sensing is a science that bridges the chemical, biological, engineering, and material sciences with foundations in chemistry spanning organic, analytical, physical, and inorganic chemistry. Therefore, the development of sensors capable of detecting the presence of analytes requires a multifaceted approach.

With the many approaches taken by chemists to develop sensors, numerous signaling strategies have emerged in the literature towards the detection

of anaytes. Even though many of these signal transduction mechanisms have been explored in the Anslyn and McDevitt research groups, the indicator-displacement assay has often proven to be a successful strategy. Chapter 2 focuses on the application of an indicator-displacement assay with a synthetic host to quantitate the amount of citrate in commercial beverages. Also, application of an ANN with the same two-component sensing ensemble allows for the determination of citrate and calcium concentrations in flavored vodkas.

Investigators, with a large knowledge base to draw from concerning molecular recognition and host design, are now able take chemical sensing into an area ripe for cultivation. This new emerging science couples the concepts of molecular sensing with array-based platforms so that sensing of multiple analytes can be accomplished. Trends are now shifting towards utilizing an array of differential sensors responsive to various classes of analytes instead of using sensors specifically designed to target one analyte. Combining the signals from all the sensors in the array generates a fingerprint response that is unique to the composition of the mixture being analyzed. In Chapter 3 and Chapter 4, this concept is employed by coupling the principles of supramolecular chemistry and pattern recognition to create new sensing protocols for the analysis of nucleotide phosphates and phosphonates in aqueous solutions.

A novel optically-based sensor array platform was described in Section 1.3.1 with versatile components that can be modified for different applications evaluating complex mixtures. We expect that by expanding this "lab-on-a-chip" technology to incorporate differential sensors and pattern recognition, analysis of

various classes of analytes within this platform has the potential to be a viable sensing device for biochemical and chemical warfare degradation products. Attributes such as high sensitivity, low detection limits, reduction of false positives, short assay times, and minimal consumption of reagents have been demonstrated in our previous reports utilizing this detection platform and show promise for the incorporation of the sensing strategies described herein.

# CHAPTER 2: COMPETITIVE INDICATOR METHODS USED FOR THE ANALYSIS OF CITRATE AND CALCIUM IN BEVERAGES

## 2.0 Introduction

As described in Chapter 1, many investigations have been carried out to develop single analyte molecular sensors. The application of these molecular sensors requires the presence of a reporter molecule capable of signaling the binding of the analyte to the host. The two most reoccurring signal transduction themes are the covalent attachment of the signaling molecule to the host or competition between the target analyte and the signaling molecule.[66]

Competition assays are the focus of this chapter. Specifically, a competitive indicator method for studying host:guest complexes is extended to systems forming I:H, $I:H_2$, and A:H complexes of indicator (I), host (H) and competing analyte (A). Methods are applied to complexes of a synthetic organic host (**2.1**) with commercially available indicators xylenol orange (**2.4**) and methylthymol blue (**2.5**). Utilizing complexometric indicators results in an observable shift in $\lambda_{max}$ upon binding of the analyte and, subsequently may enhance the sensitivity of these competition assays due to a larger dynamic range in the change of absorption. The binding constants for the association between I:H, $I:H_2$, and A:H are reported. These sensing ensembles have been tested in competitive media. Competition assays using UV-Vis spectroscopy and each

host-indicator ensemble allowed for the determination of citrate in various beverages.

Finally, pattern recognition algorithms were applied to a two-component sensing ensemble to differentiate among solutions containing various concentrations of calcium and citrate ions. The concentrations of calcium and citrate in various flavored vodkas were determined through artificial neural network (ANN) analysis. Herein, the new developments are summarized and the utility of this method is described in the context of the analysis of citrate and calcium ion in citrus beverages using a synthetic receptor paired with an optical signaling molecule and ANN.

## 2.1 Development of a Host for Citrate

The Anslyn group has used indicator-displacement assays with a series of synthetic organic hosts in order to detect various analytes.[91-95] In one system, a receptor for citrate was developed that is selective for this tris-carboxylate compound even in the presence of other common carboxylates.[92] The choice of citrate as the target analyte was due to the potential commercial interest in a sensor for citrate by beverage bottling companies.

The receptor (or host) **2.1** consists of a 2,4,6-triethylbenzene core substituted with guanidinium moieties in the 1, 3, and 5 positions. Each adjacent substituent on the benzene ring alternates above and below the plane of the ring to minimize steric interactions, causing the guanidiniums to lay on one face of the benzene ring.[96] Receptors containing similar structures to **2.1** have demonstrated

that the preorganization helps facilitate the binding of small organic guests.[91-93,97-99]

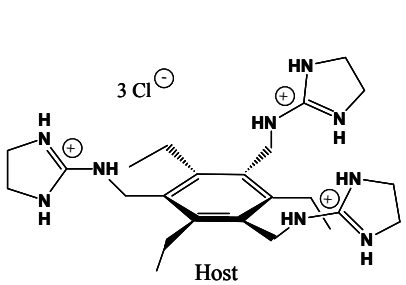


Host
**2.1**

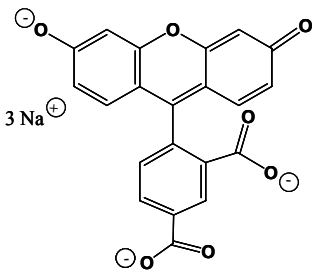


(5-carboxyfluorsescein)
**2.3**

**Scheme 2.1:** Molecular structures of host (**2.1**) and 5-carboxyfluorescein (**2.3**)

At neutral pH, citrate (**2.2**) is trianionic, and this charge leads to the ability to distinguish citrate from other possible interfering species. Host **2.1** is complementary to citrate in both charge and hydrogen bonding ability. The use of guanidiniums was employed because their geometry is conducive for the binding of carboxylates, and they remain protonated over a wider pH range than ammonium species.[100,101]

The sensing properties of **2.1** for citrate were investigated with the use of competition assays.[91] Initially, a sensing ensemble was created by introducing **2.3** (5-carboxyfluorescein) to **2.1**. As seen in Figure 2.1, the absorbance of **2.3** at pH 7.4 increases at 495 nm upon association with **2.1**. The observed increase in absorbance was rationalized to be a result of increased ionization of the phenol on the xanthene ring due to the positively charged microenvironment of the host molecule. The binding constant was found to be 4.7 x $10^3$ $M^{-1}$ under Benesi-Hildebrand[102] conditions in 25% (v/v) water in methanol at pH 7.4.

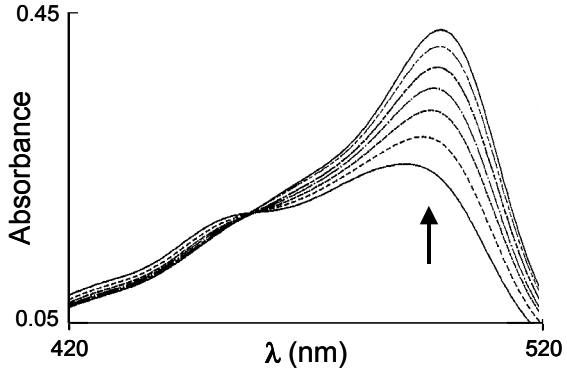


**Figure 2.1:** UV-Vis spectra of **2.3** in 25% (v/v) water in methanol with 5 mM HEPES buffer at pH 7.4. Addition of **2.1** to a solution of **2.3** at constant concentration (14 μM) causes an increase in absorbance at 495 nm (arrows indicate the direction of change in the absorbance intensity).[92]

Addition of sodium citrate to the indicator-host complex causes a decrease in the observed absorbance of fluorescein at 495 nm (Figure 2.2). It was reasoned that the 5-carboxyfluorescein (**2.3**) was expelled from the binding pocket due to the higher binding affinity of citrate with **2.1**. A binding constant for citrate with **2.1** was found to be 2.9 x $10^5$ $M^{-1}$ in this solvent system. Significantly reduced affinities were found for succinate, glutarate (both valued close to 2 x $10^2$ $M^{-1}$) and acetate (less than 10 $M^{-1}$).[92]

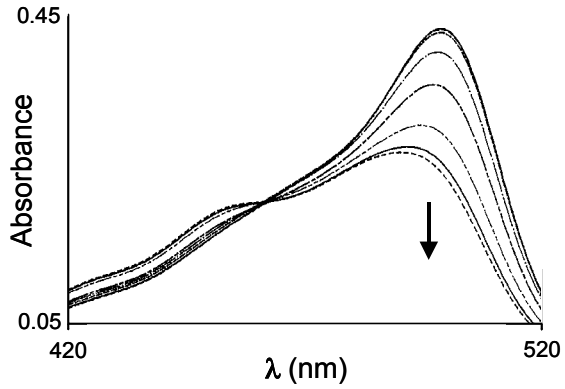


**Figure 2.2:** UV-Vis spectra of **2.3** in 25% (v/v) water in methanol with 5 mM HEPES buffer at pH 7.4. Addition of **2.2** to the sensing ensemble **2.1**:**2.3** at constant concentration (75 μM **2.1**, 14 μM **2.3**) causes a decrease in absorbance at 495 nm (arrows indicate the direction of change in the absorbance intensity).[92]

A practical use of an ensemble of **2.1** and **2.3** was demonstrated by evaluating the amount of citrate in various complex mixtures. Calibration curves were generated for varying amounts of citrate from the absorbance data obtained from the citrate competition assay. With these plots, aliquots of different citrus beverages were added to a solution of the **2.1:2.3** complex and the absorbance recorded.[91] This allowed for the analysis of citrate in commercially available beverages and further demonstrated that **2.1** possess selectivity for citrate in the presence of other competing analytes.

Although this assay was successful, three improvements were desired. One was a $\lambda_{max}$ shift, which creates a color change and therefore a larger dynamic range in the change in absorbance. Another goal was to show that many commercially available indicators could be used with the same receptor. This gives chemists larger latitude in the ability to choose indicators for displacement

assays using synthetic receptors. Third, the multi-analyte sensing capabilities of these sensing ensembles are demonstrated via application of ANN analysis. To this end, competition assays are employed with standard spectrophotometer to sense for calcium and citrate in various beverages.

## 2.2 Binding Studies

### 2.2.1 Selection of the Indicators and Experimental Conditions

Using competition assays for the evaluation of analytes in solution requires that the indicator form a complex with the ligand or host molecule. Another requirement is that the absorption spectra of the complexed form differ significantly from the absorption spectra of the uncomplexed form. The choice of indicators in this study was guided by two factors. First, the binding of carboxylates with guanidinium groups imbedded in aminoimidazoline groups is well precedented,[91-95] and therefore the use of complexometric indicators possessing carboxylates in their structure were explored. Second, we chose indicators that change color as a function of pH, thereby expecting similar color changes within the microenvironment of the host. Xylenol orange (**2.4**) and methylthymol blue (**2.5**) were chosen as the indicators for the purposes of our studies.

At neutral pH, metal cations typically coordinate to the iminiodiacetic acid residues and the auxochromic phenol oxygen of **2.4** and **2.5** inducing a shift in the $\lambda_{max}$.[103-106] We expected that complexation of **2.4** or **2.5** to **2.1** would result in a similar color change of the indicator due to increased ionization of the phenols. The structural features of these two indicators (I) clearly show that there are two

similar iminiodiacetic acid binding sites that can associate with host **2.1** (H), giving I:H and I:$H_2$ molecular complexes (Scheme 2.2).

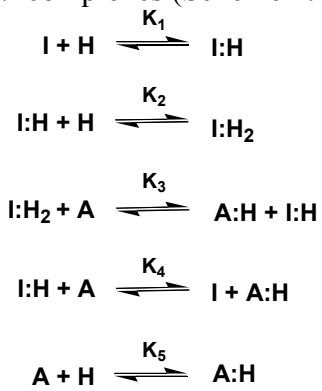


**Scheme 2.2:** Equilibria for the systems studied by UV-Vis spectroscopy.

For direct comparison to the studies mentioned in Section 2.1, the studies described here were conducted on a UV-Vis spectrophotometer using solutions containing 25 % (v/v) water in methanol mixtures buffered at pH of 7.5. A sulfonate buffer (4-(2-hydroxyethyl)-1-piperazine ethanesulfonic acid, or HEPES) was employed to avoid competitive media.[92] In those studies, the use of 25 % (v/v) water in methanol mixtures enhanced binding of the host to the analyte by providing hydrophobic pockets that encouraged charge pairing.

### 2.2.2 BINDING STOICHIOMETRY

To both explore the stoichiometry of binding and to measure the affinity constants, we first studied the associative properties of **2.1** with **2.4** and **2.5**. Titration experiments were conducted to determine the binding constants for each dye with host **2.1**. As described previously, host **2.1** associates with **2.3** in a 1:1 fashion. However, the dyes used in these studies (**2.4** and **2.5**) are expected to

associate with the host giving I:H and $I:H_2$ complexes. This expectation is borne out by the lack of sharp isosbestic points.

### 2.2.3 BINDING DATA

The absorbance of **2.4** (Figure 2.3) at pH 7.5 increases at 577 nm upon association with **2.1,** while the absorbance decreases at 445 nm (solutions change from an orange color to a pink-red). Similarly, the absorbance of **2.5** (Figure 2.4) at pH 7.5 increases at 607 nm upon addition of **2.1** with a decrease in absorbance at 454 nm (solutions change from a light yellow to a cobalt blue). It is reasoned that the binding of the positively-charged host molecule to the carboxylates on the indicator would lower the p$K_a$ of the indicator phenol groups due to the positive microenvironment present in the host. The observed color changes correlate with the indicators acting as if they are in a more basic microenvironment. The increased ionization state of the indicators is due to the positive charges on the receptor, and the increased electron density on the auxochromic oxygen leads to the observed $\lambda_{max}$ changes.

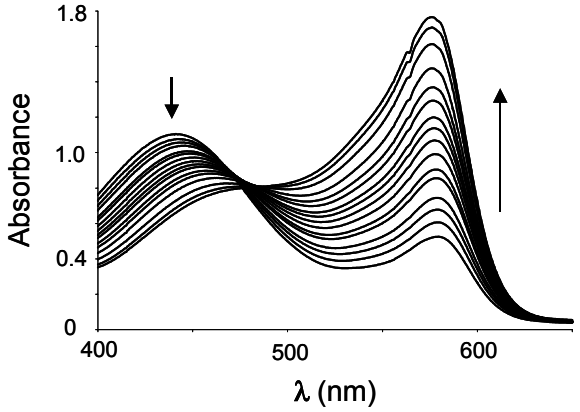


**Figure 2.3:** UV-Vis spectra of **2.4** in 25% (v/v) water in methanol with 10 mM HEPES buffer at pH 7.5. Addition of **2.1** to a solution of **2.4** at constant concentration (55 μM) causes and increase of absorbance at 577 nm and a decrease in absorbance at 445 nm (arrows indicate the direction of change in the absorbance intensity).

In Figures 2.3 and 2.4, a large change in absorbance was observed with the addition of **2.1** to each indicator. For instance, the percent difference in absorbance at 577 nm between the absorbance of the dye in solution and the absorbance of the **2.4**:**2.1** complex in Figure 2.3 was 238%, and the percent difference in absorbance at 607 nm in Figure 2.4 was calculated to be 521%. This is a significantly larger dynamic range in change in signal compared to the 73% increase in signal observed with the addition of **2.1** to 5-carboxyfluorescein (Figure 2.1). The dramatic increase in signal in both cases with indicators **2.4** and **2.5** is attributed to their ability to shift their $\lambda_{max}$ upon complexation with host **2.1**.

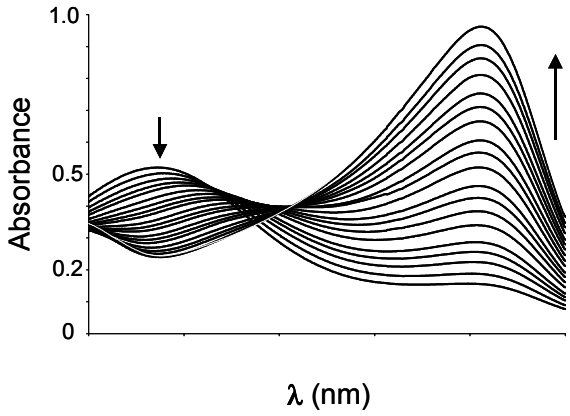


**Figure 2.4:** UV-Vis spectra of **2.5** in 25% (v/v) water in methanol with 10 mM HEPES buffer at pH 7.5. Addition of **2.1** to a solution of **2.5** at constant concentration (55 mM) causes an increase in absorbance at 607 nm and a decrease in absorbance at 454 nm (arrows indicate the direction of change in the absorbance intensity).

### 2.2.4 DERIVATION OF BINDING EQUATIONS

The system studied contained 1:1 (I:H) and 1:2 ($I:H_2$) complexes of indicator (I) with host (H). The following Eqs. 2.1 and 2.2 describe the interactions between host (**2.1**) and indicator (**2.4** or **2.5**).

$$I + H \rightleftharpoons IH \qquad \text{Eq. 2.1}$$

$$IH + H \rightleftharpoons IH_2 \qquad \text{Eq. 2.2}$$

The absorbance of the solution of xylenol orange ($A_o$) prior to the addition of host is described by Beer's Law, Eq. 2.3;

$$A_o = \varepsilon \cdot b \cdot [I] \qquad \text{Eq. 2.3}$$

where ε is the molar absorptivity of the indicator, b is the path length of light through the sample solution, and [I] is the concentration of the indicator present.

After the addition of host, the equation for describing all the absorbing species (A) in the solution becomes:

$$A = \varepsilon_I \cdot b \cdot [I_i] + \varepsilon_H \cdot b \cdot [H_i] + \varepsilon_{IH} \cdot b \cdot [IH] + \varepsilon_{IH_2} \cdot b \cdot [IH_2] \qquad \text{Eq. 2.4}$$

where $[I_i]$ and $[H_i]$ represent the concentration of the free indicator and host in solution, respectively, and [IH] and $[IH_2]$ are the concentrations of any complexes that may form between the them.

The total concentration of each species ($I_T$ and $H_T$) is depicted by the mass balance equations for both the indicator and the host molecule.

$$[I_T] = [I_i] + [IH] + [IH_2] \qquad \text{Eq. 2.5}$$

$$[H_T] = [H_i] + [IH] + 2 \cdot [IH_2] \qquad \text{Eq. 2.6}$$

Solving Eq. 2.5 and Eq. 2.6 for $[I_i]$ and $[H_i]$, respectively and incorporating the expressions into equation 2.4 gives Eq. 2.7.

$$\begin{aligned} A = {} & \varepsilon_I \cdot b\left([I_T] - [IH] - [IH_2]\right) + \varepsilon_H \cdot b\left([H_T] - [IH] - 2 \cdot [IH_2]\right) \\ & + \varepsilon_{IH} \cdot b \cdot [IH] + \varepsilon_{IH_2} \cdot b \cdot [IH_2] \end{aligned} \qquad \text{Eq. 2.7}$$

Since the host has no absorbance at the wavelength that is being monitored, the $\varepsilon_H$ term becomes zero. Upon eliminating this term and combining like terms, the equation becomes:

$$A = \varepsilon_I \cdot b \cdot [I_T] + (\varepsilon_{IH} - \varepsilon_I) \cdot b \cdot [IH] + (\varepsilon_{IH_2} - \varepsilon_I) \cdot b \cdot [IH_2] \qquad \text{Eq. 2.8}$$

Dividing the path length from each side of the equation gives:

$$\frac{A}{b} = \varepsilon_I \cdot [I_T] + \Delta\varepsilon_1 \cdot [IH] + \Delta\varepsilon_2 \cdot [IH_2] \qquad \text{Eq. 2.9}$$

where $\Delta\varepsilon_1 = \varepsilon_{IH} - \varepsilon_I$ and $\Delta\varepsilon_2 = \varepsilon_{IH_2} - \varepsilon_I$. The equilibrium constants in this system are given by:

$$K_1 = \frac{[IH]}{[H_i] \cdot [I_i]} \qquad \text{Eq. 2.10}$$

$$K_2 = \frac{[IH_2]}{[IH] \cdot [H_i]} \qquad \text{Eq. 2.11}$$

Rearrangement of these expressions and substitution into Eq. 2.9 gives the result:

$$\frac{A}{b} = \varepsilon_I \cdot [I_T] + \Delta\varepsilon_1 \cdot \left(K_1 \cdot [H_i] \cdot [I_i]\right) + \Delta\varepsilon_2 \cdot \left(K_2 \cdot K_1 \cdot [H_i]^2 \cdot [I_i]\right) \qquad \text{Eq. 2.12}$$

Since $[I_T]$ is held constant, the absorbance of the indicator prior to the first addition of host ($A_0$) is subtracted from each subsequent absorbance reading after the addition of the host ($A_i$). This results leads to the $\varepsilon_I$ term dropping out of the expression.

$$\frac{\Delta A}{b} = \Delta\varepsilon_1 \cdot \left(K_1 \cdot [H_i] \cdot [I_i]\right) + \Delta\varepsilon_2 \cdot \left(K_2 \cdot K_1 \cdot [H_i]^2 \cdot [I_i]\right) \qquad \text{Eq. 2.13}$$

As mentioned earlier, the equilibrium expressions can be rewritten as:

$$[IH] = K_1 \cdot [H_i] \cdot [I_i] \qquad \text{Eq. 2.14}$$

$$[IH_2] = K_2 \cdot [H_i]^2 \cdot [I_i] \qquad \text{Eq. 2.15}$$

Using these values and substituting into the mass balance Eq. 2.5 and solving for $[I_i]$ will give the equation:

$$[I_i] = \frac{[I_T]}{1 + K_1 \cdot [H_i] + K_2 \cdot K_1 \cdot [H_i]^2} \qquad \text{Eq. 2.16}$$

Combining Eq. 2.16 with Eq. 2.13 results in the equation for the binding isotherm for a 1:2 $[I:H_2]$ complex.

$$\frac{\Delta A}{b} = \frac{(K_1 \cdot [H_i] \cdot [I_T]) \cdot (\Delta\varepsilon_1 + \Delta\varepsilon_2 \cdot K_2 \cdot [H_i])}{1 + K_1 \cdot [H_i] + K_2 \cdot K_1 [H_i]^2} \qquad \text{Eq. 2.17}$$

The term $[H_T]$ is a value that can be determined experimentally, where as, the concentration of free host, $[H_i]$, cannot be measured directly. This creates the need to relate $[H_i]$ to $[H_T]$ and can be accomplished by substituting Eq. 2.16 into the rearranged form of Eq. 2.14, giving Eq. 2.18.

$$[IH] = \frac{K_1 \cdot [H_i] \cdot [I_T]}{1 + K_1 \cdot [H_i] + K_2 \cdot K_1 \cdot [H_i]^2} \qquad \text{Eq. 2.18}$$

Now, substitute Eq. 2.18 into the mass balance equation for $[H_T]$. This relates the total concentration of host to the concentration of free host in solution.

$$[H_T] = [H_i] + \left( \frac{K_1 \cdot [H_i] \cdot [I_T]}{1 + K_1 \cdot [H_i] + K_2 \cdot K_1 \cdot [H_i]^2} \right) + \left( \frac{2 \cdot K_2 \cdot K_1 \cdot [I_T] \cdot [H_i]^2}{1 + K_1 \cdot [H_i] + K_2 \cdot K_1 \cdot [H_i]^2} \right)$$

Eq. 2.19

Rearrangement of Eq. 2.19 in order to solve for $[H_i]$ gives the following cubic expression:

$$K_1 \cdot K_2 \cdot [H_i]^3 + K_1\left(2 \cdot K_2 \cdot [I_T] - K_2 \cdot [H_T] + 1\right) \cdot [H_i]^2 + \left(K_1 \cdot [I_T] - K_1 \cdot [H_T] + 1\right) \cdot [H_i] - [H_T] = 0 \quad \text{Eq. 2.20}$$

Using Eq. 2.17 and Eq. 2.20, it is possible to extract a binding constant from a plot of the change in absorbance ($\Delta A$) versus the total concentration of indicator $[I_T]$.

### 2.2.5 CURVE FITTING ANALYSIS

As shown in Figure 2.5 A and B, addition of citrate to the indicator-host complexes causes a reverse in the observed absorbance of both xylenol orange and methylthymol blue at 577 nm and 607 nm, respectively. As seen with the citrate assay employing 5-carboxyfluorescein, the indicator is expelled from the binding pocket due to the higher binding affinity of **2.1** with citrate (Scheme 2.3).

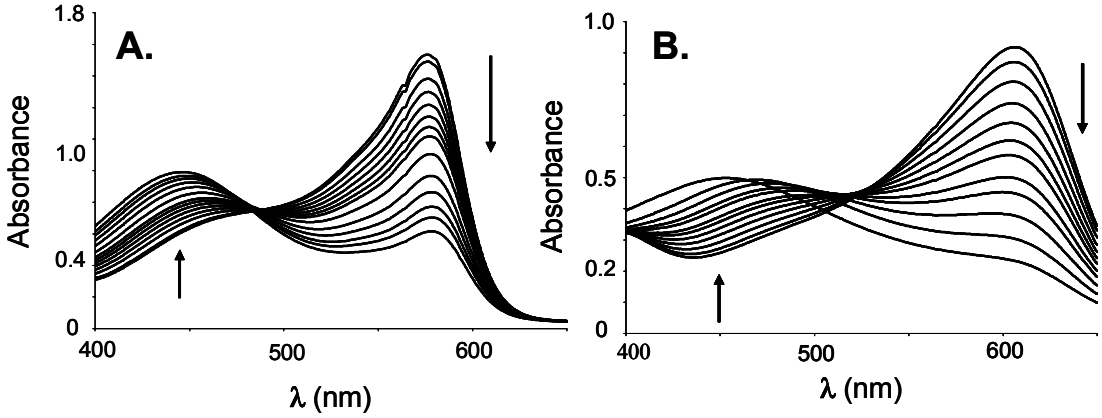


**Figure 2.5:** UV-Vis spectra of **2.4** and 2.5 in 25% (v/v) water in methanol with 10 mM HEPES buffer at pH 7.5. (A) Addition of **2.2** to a solution of **2.4**:**2.1** at constant concentration (55 μM **2.4**, 1.13 mM **2.1**) causes a decrease in absorbance at 577 nm and an increase in absorbance at 445 nm. (B) Addition of **2.2** to a solution of **2.5**:**2.1** at constant concentration (55 μM **2.5**, 1.13 mM **2.1**) causes a decrease in absorbance at 607 nm and an increase of absorbance at 454 nm (arrows indicate the direction of change in the absorbance intensity)

Extraction of the binding constants, $K_1$ and $K_2$, for the association between each indicator molecule and the host is complicated. There are four variables: two binding constants ($K_1$ and $K_2$), and two different extinction coefficients (1:1 indicator-host complex, and 1:2 indicator-host complex). A method for determining 1:1 and 1:2 binding constants from optical spectroscopy data has been discussed.[45-49,107]

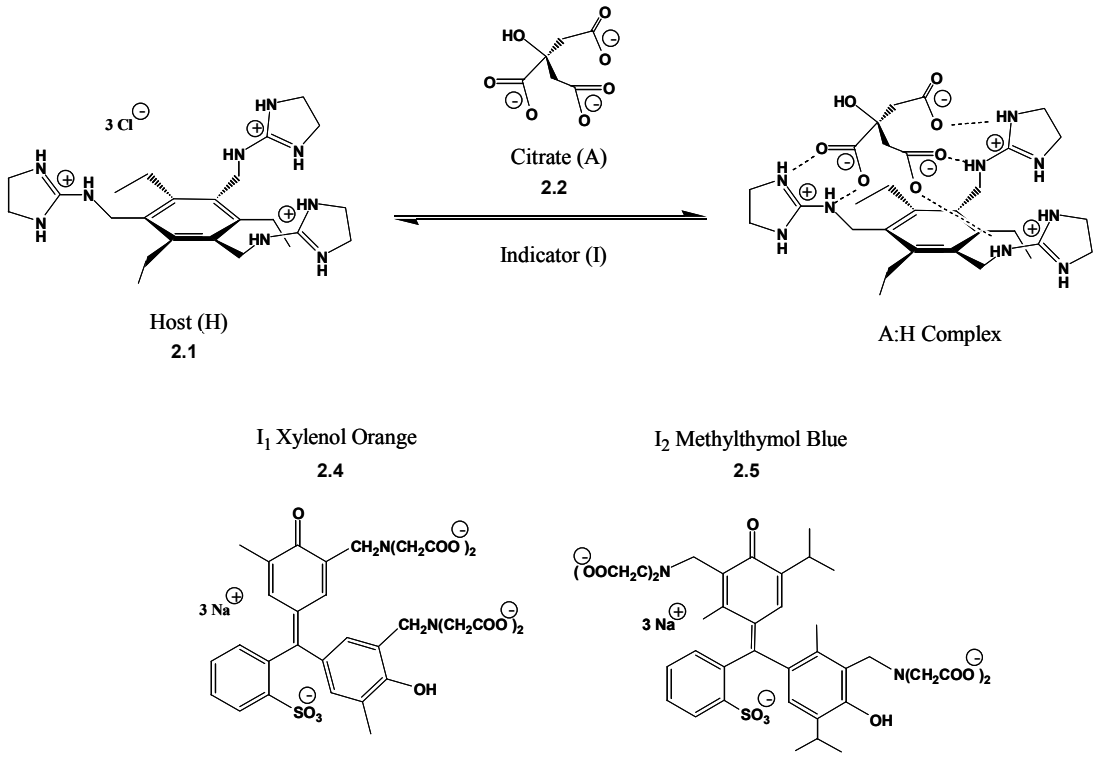


**Scheme 2.3:** Molecular structures of the host (**2.1**) and indicators (**2.4** and **2.5**) used to sense for citrate.

The program Mathematica 3.0 was used to solve Eq. 2.20 for $[H_i]$ with multiple values of $[H_T]$ and several initial estimates of $K_1$, $K_2$, $\Delta\varepsilon_1$, and $\Delta\varepsilon_2$. Each value for $[H_i]$ is substituted into Eq. 2.17. The fit of Eq. 2.17 to the data is accomplished by prompting the user for initial estimates for $K_1$, $K_2$, $\Delta\varepsilon_1$, and $\Delta\varepsilon_2$. The model equation (Eq. 2.17) is overlaid graphically with the experimental values obtained for $\Delta A/b$ (the path length is 1.00 cm) and $[H_T]$. The values $K_1$, $K_2$, $\Delta\varepsilon_1$, and $\Delta\varepsilon_2$ are modified and the data replotted until the best fit between experimental data and the model is visually achieved, as shown in Figure 2.6.

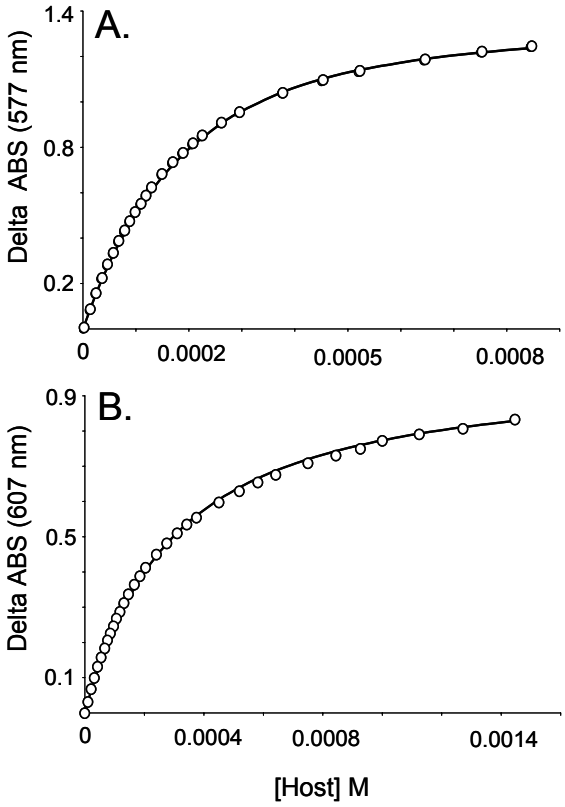


**Figure 2.6:** Theoretical fit (**-**) of Eq. 2.17 to the experimental data (○) obtained from ΔA as a function of the addition of **2.1** to each indicator. (A) Isotherm plot for addition of **2.1** to **2.4** (λ = 577nm). (B) Isotherm plot for the addition of **2.1** to **2.5** (λ = 607nm).

The binding constants determined for the **2.4:2.1** molecular complex were $K_1$= 7.05 x $10^3$ $M^{-1}$ and $K_2$ = 2.08 x $10^3$ $M^{-1}$. The affinity constants determined for the **2.5:2.1** molecular complex were $K_1$= 3.95 x $10^3$ $M^{-1}$ and $K_2$ = 1.10 x $10^2$ $M^{-1}$. These results show that xylenol orange has a larger affinity for **2.1** than methylthymol blue. This observation may be attributed to the presence of the isopropyl groups on methythymol blue as opposed to the methyl groups at the

corresponding positions in the xylenol orange structure. The added steric bulk on **2.5** could hinder access of **2.1** to the indicator binding sites, resulting in slightly smaller binding constant values.

The equilibrium equations given in Scheme 2.2 for the displacement of the indicators upon addition of **2.2** are as follows:

$$K_3 = \frac{[AH]\cdot[IH]}{[IH_2]\cdot[A]} \qquad \text{Eq. 2.21}$$

$$K_4 = \frac{[AH]\cdot[I]}{[IH]\cdot[A]} \qquad \text{Eq. 2.22}$$

The equilibrium expression for the association of host **1** with citrate is:

$$K_5 = \frac{[AH]}{[H]\cdot[A]} \qquad \text{Eq. 2.23}$$

Hence, the displacement constants $K_3$ and $K_4$ can be determined by using the following relationships:

$$K_3 = \frac{K_5}{K_2} \qquad \text{Eq. 2.24}$$

$$K_4 = \frac{K_5}{K_1} \qquad \text{Eq. 2.25}$$

With xylenol orange, the values for $K_3$ and $K_4$ obtained from Eqs. 2.24 and 2.25 are $1.39 \times 10^2$ $M^{-1}$ and 41.1 $M^{-1}$, respectively. In the methylthymol blue studies, the values for $K_3$ and $K_4$ obtained from Eqs. 2.24 and 2.25 are $2.64 \times 10^3$

$M^{-1}$ and 73.4 $M^{-1}$, respectively. These values for $K_3$ and $K_4$ were calculated using the binding constant ($K_5$) presented earlier.[91] It was reasoned previously that the association constants for methylthymol blue to **2.1** were smaller than the corresponding $K_1$ and $K_2$ values for xylenol orange due to added steric bulk on the methylthymol blue structure. It follows that the displacement constants for xylenol orange upon introduction of citrate are smaller than the corresponding $K_3$ and $K_4$ values for methylthymol blue because of the stronger association of the **2.4**:**2.1** complex. The association of the **2.5**:**2.1** complex is slightly weaker than the **2.4**:**2.1** complex and therefore the **2.5**:**2.1** complex will disassociate more readily in order for the **2.1**:**2.2** complex to form upon introduction of citrate.

## 2.3 Beverage Analysis

### 2.3.1 CITRATE IN BEVERAGES

In order to demonstrate that these sensing systems can be employed for practical uses, calibration curves were generated for citrate (Figure 2.7) in order to evaluate various citrus beverages. The determination of citrate in various beverages was performed by UV-Vis spectroscopy in 10 mM HEPES buffer at pH 7.5 with a 25% (v/v) water in methanol mixture.

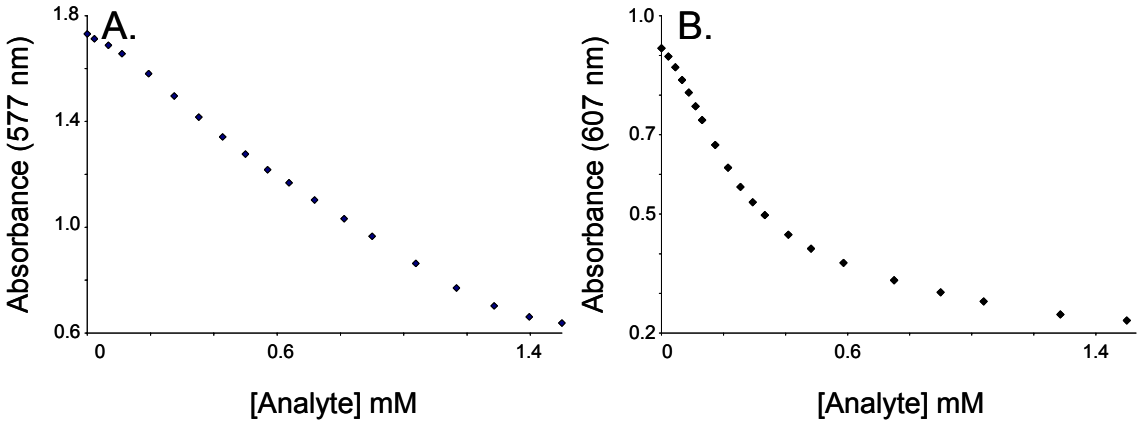


**Figure 2.7:** Calibration curves used for the citrate assay (25% (v/v) water in methanol with 10 mM HEPES buffer at pH 7.5). (A) UV-Vis calibration curve using **2.4** at the indicator (55 μM **2.4**, 1.13 mM **2.1**, λ = 577 nm). (B) UV-Vis calibration curve using **2.5** at the indicator (55 μM **2.5**, 1.13 mM **2.1**, λ = 607 nm).

For each assay utilizing a different indicator, aliquots ranging between 10 and 400 μL of each type of beverage were added to the sensing ensemble (1.00 mL). An absorbance reading was taken, and the citrate concentration was determined from the calibration curve. These values are reported in Table 2.1. The citrate concentrations determined for Sprite® and Snapple® Starfruit drink by each sensing system are in agreement within 10% of each other. The values calculated with the two citrate assays for Schweppes® tonic water differ by 13%. Based upon previous results, it is known that **2.1** is selective for citrate in these kinds of beverages, and this data shows that this novel colorimetric competition method works well to quantitate citrate in a practical application.

| | Concentration (mM) | |
|---|---|---|
| | **2.2** + **2.4**:**2.1** | **2.2** + **2.5**:**2.1** |
| Sprite | 4.9 ± 0.5 | 4.4 ± 0.3 |
| Snapple (Starfruit) | 10.8 ± 0.9 | 9.6 ± 1 |
| Tonic Water (Schweppes) | 13.2 ± 2 | 10.9 ± 3 |

**Table 2.1:** Concentration of citrate (mM) in beverages determined by different sensing systems. The reported values shown are the average value ± standard deviation of three measurements.

### 2.3.2 CITRATE AND CALCIUM IN BEVERAGES USING ARTIFICIAL NEURAL NETWORKS

Recently, the simultaneous detection of two structurally similar analytes, tartrate and malate, was demonstrated via spectrophotometric analysis of two indicator displacement assays utilizing two different synthetic hosts and two different indicators.[108] Application of an ANN allowed for the evaluation of the relative amounts of each analyte in unknown solutions. The power behind this simple approach is that it creates multi-analyte sensing protocol in the absence of an array setting. Despite the success of this approach, two additional levels of complexity were sought. First, further demonstrate the versatility of this method by extending it to systems using complexometric dyes capable of forming 1:1 and 2:1 host:guest complexes (Scheme 2.4). Second, employ this method for practical uses through the analysis of commercially available flavored vodkas. It is expected that a multianalyte sensing scheme dependent on the analysis of homogeneous solutions in a UV-Visible spectrophometer would hold greater potential for utility among chemists due to the relative availability of this type of instrumentation.

The host (**2.1**) and indicator, xylenol orange (**2.4**), discussed earlier were chosen for this study due to their established affinities for citrate (**2.2**) and calcium (Ca(II)), respectively.[109] The presence of the guanidinium groups on the host **2.1** is known to impart affinity to carboxylates,[91-95] while the iminiodiacetic acid moieties on the indicator **2.4** have been shown to bind divalent cations like calcium.[103-106] Also, the xylenol orange indicator was chosen due to the characteristic color change or $\lambda_{max}$ shift observed earlier in similar systems resulting in a larger dynamic range with which to work.

The signaling mechanism envisioned is an indicator-displacement assay which has often been exploited by the Anslyn group.[91-95] The signaling scheme is executed by adding a host molecule to an indicator adorned with binding groups similar in charge or geometry as the target analyte. Once a H:I complex is formed, the analyte of interest is introduced and the H:I equilibrium is disrupted. As the analyte binds preferentially to the host, an optically measurable response results due to the changes in the microenvironment of the indicator.

The training set (matrix) needed for the identification and quantification of calcium and citrate was carried out by obtaining UV-Visible spectra of a two-component sensing ensemble of **2.1** and **2.4** in solution. With this approach, several absorbance measurements at different wavelengths from a solution containing this sensing ensemble can serve as unique data inputs (or a fingerprint response) allowing for identification and quantification of components present in the solution. In this regard, the concentration of the host and indicator were maintained at a constant concentration while separate UV-Visible spectra were

obtained for each addition of various amounts of calcium and citrate. Figure 2.8 is a general outline for the matrix of spectra envisioned for the training set.

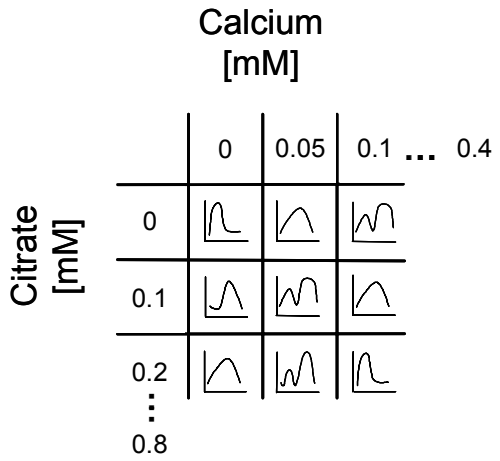


**Figure 2.8:** The approach taken to obtain data via UV-Vis spectroscopy for the two-component sensing ensemble, where spectra were recorded at various concentrations (mM) of calcium and citrate.

Eighty discrete spectra resulted by systematically changing the concentrations of calcium in 50 μM increments ranging between 0 and 400 μM and also changing the concentrations of citrate in 100 μM increments ranging between 0 and 800 μM. An example of the spectral difference between the binding of varying ratios of calcium and citrate to **2.1** and **2.4** is illustrated in Figure 2.9. These two spectra show that a unique response is detected when a complexiметric dye is combined with a synthetic receptor upon exposure to mixtures of two different analytes.

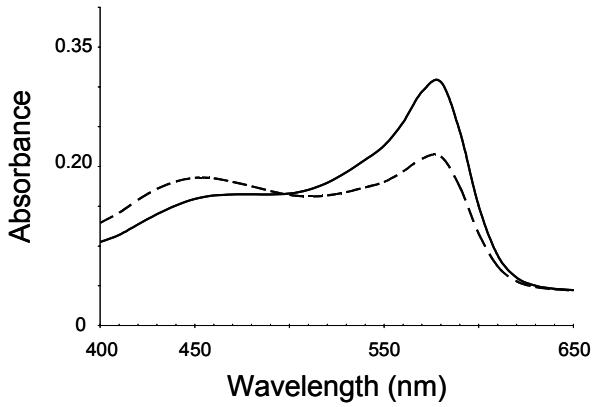


**Figure 2.9:** Representative UV-Vis spectra of the indicator-displacement assays created when a solution containing **2.4** (240 μM) and **2.1** (10 μM) is titrated with various concentrations of calcium and **2.2** in 25% (v/v) vodka in water with 10 mM HEPES buffer at pH 7.5. [(▬)Calcium at 400 μM and citrate at 100 μM] and [(— —) Calcium at 50 μM and citrate at 600 μM] Inside tick marks on the x-axis illustrate the 25 wavelengths chosen to use in the ANN analysis.

As shown in Scheme 2.4, the equilibria of this system are complex. Detection of these complexes would normally prove to be difficult because many of the species that may exist in the solution do not contain chromophoric groups for optical monitoring by UV-Visible or fluorescence spectroscopy. In fact, only the presence of the complexometric dye allows for optical monitoring of the events occurring in the solution. However, the spectrophotometric changes that occur upon introduction of different analytes to the solution are subtle (Figure 2.9) and these subtle differences can be extracted quantitatively through the application of pattern recognition.

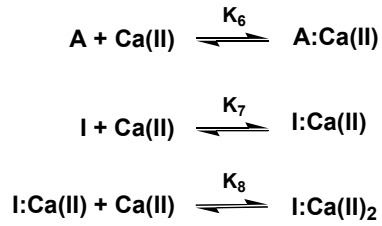


**Scheme 2.4:** Equilibria of the extended systems studied.

Supervised learning with pattern recognition protocols was accomplished using mulit-layer perceptron (MLP) artificial neural networks (ANN).[68,88,90] The diagram in Figure 2.10 illustrates the typical organization of the components within a multilayer ANN. The structure of an ANN can be tailored to the problem being solved. For our purposes, the number of units in the input layer is equal to the number of wavelengths taken from each UV-Visible spectrum in the training set. The output layers are chosen to be equal to the number of predictions desired from the network. For our studies, the network is expected to predict the concentrations of calcium and citrate. The intermediate layers ("hidden layers") positioned between the input layers and the output layers were selected to be half the number of the input layers. The connections between each of the layers (Figure 2.10) allow for each component (or neuron) to interact with each other and extend the ability of the network to generate more complex algorithms for a range of difficult applications.

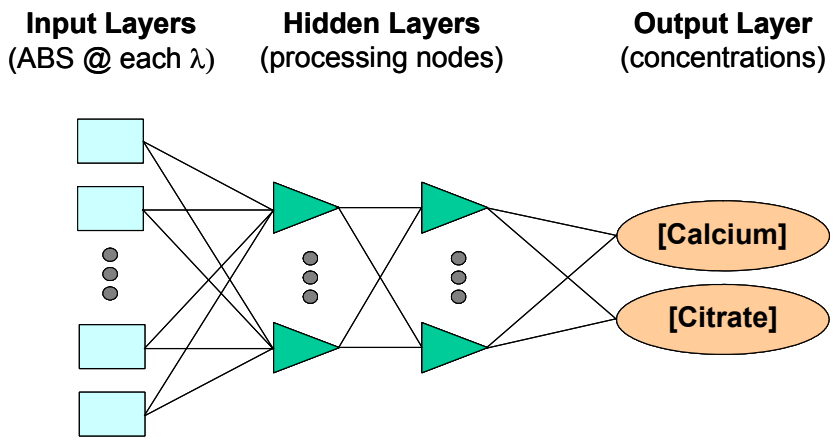


**Figure 2.10:** General representation of the multilayer ANN used for the analysis of flavored vodkas. The ANN is composed of an input layer, a variable number of hidden layers, and an output layer.

With the network trained, "unknowns" or inputs not present in the matrix can be supplied into the trained network so that the previously formed algorithms can attempt to calculate an output value. All but four of the spectra were used to train the ANN using 25 wavelengths from each titration. The four traces that were omitted from the training set were utilized as test points to evaluate the network's ability to extrapolate and therefore gage the performance of the ANN matrix. The absolute error within the matrix for the output values of the test points ranged from 2.2% to 17% (Table 2.2A).

**A**

| Real Values | | Predicted Values | |
|---|---|---|---|
| [Citrate (mM)] | [Calcium (mM)] | [Citrate (mM)] | [Calcium (mM)] |
| 0.00 | 0.10 | 0.03 +/- 0.01 (3.4%) | 0.12 +/- 0.04 (14%) |
| 0.20 | 0.40 | 0.15 +/- 0.03 (27%) | 0.37 +/- 0.01 (9.5%) |
| 0.40 | 0.15 | 0.347 +/- 0.005 (22.1%) | 0.121 +/- 0.002 (30.1%) |
| 0.60 | 0.20 | 0.56 +/- 0.01 (7.7%) | 0.179 +/- 0.001 (11.5%) |
| 0.80 | 0.35 | 0.769 +/- 0.0005 (4.41%) | 0.037 +/- 0.009 (4.4%) |

**B**

| Vodka | Predicted Values from ANN | | NMR Analysis |
|---|---|---|---|
| Flavor | [Citrate (mM)] | [Calcium (mM)] | [Citrate (mM)] |
| Citrus Twist | 0.98 | 0.72 | 0.90 |
| Orange | 0.31 | 0.21 | 0.44 |
| Vanilla | 1.18 | 0.74 | 1.16 |
| Green Apple | 1.55 | 0.02 | 1.04 |
| Raspberry | 1.37 | 0.11 | 1.30 |

**Table 2.2:** (A) Concentration of citrate (mM) and calcium (mM) in the validation test points samples determined by the two-component sensing system and ANN analysis. The reported values shown are the average value + standard deviation of three measurements with the percent different shown in parenthesis. (B) Concentration of citrate (mM) and calcium (mM) in various flavored Smirnoff ® vodkas determined by ANN and NMR analysis.

Despite the fact that the relative error associated with the output values for each test point was less than 30%, independent verification of the individual citrate concentrations of the unknowns reported for the flavored vodka samples was carried out by other techniques. Given the good correlation between citrate and Ca(II) found in Table 2.2, the focus here is on one component for verification: citrate. The amount of citrate present in each flavored vodka sample was accomplished by a NMR analysis. As shown in Table 2.2B, verification of citrate concentrations by NMR gave values with a percent difference ranging from 1.7% for the vanilla flavor to 33% for the green apple flavor. These values are in good agreement, but it is believed that increasing the number of spectra obtained for the training matrix would improve the accuracy and reduce the error of the

methodology presented here. In addition, it was observed that the values reported by both the ANN and the NMR methods indicate a trend of increasing citrate concentrations in the vanilla, green apple, and raspberry flavored vodkas compared to the orange and citrus twist flavors.

In conclusion, the combination of indicator-displacement assays and a synthetic host with pattern recognition algorithms generates a useful sensing strategy. Also, we successfully extended this method to encompass a practical application such as the analysis of commercially flavored vodkas. This detection method demonstrated that concentrations of more than one analyte can be determined in a single analysis without the need for an array or sophisticated instrumentation.

## 2.4 Summary

The competitive indicator method has been extended to systems containing both 1:1 and 1:2 molecular complexes. Such competition assays give a facile method of determining the concentration of a target analyte without introducing additional covalent structure in the synthetic receptor. In general, we predict that the use of complexometric dyes that have similar functionalities to that of the analyte of interest can be used to generate many different colorimetric competition assays.

In addition, the application of ANNs to a set of UV-Visible spectra extends the utility of indicator-displacement assays to analyze two analytes with one host and one indicator without the need for an array platform. In conclusion,

sophisticated hosts can be interfaced with different indicators to create simple but powerful sensing systems for the analysis of analytes in aqueous media.

## 2.5 Experimental

### 2.5.1 MATERIALS

All the solvents used in spectrophotometric studies were of spectroscopic grade and purchased from Aldrich. Xylenol orange and methylthymol blue were obtained from Aldrich and used without further purification. The calcium nitrate was obtained from Fisher Scientific and used without further purification. Buffer components were of reagent grade. The synthesis of **2.1** has been previously reported.[92]

### 2.5.2 ABSORPTION STUDIES

The absorption spectra were recorded on a Beckman DU-640 UV/Visible spectrophotometer. All spectrophotometric measurements were done at a constant pH (7.5) in 10 mM HEPES at room temperature (25$^{o}$C). Solutions were measured in a 1.00 cm (3 mL) quartz cuvette. The solvent system employed for all the titration experiments was a 25 % (v/v) water in methanol mixture.

The first set of absorption titrations (adding **2.1** to **2.4** and **2.1** to **2.5**) were performed by keeping the concentration of the indicator constant (55 μM) while varying the concentration of **2.1**. Data obtained from these titrations were used in the determination of affinity constants for **2.1** to **2.4** and **2.1** to **2.5**. The second set of absorption titrations (adding **2.2** to **2.1**:**2.4** and **2.2** to **2.1**:**2.5**) were performed by keeping both the concentration of each indicator **2.4** and **2.5** (55 μM) and **2.1** (1.13 mM) constant, while varying the concentration of **2.2**. Data

obtained from these titrations were used to generate calibration curves for citrate (Table 2.1).

The second set of absorption titrations (generation of the matrix for the ANN) were performed by keeping the concentration of the $H_2$:I solution constant (0.24 mM **2.1** and 0.01 mM **2.4**) and adding both $Ca(NO_3)_2$ and **2.2** in varying concentrations to separate solutions of **2.1**:**2.5**. All solutions were buffered at pH 7.5 with HEPES buffer (10 mM) in 75% Smirnoff Vodka in water (v/v). Nine separate solutions were made that contained 0.5 mL of the $H_2I$ solution, 100 μL of a 10 mM $Ca(NO_3)_2$, and aliquots of a 20 mM Citrate solution brought to a volume of 1.00 mL with the solvent system described above. Next, nine other solutions were prepared in the same manner without the addition of the $Ca(NO_3)_2$ solution. For the "leave-one-out" strategy, four test solutions were prepared to evaluate the network's ability to extrapolate and are shown in Table 2.2.

### 2.4.3 EXTRACTION OF BINDING CONSTANTS

The binding constants of **2.1** to each indicator was determined from the data obtained from the two titration experiments described earlier. The absorbance was recorded at 577 nm for the addition of **2.1** to **2.4** assay and 607 nm for the addition of **2.1** to **2.5** assay. The binding constants were determined form the plot of ($\Delta A/b$) vs. total citrate concentration using Eq. 2.17 where b = 1.00 cm, $[H_i]$ was found using Eq. 2.20, $[I_T]$ is the total indicator concentration (55 μM), $\Delta\varepsilon 1 = \varepsilon_{I:H} - \varepsilon_I$ and $\Delta\varepsilon_2 = \varepsilon_{I:H_2} - \varepsilon_I$. The values used for $[H_i]$ were found by solving Eq. 2.20 in Mathematica 3.0 for each $[H_T]$ known experimentally (0-1.4 mM) and initial estimates of $K_1$, $K_2$, $\Delta\varepsilon_1$, and $\Delta\varepsilon_2$. The values for $\Delta\varepsilon_1$ and $\Delta\varepsilon_2$ for

the **2.1** + **2.4** assay were found to be 2.41 x $10^4$ $cm^{-1}$ $M^{-1}$ and 1.13 x $10^4$ $cm^{-1}$ $M^{-1}$, respectively. The values for $\Delta\varepsilon_1$ and $\Delta\varepsilon_2$ for the **2.1** + **2.5** assay were found to be 2.75 x $10^4$ $cm^{-1}$ $M^{-1}$ and 8.19 x $10^3$ $cm^{-1}$ $M^{-1}$, respectively.

### 2.5.4 EVALUATION OF BEVERAGES

For the UV-Vis citrate assay, sample preparation was dependent on the beverage being analyzed. The tonic water and Sprite® samples were sonicated and the pH of each sample was then adjusted to 7.5 with aqueous sodium hydroxide. The Snapple® fruit drink was filtered. This solution was then brought to a pH of 7.5 with additions of aqueous sodium hydroxide. An aliquot (25.0 mL) of each beverage sample was lyophilized to remove the water. The residue was then re-dissolved in 25% (v/v) water in methanol (10.0 mL). An aliquot (300 μL) of this beverage solution was added to the sensing ensemble (55 μM **2.4** or **2.5** and 1.13 mM **2.1**) and brought to a total volume of 2.00 mL. Then subsequent portions of this solution (10-200 μL) were added to the sensing ensemble (1.00 mL). An absorbance value was recorded for each addition and the corresponding citrate concentration value was obtained from the calibration curve (Figure 2.8). The final values reported in Table 2.1 were obtained by multiplying the value determined from the calibration curve by the dilution factor.

For the analysis of flavored vodkas, sample preparation proceeded by taking an aliquot (25.0 mL) of each flavored vodka and evaporating any ethanol. To each residue, 100 mL of deionized water was added and each sample was lyophilized to remove the water. The residue was then dissolved in 25% (v/v) water in vodka (5.0 mL). An aliquot (100 μL) of this beverage solution was

added to the sensing ensemble (0.2 mM **2.1** and 0.01 mM **2.4**) and brought to a total volume of 1.00 mL. An absorbance value was recorded three times for each sample and the corresponding citrate concentration and calcium values were obtained from the matrix (Table 2.2). The final values reported in Table 2.2 were obtained by multiplying the value determined from the ANN by the dilution factor.

### 2.5.6 NEURAL NETWORK PROCESSING

Processing of the UV-Vis measurements was accomplished using Statistica Artificial Neural Network software (version 5.5) for the multi-layered perceptron MLP analysis. No pre-processing of the data was attempted.

# CHAPTER 3: DIFFERENTIAL RECEPTORS CREATE PATTERNS DIAGNOSTIC FOR NUCLEOTIDE PHOSPHATES

## 3.0 Introduction

In recent years, approaches to chemical sensing have been shifting towards the development of devices capable of simultaneous detection of multiple analytes rather than single analyte sensors.[75,78,79,110,111] In the previous chapter, indicator-displacement assays were shown the ability to create mulitanalyte sensing schemes without the use of an array platform. Another application for the indicator-displacement assay is discussed here in the context of a multi-component sensing array device.

In this regard, a resin-bound library of receptors is integrated into a multicomponent sensing device. Optimization of the experimental conditions necessary for successfully signaling the presence of various nucleotide phosphates in solution using an indicator-displacement assay is discussed. Specifically, each chemosensor is placed into a micromachined cavity within a silicon wafer, and the optical changes observed by a charged-coupled device (CCD) result in near-real-time digital analysis of solutions. Also, the application of principal component analysis (PCA) to quantitatively compare the data sets from each analysis is presented. In summary, a multi-faceted approach was used to develop a combinatorial sensor system capable of sensing biologically relevant phosphates.

## 3.1 Development of Combinatorial Receptors for Nucleotide Phosphates

The Anslyn, McDevitt, and Shear groups have exploited the use of resins modified with known chemical indicators [81], enzymes[85], and immunoglobulins[84] to detect many analytes in complex fluids within the array platform. In one approach, a combinatorial library of resin-bound receptors was developed in an effort to combine the University of Texas sensor array technology with the power of combinatorial chemistry[97]. Based on these studies, adenosine 5'-triphosphate (ATP) was chosen as the target analyte for proof of principle and potential applications in medical diagnostics and microbiology.

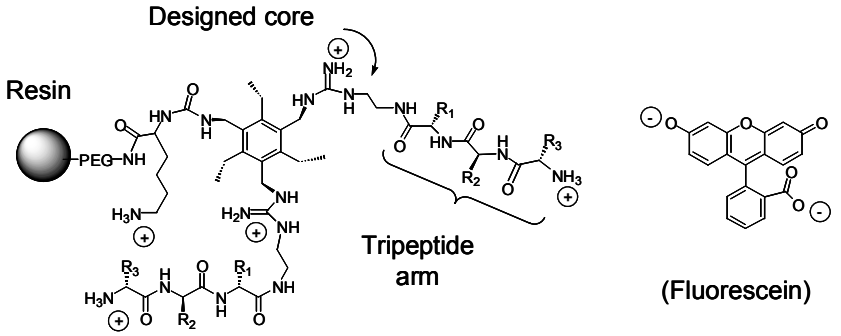


**Scheme 3.1:** General molecular structure of combinatorial resin-bound receptor library (**3.1**) and fluorescein (**3.2**) used to sense for nucleotide phosphates in the array platform.

The design of the anchored receptor (**3.1**) includes a 1,3,5-trisubstituted-2,4,6-triethylbenzene scaffold coupled with peptide libraries (Scheme 3.1). The scaffold was linked to the resin bead via a urea linkage to a lysine. The scaffold

places adjacent groups alternating up and down with respect to the plane formed by the benzene ring, creating a preorganized cavity for binding interactions.[66,112] This scaffold also possesses two guanidinium groups to impart an affinity for nucleotide triphosphates and these guanidiniums are appended with tripeptides to incur differential binding properties. At neutral pH, nucleotide phosphates are anionic and are expected to bind to these cationic resin-bound receptors. The split-and-pool method[27] that was used to generate the combinatorial library of sensors gave a maximum of 4913 possible tripeptides.

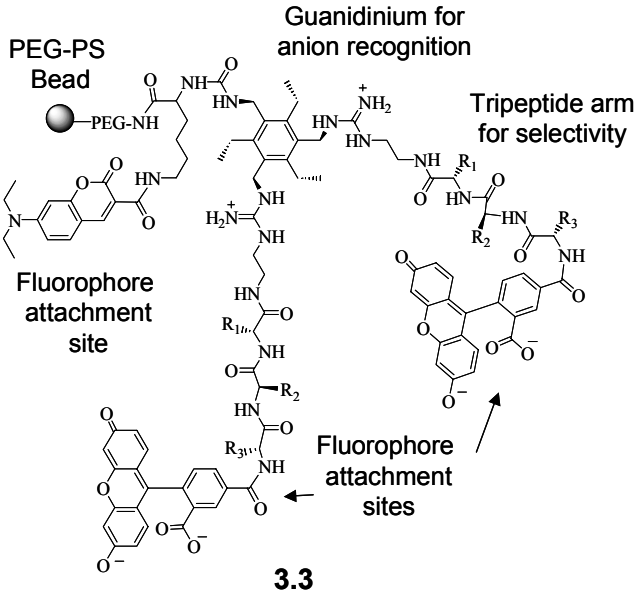


**Scheme 3.2:** General molecular structure of initial combinatorial resin-bound receptor library with attached fluorphores (**3.3**) used for screening and conventional fluorometer studies of nucleotide phosphates.

The previous screening of the library (**3.3**) against ATP and sequencing the "hits" led to the identification of tripeptide sequences that were good

candidates for binding the target analyte. Fluorescently labeled N-methylanthraniloyl-ATP (MANT-ATP) was used to screen the combinatorial library of receptors (**3.3**) for members that were selective for ATP.[97] Approximately 15% of the library members were found to bind MANT-ATP to varying degrees. Several of the highly fluorescent sensors ("hits") and a few of the nonfluorescent sensors ("misses") were removed and sequenced. From the sequencing results, three members that were fluorescent and one member that was not fluorescent were arbitrarily chosen for resynthesis in bulk quantities. These sensors (**3.3)** shown in Scheme 3.2 also included the addition of an attached 5-carboxyfluorescein molecule at the end of the tripeptide arms to be used in further fluorescent studies.

Fluorescent studies were done in a conventional fluorometer using a "monolayer" of beads of one member (Ser-Tyr-Ser) in the **3.3** library to study the stoichiometry and affinity constant of these sensors with various nucleotide phosphates.[97] The monolayer consists of a thin layer of beads sandwiched between two layers of gold mesh on a glass slide. An increase in the emission of fluorescein was observed upon binding of ATP (Figure 3.1). A binding constant of $3.4*10^3$ $M^{-1}$ was calculated from these studies.[97] A large spectral response was observed upon addition of ATP compared to that of adenosine 5'-monophosphate (AMP) and guanosine 5'-triphosphate (GTP) in a sulphonate (4-(2-hydroxyethyl)piperazine ethanesulfonic acid-*N*-(2-hydroxyethyl)piperazine-*N*'-(2-ethanesulfonic acid)) or HEPES buffer at pH 7.4. These results suggest that selected members of the **3.3** library are responsive to nucleotide phosphates.

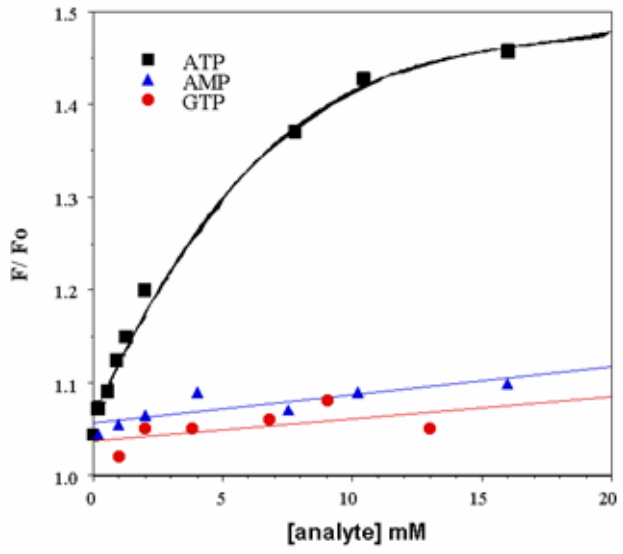


**Figure 3.1:** Isotherm plots of the Ser-Tyr-Ser library (**3.3)** member in 200 mM HEPES buffer solution at pH 7.4. Comparison of fluorescence response to additions of ATP, GTP, and AMP solutions shows **3.3** selectivity of ATP over the other phosphates.[97]

Earlier, it was postulated that this combinatorial library of receptors biased toward a class of analytes would be effective in an array setting. To this end, a library of chemosensors (**3.1**) was integrated into a chip-based array platform in order to develop a more versatile strategy for characterizing nucleotide phosphates in aqueous solutions.[81,82] The objective of this dissertation work is to determine whether the patterns generated by a library of receptors in an array can discriminate between structurally similar compounds like ATP and GTP.

## 3.2 Array Platform Studies

### 3.2.1 Selection of Indicator and Experimental Conditions

As mentioned earlier, the optical assay envisioned was an indicator-displacement assay between the resin-bound receptor and an anionic dye molecule. Fluorescein (**3.2**) was chosen because it has been proven successful in earlier studies[97] with a similar library of receptors (**3.3**), and it is commercially available. It possesses a carboxylate and phenol on the xanthene ring that is known to change color with protination state.[113] Since this probe is a pH indicator, all solutions were buffered with HEPES at pH 7.5. At this pH, it was expected that the fluorescein would be present in its dianionic form and associate in some fashion with the cationic resin-bound receptor resulting in a color change to each resin bead. Introduction of ATP to the sensing ensemble would disrupt this association and, upon formation of an ATP-receptor interaction, cause a measurable color change (Figure 3.2). In other words, sensing of nucleotide phosphates will be accomplished with indicator-displacement assays by optically monitoring intensity changes in the signal of the dye molecule as the analyte binds.

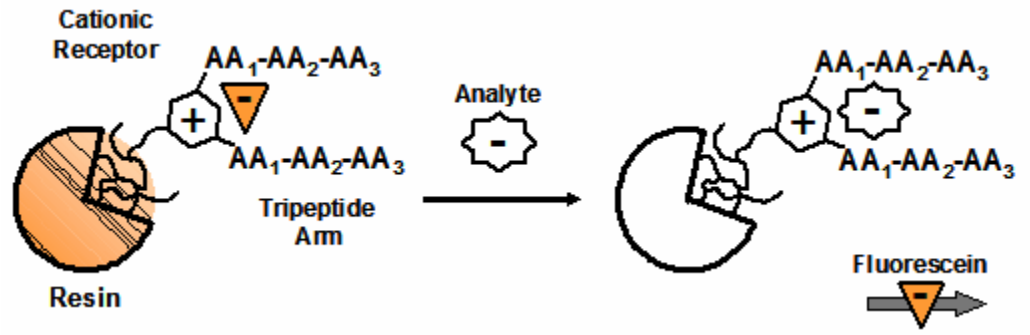


**Figure 3.2:** Signal transduction scheme used to detect nucleotide phosphates within the resin-bound sensor (**3.1**). $AA_n$ = amino acid.

To explore the feasibility of the dye displacement assay, a series of experiments were completed using a variety of different experimental conditions. All optical measurements are done colorimetrically using bright-field microscopy in order to avoid difficulties associated with epi-fluorescence measurements. Despite the fluorescent nature of fluorescein, the dye is used as a colorimetric indicator in these studies. Local concentrations of dye in the bead interior leads to high effective loading levels allowing for the completion of absorbance based measurements.

### 3.2.2 ASSAY OPTIMIZATION

There are several important issues to consider in the development of a new sensing protocol for a library of receptors (**3.1**) attached to solid supports. In order to sense for nucleotide phosphates, the anchored receptors (**3.1**) should undergo reversible and selective binding of the analyte. The optical changes that result due to the association of **3.2** to the anchored receptor (**3.1**) are determined, and the mechanisms associated with the binding of nucleotide phosphate and dye

to the receptor on the resin is also rationalized. Hence, a series of experiments are outlined throughout this section in order to investigate these scientific questions.

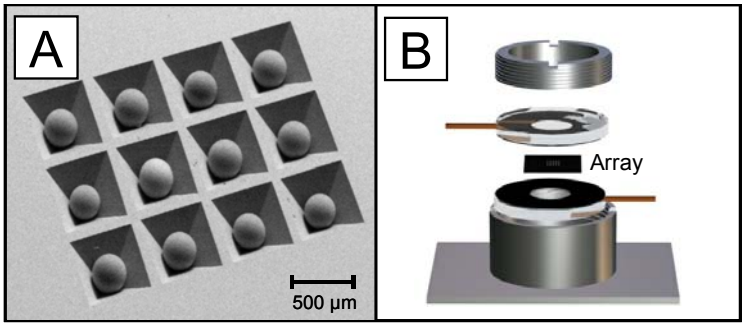


**Figure 3.3:** (A) Scanning electron micrograph of representative 3 x 4 microarray containing glass beads.[114] (B) Design of flow cell used in experiments.

Since the library of resin-bound receptors (**3.1**) had 4913 unique members, each parameter investigated within the array used a 7 x 5 array platform to maximize the number of candidates screened in each experiment. A scanning electron micrograph of a representative 3 x 4 array platform is shown in Figure 3.3A. Sample delivery to the chemosensors occurs using a previously described flow cell.[81] A schematic of the flow cell is shown in Figure 3.3B. The sample is introduced over the array and passes around and through the beads to exit the bottom of the wells. Red, green, and blue (RGB) transmitted light intensity values are recorded for each bead in the array over the period of the assay via a CCD. "Effective absorbance" values for each color channel can then be calculated according to Beer's Law (Eq. 3.1).

$$A = -\log \frac{I}{I_o} \qquad \text{Eq. 3.1}$$

Included in each experiment within the array are five control beads that consist of the same matrix as those used in the synthesis of **3.1** (TentaGel-$NH_2$) and were chemically derivatized with acetic anhyride (**3.4**) and 5-carboxyfluorescein (**3.5**). With this arrangement, the acetylated resins (**3.4**) function as blanks and the fluorescein-appended resins (**3.5**) allow for the pH of the solutions passing through the flow cell to be monitored.

First, the binding properties of **3.2** to **3.1** were investigated. This was accomplished by randomly choosing thirty beads from the series of receptors (**3.1**), three blank beads (**3.4**), and two resin-bound fluorescein beads (**3.5**) and placing them into the microarray (Figure **3.4A**). A 0.03 mM solution of **3.2** was introduced into the array with the eluting buffer (25 mM HEPES pH 7.5) at 1 mL/min. The CCD camera recorded the dye solution passing through the array for 12 min. Since the $\lambda_{max}$ for fluorescein lies within the blue channel region, "effective absorbance" values ($A_B$) were calculated using Eq. 3.2 (See Experimental).

$$A_B = -\log \frac{I_B}{I_{B_o}} \qquad \text{Eq. 3.2}$$

Figure 3.4B is a graphical representation of the images collected by the CCD camera during this experiment. This plot demonstrates that the library of receptors (**3.1**) associate with **3.2** to varying degrees. Blank beads (bead #1 in Figure 3.4B) developed little or no orange color indicating that the dye did not associate within the matrix of the bead through hydrophobic effects. Fluorescein beads (**3.5**) remained unchanged throughout the assay indicating that the pH remains constant (data not shown). It is also interesting to note that beads with

faster rates of dye uptake do not necessarily retain or associate with more fluorescein (or have a higher $A_B$ value). These observations are consistent with the presence of some amount of chemical diversity associated with each member within the **3.1** library.

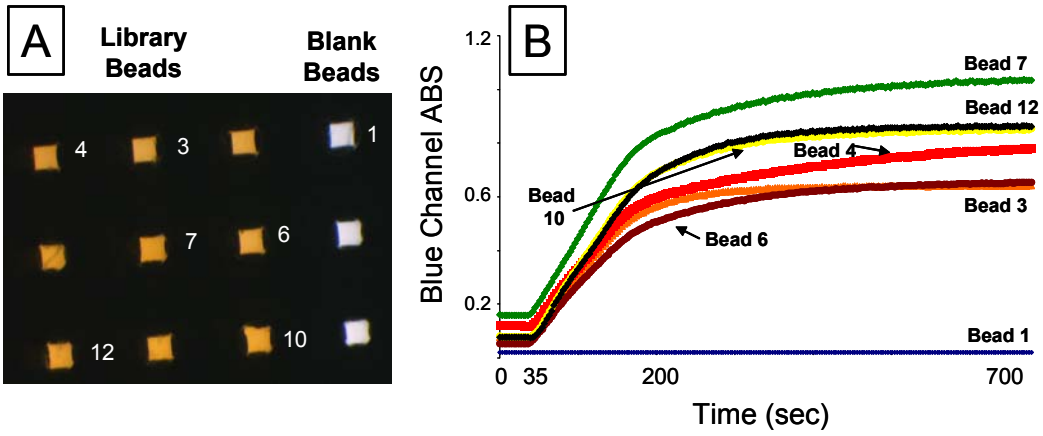


**Figure 3.4:** Differential dye (**3.2**) binding to the library of receptors (**3.1,** Beads 3, 4, 6, 7, 10 and 12). (A) Representative image of the chemosensors studied within the array after a solution of 3.2 was introduced. (B) Graphical representation of the data taken by the CCD camera upon an injection of 0.03 M solution of **3.2** to the array of beads with eluting 25 mM HEPES buffer at pH 7.5. (Bead #1 (**3.4**) took up little or no dye.)

Ultimately, it was envisioned to be able to compare the responses of one resin-bound member of the library (**3.1**) to different nucleotide phosphates. In order to obtain any relevant statistical information from these types of experiments, a way of reproducibly returning each chemosensor to the same "zero point" or baseline for repeated analysis needed to be determined. This was

accomplished through the removal of the residual dye after data extraction for a set time period (5 min) by flowing a 30 mM sodium hydroxide solution over the array containing the dye-loaded beads at a flow rate of 1mL/min so that charge pairing between the dye (or the analyte) and the receptor would be disrupted, thus allowing these compounds to be removed from the bead. Next, a small amount (2.0 mL at a flow rate of 1mL/min for 5 min) of 10 mM hydrochloric acid would be introduced to the array of beads with eluting buffer in an attempt to return the microenvironment close to the original value. Finally, the original flowing buffer (pH = 7.5) was reintroduced into the flow cell.

At this point, studies on the reproducibility of indicator uptake were performed. Although the relative concentration of receptors on each bead is unknown,[115] it is only required for the purposes of the displacement assay that the same absorbance value result within each library bead upon introduction of **3.2** from trial to trial. On a molecular level, one can consider each library bead as a single receptor with ***n*** binding sites. Hence, experiments were designed to test the reproducibility of the **3.1**:**3.2** association by introducing various concentrations of fluorescein in 25 mM HEPES (pH 7.5) to an array containing the resin-bound library of receptors (**3.1**).

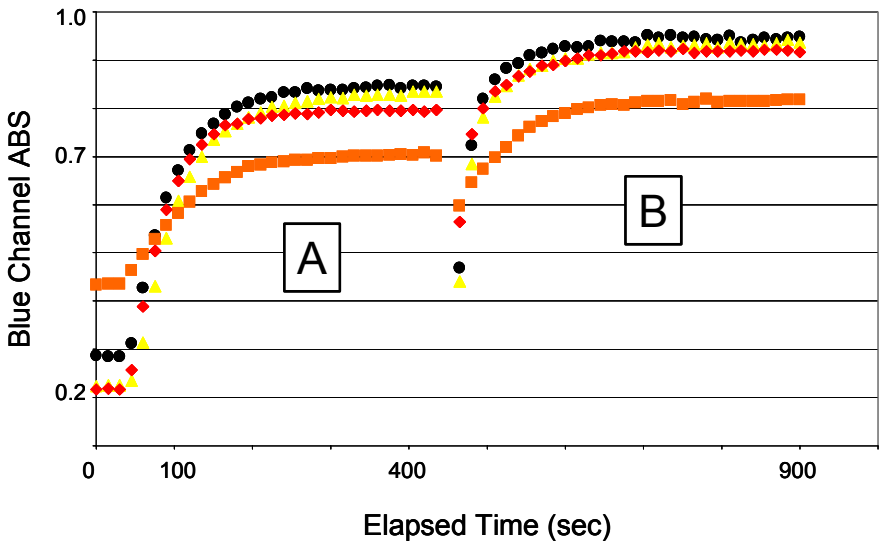


**Figure 3.5:** Absorbance values plotted over time for an array containing four members of **3.1** library in eluting 25 mM HEPES buffer at pH 7.5. (A) Addition (2.0 mL pulse) of **3.2** solution at 0.30 mM. (B) Addition (2.0 mL pulse) of **3.2** solution at 3.0 mM.

Two separate absorbance plots of a dye pulse introduced into an array of library beads over time at two different concentrations are shown in Figure 3.5. After testing several different concentrations of dye solutions, it was determined that one pulse of dye at a concentration of 0.3 mM in 25 mM HEPES (pH 7.5) at the flow rate of 1.0 mL/min gave the most reproducible regeneration of color from trial to trial for each bead compared to itself. A second 2.0 mL pulse of the dye at the same concentration was integrated into the assay protocol to insure saturation of all the binding sites on the receptor. This establishes a stable signal in the presence of eluting buffer in repeated trials and maximizes the dynamic range with which to work. As shown in Figure 3.5B, a dye pulse at a concentration of 3.0 mM into the array of library beads caused a significant

increase in absorbance values. Unlike in previous dye uptake studies, there was no noticeable amount of dye removed from the **3.1** library beads by the typical wash sequence. This was reasoned to be the result of exceeding the solubility limit of the sensing ensemble and generating a precipitate.

As emphasized above, one of the primary goals of this effort involves the development of dye displacement assays for discrimination of structurally similar phosphonate analytes using combinatorial-bead arrays. As such, each bead constitutes a new and unknown sensing ensemble whose properties and characteristics differ from neighboring microsensors. To develop practical sensor systems, it is convenient to be able to refresh and re-use chip ensembles so that the reproducibility and discrimination capacity of the array can be deciphered. Further, the definition of the assay conditions that yield the best analytical characteristics much be defined and optimized using a series of sequential trials with the same population of beads.

Table 3.1 illustrates the reproducibility of signal from trial to trial in one experiment for the dye uptake protocol devised for ten **3.1** chemosensors in a microarray. The number reported for each bead is the average of thirty absorbance values calculated from images taken 5 sec apart by the CCD camera of the microarray with eluting buffer at 1mL/min after injection of the two dye pulses under ideal conditions. The variability in the absorbance values for dye uptake ranged from 0.4-6.0% standard deviation over six trials.

| Bead Indext Number | Absorbance Values (Average of 30 images) Trial 1 | Trial 2 | Trial 3 | Trial 4 | Trial 5 | Trial 6 | Average | Standard Deviation (%) |
|---|---|---|---|---|---|---|---|---|
| 1 | 0.822 | 0.716 | 0.719 | 0.704 | 0.714 | 0.725 | 0.733 | 6.0 |
| 2 | 0.845 | 0.845 | 0.843 | 0.839 | 0.837 | 0.841 | 0.841 | 0.4 |
| 3 | 0.844 | 0.817 | 0.819 | 0.814 | 0.821 | 0.837 | 0.825 | 1.5 |
| 4 | 0.852 | 0.833 | 0.832 | 0.833 | 0.840 | 0.853 | 0.841 | 1.1 |
| 5 | 0.827 | 0.812 | 0.812 | 0.805 | 0.812 | 0.818 | 0.814 | 0.9 |
| 6 | 0.826 | 0.824 | 0.826 | 0.823 | 0.830 | 0.842 | 0.829 | 0.8 |
| 7 | 0.840 | 0.833 | 0.832 | 0.827 | 0.832 | 0.852 | 0.836 | 1.1 |
| 8 | 0.837 | 0.814 | 0.815 | 0.810 | 0.815 | 0.825 | 0.819 | 1.2 |
| 9 | 0.848 | 0.848 | 0.848 | 0.846 | 0.850 | 0.859 | 0.850 | 0.5 |
| 10 | 0.857 | 0.847 | 0.851 | 0.852 | 0.857 | 0.869 | 0.856 | 0.9 |

**Table 3.1:** Average absorbance values of ten chemosensor**s** (**3.1**) reported after the dye uptake procedure was executed six times. Absorbance values acquired for each chemosensor was done while eluting 25 mM HEPES buffer (pH 7.5) and a wash sequence was performed before the next set of dye pulses was injected into the microarray.

The ability of this sensing ensemble (**3.1**:**3.2**) to detect the presence of ATP was studied next. An array of beads containing thirty **3.1**, three **3.4**, and two **3.5** chemosensors were placed into the flow cell and studied. Dye uptake proceeded as described above. Following dye loading, the CCD camera was used to take images of the microarray with 25 mM HEPES buffer (pH 7.5) eluting through the flow cell and their time dependent color data was recorded on the computer. Then, a 20 mM ATP sample (in 25 mM HEPES at pH 7.5) is introduced into the array. The array was exposed to this sample for 2 min while the CCD continued to record images of the microarray. Once the sample had exited the flow cell, the buffer continued to elute over the microarray for 5 min. The wash sequence was completed in an attempt to bring the chemosensors back to their original "zero point." The total time for each assay is 30 min.

The assay was repeated three times, and the data extraction and RGB analysis of these trials yields the following plot (Figure 3.6). The absorbance traces seen in Figure 3.6 show that each sensing ensemble (**3.1**:**3.2**) maintains color in the presence of flowing buffer. However, upon injection of ATP, the absorbance values increase initially and then fall off at different rates. This initial increase in color was attributed to a microenvironmental pH change to the fluorescein from the formed association between **3.1** and ATP and subsequent expulsion of the dye molecule from the binding pocket of **3.1**. The disappearance of color from each bead thereafter is rationalized to be the result of the dye molecule, now free from the binding pocket, being washed out of the flow cell by the eluting buffer. Notably, the off rates, or absorbance trace slopes observed from Figure 3.6, for **3.2** from each library bead are reproducibly different. The variability of signal for each individual bead compared to itself from trial-to-trial is less than 5%. The response of the control beads was the same as seen in previous experiments described earlier. Displacement rates, however, quantified by slope measurements vary from bead to bead within an individual trial ranged from by 7.0 – 86.0%.

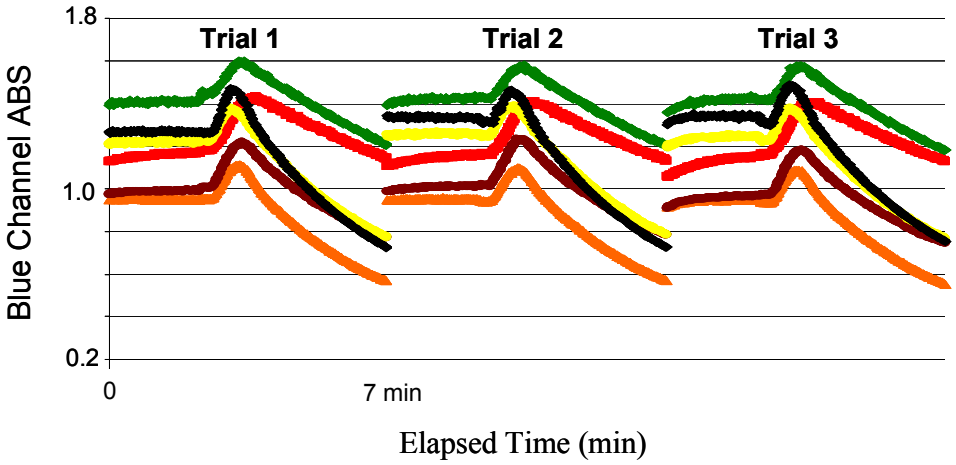


**Figure 3.6:** Absorbance values plotted over time elapsed (7 min) for **3.1**:**3.2** in eluting 25 mM HEPES buffer at pH 7.5 upon successive cycles of dye uptake, 20 mM ATP solution injections, and the wash sequence.

To summarize the conditions used for the dye displacement assays, dye uptake proceeds with a 2.0 mL injection of a 3.0 x $10^{-4}$ M fluorescein dye in a 25 mM HEPES solution at pH 7.5 via the fluid delivery system. A second 2.0 mL injection of the dye solution is introduced to the array in order to more completely load the library bead receptor sites with fluorescein. A buffered solution is allowed then to pass through the flow cell for 5 min in order to achieve a stable initial starting point for the assay. At this time, RGB absorbance data is obtained for each bead in the array. The CCD camera continues to record data as the nucleotide phosphate sample is injected into the array. Data extraction and processing (See Experimental) allows for calculation of the dye displacement rates of each bead after analyte injection. The residual dye within the library beads is rinsed out through a series of basic and acidic solution washes. These

assay conditions allowed for a reproducible method for optically monitoring the uptake and displacement of fluorescein from a combinatorial library of resin-bound receptors towards the detection of various nucleotide phosphonates in solution.

## 3.3 Nucleotide Phosphate Detection

### 3.3.1 BINDING DATA

As mentioned earlier, the purpose of our work is to determine whether the combined signals from a library of receptors in an array can create a fingerprint response that allows for discrimination of structurally similar compounds like ATP, GTP, and AMP. In Section 3.2, many experimental conditions were elucidated and tested in order to develop an assay that would reproducibly generate a **3.1**:**3.2** sensing ensemble that signals the presence of a nucleotide phosphate within the array platform. As seen in Scheme 3.3, the three samples to be studied only vary slightly in structure (i.e. ATP vs. GTP only varies in the type of nucleotide base, and ATP vs. AMP varies by the number of phosphate esters). Here, experiments are described so that the optical responses from the library of receptors upon introduction of these three different samples could be monitored and evaluated.

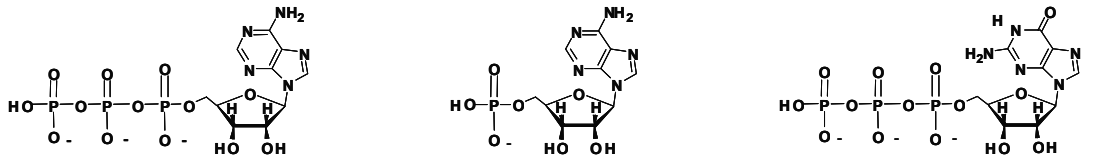

adenosine 5'-triphosphate (ATP)

adenosine 5'-monophosphate (AMP)

guanosine 5'-triphosphate (GTP)

**Scheme 3.3:** Molecular structures of the various nucleotide phosphates studied.

In one experiment, thirty beads from the library were randomly chosen, given an index number, and placed in a micromachined chip-based array platform. The RGB intensity values for the thirty library beads in the array were recorded over time after a 2.0 mL injection of a 20 mM sample of ATP, GTP, or AMP in 25 mM HEPES buffer (pH 7.5). Three trials were performed for each sample for a total of nine trials, and absorbance values were calculated by taking the negative log of the ratio of the blue channel intensity over the red channel intensity for each bead.[81,82] Figure 3.7A shows representative normalized absorbance traces for two of the beads in the array after an injection of GTP. Figure 3.7B shows a trace of the same two beads after an injection of AMP. The range of relative standard deviation for regeneration of signal for each bead trial to trial in this experiment was 1.2 - 2.6%.

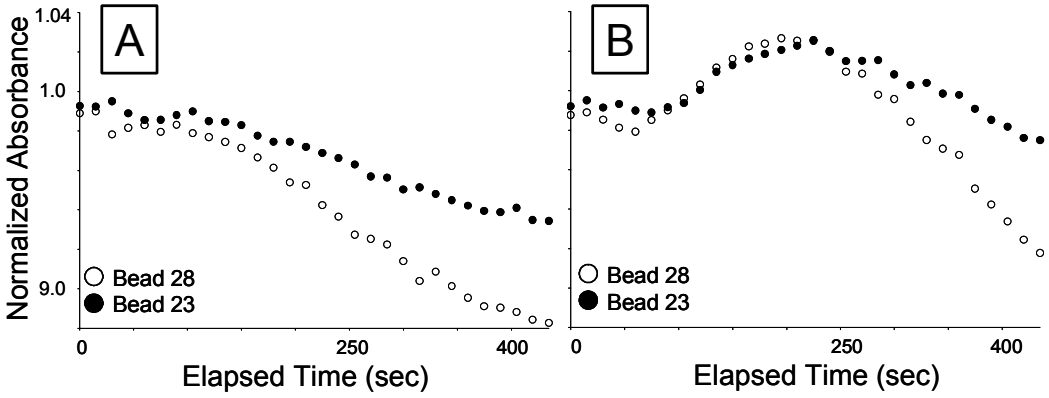


**Figure 3.7:** Absorbance values plotted over time for **3.1:3.2** in eluting 25 mM HEPES buffer at pH 7.5. (A) Addition (2.0 mL pulse) of 20 mM GTP solution in 25 mM HEPES (pH 7.5). (B) Addition (2.0 mL pulse) of 20 mM AMP solution in 25 mM HEPES (pH 7.5). To aid in slope comparison, the plots were shifted so that the average of the initial 30 points prior to sample injection (not shown) had an absorbance of 1.00.

In Figure 3.7, A and B show representative normalized absorbance traces for two of the beads in the array after an injection of GTP and AMP, respectively. The slope of the absorbance values from 210-435 seconds was calculated for each bead in each sample, and these values were used in the analysis because the indicator-displacement rates were found to be most reproducible in this region for comparison. Only two of the thirty beads are displayed in Figure 3.7 and the plots were shifted so that the average of the initial 30 points prior to sample injection (not shown) had an absorbance of 1.00 to help aid in slope comparison. The slope of bead 28 differs by 40% between the AMP and GTP trials. Whereas, the slope value for bead 23 in each plot differs by only 26%. Although these slopes are easily differentiated by qualitative visual inspection, the rates of displacement for

several trials can be compared more quantitatively using pattern recognition algorithms as described below.

### 3.3.2 APPLICATION OF PRINCIPAL COMPONENT ANALYSIS

The method of principle component analysis (PCA) was utilized to reduce the dimensionality of the data set. For each of the nine trials, a slope value was recorded for each of the thirty beads. To identify patterns in the data, a principal component (PC) axis is calculated to lie along the line of maximum variance in the original data. Subsequent PC axes lie along lines describing diminishing levels of variance. The coordinates of the sample relative to the PC axes are termed scores and can be used as an indicator of correlation between analytes. Proximity in space on a score plot directly correlates to similarities in indicator displacement rates. Figure 3.8 shows a two dimensional score plot for the first two principal components (PC1 and PC2) with clustering of the AMP, GTP and ATP samples with one possible ATP outlier. PCA demonstrates that the array of library sensors can differentiate between structurally similar molecules such as AMP, GTP and ATP.

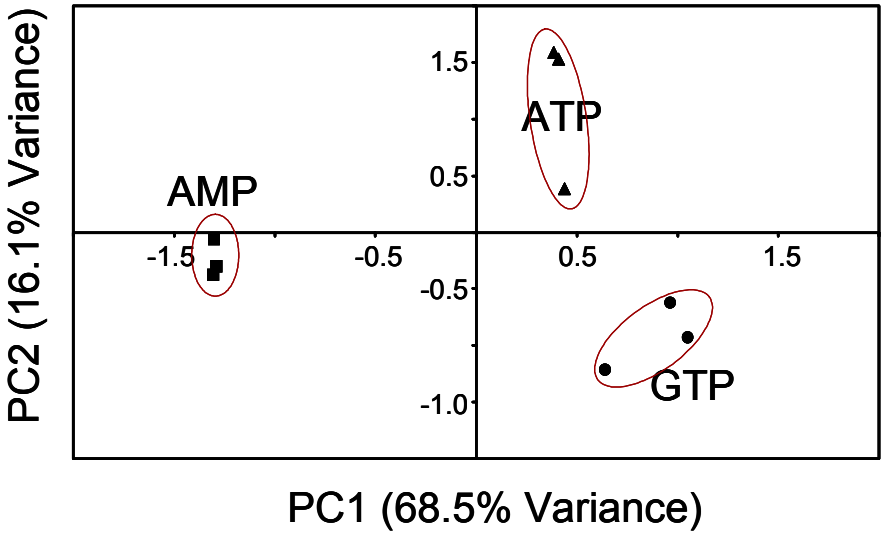


**Figure 3.8:** Principle component analysis plot of the three trials for each nucleotide phosphate sample (▲ATP, ♦GTP, ■AMP). Red circles have no statistical meaning and are only drawn to help aid in sample comparison.

### 3.3.3 SEQUENCING RESULTS

Factor loading values can be used to evaluate the individual sensors in the array. The values correspond to the cosine of the angle between a principal component axis and the original variable axis. Therefore, similar loading values correspond to similar sensor responses. Furthermore, loading values approaching 1 or -1 indicate that the individual sensor played a significant role in the formation of a particular component axis (Figure 3.9).

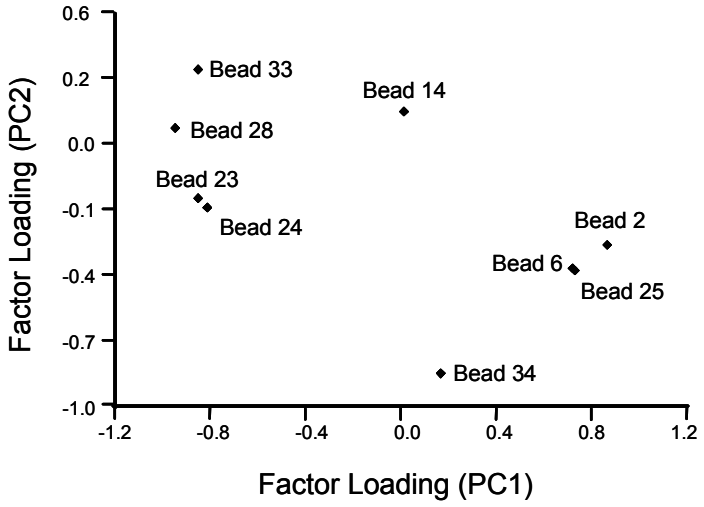


**Figure 3.9:** Factor Loading Plot of the nine library (**3.1**) beads chosen for microsequencing.

Only nine beads were analyzed due to the high cost of peptide microsequencing. Eight beads were chosen to be sequenced on the basis of their large and nearly overlapping factor loading values (Figure 3.9 and Table 3.2). Bead 14, which possessed the lowest values for each PC axis, was sequenced to elucidate which receptors elicit minimal discrimination. It is interesting to note that beads with high loading values possess serine (or the structurally similar amino acid threonine) and other aromatic amino acids, as found in our earlier screening of this library.[97] Since 86% of the beads in the array had a factor loading value with an absolute magnitude greater than 0.7 on PC1, it is thought that the combination of these differential receptors is necessary for analyte discrimination.

| Tripeptide Sequence | Factor Loading (PC1) | Factor Loading (PC2) | Bead Index Number |
|---|---|---|---|
| Asp-Asn-Ser | -0.98 | 0.14 | 28 |
| Phe-Trp-Phe | -0.88 | -0.16 | 23 |
| Thr-Thr-Ser | -0.88 | 0.39 | 33 |
| Val-Asn-Tyr | -0.84 | -0.20 | 24 |
| Val-Pro-Ala | 0.01 | 0.21 | 14 |
| Ala-Met-Thr | 0.17 | -0.91 | 34 |
| Val-Gly-Ile | 0.74 | -0.46 | 6 |
| Ser-His-Tyr | 0.75 | -0.47 | 25 |
| Thr-Thr-Ile | 0.89 | -0.36 | 2 |

**Table 3.2:** Sequencing results and Factor Loading Values for the first two principal components (PC1 and PC2).

Even though statistical analysis of the sequencing results cannot be performed due to the small number of beads analyzed, some conclusions can be drawn for discussion nontheless. In Table 3.3, the amino acids found on each bead and the distribution by position is catalogued. Of the seventeen amino acids used in the synthesis of this library (**3.1**), several amino acids did not appear in sequenced beads: glutamic acid, glutamine, and leucine. The most commonly occurring amino acid was threonine and the two other amino acids (serine and valine).

| | Hydrophilic | | | | | | | Hydrophobic | | | | | | | | Special | |
|---|---|---|---|---|---|---|---|---|---|---|---|---|---|---|---|---|---|
| Amino Acid | His | Asp | Glu | Ser | Thr | Asn | Gln | Ala | Val | Ile | Leu | Met | Phe | Tyr | Trp | Gly | Pro |
| Located on C' | | 1 | | 1 | 2 | | | 1 | 3 | | | | 1 | | | | |
| Located in Middle | 1 | | | | 2 | 2 | | | | | | 1 | | | 1 | 1 | 1 |
| Located on N' | | | | 2 | 1 | | | 1 | | 2 | | | 1 | 2 | | | |
| Total Residues | 1 | 1 | 0 | 3 | 5 | 2 | 0 | 2 | 3 | 2 | 0 | 1 | 2 | 2 | 1 | 1 | 1 |

**Table 3.3.** Amino acid distribution by position.

## 3.4 Summary

A colorimetric displacement assay was performed and time dependent imaging studies of the selected sensing ensembles result in differential responses upon addition of ATP, AMP, or GTP. An advantage to this approach is that it creates an array of sensors that gives a fingerprint response for each analyte. Principal component analysis indicates that the library of chemosensors can differentiate between ATP, GTP and AMP. Based upon factor loading values, individual sensors from the library were sequenced to elucidate their chemical composition.

In conclusion, the use of a combinatorial library of sensors and indicator-displacement assays in the context of a chip-based array allows for the differentiation of structurally similar analytes in aqueous solutions. The coupling of supramolecular chemistry principles with pattern recognition lead to this new protocol for sensing.

## 3.5 Experimental

### 3.5.1 MATERIALS

Triethylamine ($Et_3N$) and dichloromethane (DCM) were refluxed over calcium hydride and distilled when noted. Methanol was obtained from Fisher Scientific. Sure seal anhydrous dimethylformamide (DMF), ATP, acetic anhydride, GTP, AMP, diisopropylethylamine (DIEA), dicyclohexylcarbodiimide (DCC), and fluorescein were obtained from Aldrich and used without further purification. The compound 5(6)-carboxyfluorescein was obtained from Molecular Probes, Inc. (Eugene, OR). The TentaGel amine (TentaGel-$NH_2$) resins (loading of 0.29 mmol/g), and 1-hydroxybenzotriazole (HOBt) were obtained from NovaBiochem. The buffer 4-(2-hydroxyethyl)piperazine ethanesulfonic acid-*N*-(2-hydroxyethyl)piperazine-*N*'-(2-ethanesulfonic acid) (HEPES) was of reagent grade and all buffered solutions were brought to pH 7.5 by adjusting with the addition of sodium hydroxide (NaOH). The synthesis of **3.1** has been previously reported.[81,97]

### 3.5.2 SYNTHESIS OF CONTROL CHEMOSENSORS

*Formation of the Acetylated TentaGel-$NH_2$ resin* (**3.4**). The preparation of compound **3.4** went as follows: 3.0 mL (32 mmol) of acetic anhydride and 57 μL (0.6 mmol) of $Et_3N$ were added to 200 mg of pre-washed TentaGel-$NH_2$ resin (0.29 mmol/g) to react for 1 hr. The acetylated resins were rinsed. The first solution used in these series of rinses was DMF and the last was MeOH. The

ninhydrin test was negative. The resin were dried *in vacuo* for 4 hr and stored at 4°C.

*Formation of the TentaGel-$NH_2$ resin bound 5(6)-carboxyfluorescein* **(3.5).** Under argon**,** 5 mL of anhydrous DMF, 0.05 mg ($1.4x10^{-4}$ mmol) of 5(6)-carboxyfluorescein, 0.29 mg ($1.4x10^{-3}$ mmol) DCC, and 0.19 mg ($1.4x10^{-3}$ mmol) HOBt were combined and allowed to stir for 30 min. In a separate reaction vessel, 200.0 mg (0.06 mmol amine) of TentaGel-$NH_2$ resin was rinsed with the following solutions for 1 min: DMF, MeOH, 10% DIEA in DCM, DCM (twice), MeOH, and DMF. The coupling agent and 0.25 μL ($1.4x10^{-3}$ mmol) of DIEA were added to the pre-rinsed resin and allowed to react for 1 hr. The resin were rinsed three times with DMF and three times with MeOH (or until the color in each wash disappeared) and dried *in vacuo* for 4 hr and stored at 4°C.

### 3.5.3 INSTRUMENTATION

The components of the micromachined array analysis system have been previously described.[81] In short, individually addressable microbeads were placed into chemically etched cavities on a silicon wafer chip. The chip loaded with microbeads was placed into a flow cell. The flow cell was positioned on an Olympus SZX12 stereomicroscope stage that allowed for bottom illumination (transmission) of the microbeads within the array to be observed through the microscope optics. Solutions were introduced into the flow cell using an Amersham Pharmacia Biotech ÄKTA Fast Protein Liquid Chromatograph (FPLC) controlled by Unicorn 3.0 Software. The design of the flow cell allowed for fluids to be introduced to the top of the array and forced down through each

bead-containing well and out through the drain. Optical changes occurring within each bead in the array were observed through the microscope optics and captured for analysis using a charge-coupled device (CCD) in conjunction with Image Pro Plus 4.0 software (Media Cybernetics).

### 3.5.4 ASSAY CONDITIONS

Each assay was performed at room temperature under continuous flow conditions. Indicator uptake proceeded with two cycles of 2.0 mL injections of a 0.30 mM fluorescein dye in a 25 mM HEPES buffer solution at pH 7.5 via the fluid delivery system. To remove excess dye within the beads, the buffered solution was allowed to pass through the flow cell at 1 mL/min for 5 min. At this time, the CCD camera captured an image sequence file and the data was recorded for later analysis. Next, a 2.0 mL nucleotide phosphate sample (20 mM) in a 25 mM HEPES buffer solution at pH 7.5 was injected into the array, and the CCD camera recorded the disappearance of the indicator by the analyte. Finally, the residual indicator within the library beads was rinsed out through a series of basic (30 mM NaOH) and acidic (10 mM HCl) solution washes. The typical standard deviation for regeneration of signal for each bead trial-to-trial ranged in these experiments from 0.2 – 7.0%.

### 3.5.5 DATA COLLECTION AND PROCESSING.

Images of the array captured by the CCD camera were analyzed by drawing areas of interest (AOI) in the central region of each bead and evaluating their average red, green, and blue (RGB) intensities. Prior to the measurements, the CCD imaging protocol was adjusted using a standard white balance

procedure. The library beads in the colorimetric assay developed an orange coloration that was quantified by measuring the average blue pixel intensity yielded by the CCD. This intensity, $I_B$, was converted to the effective blue absorbance, $A_B$, using Beer's Law ($A_B = - \log (I_B/I_R)$), where $I_R$ was the average red pixel intensity for each bead in each image captured by the CCD camera. Statistica Factor Analysis software (version 5.5) was utilized for the principal component analysis (PCA). Blank beads (i.e. acylated Tentagel resins) demonstrated that the indicator did not absorb hydrophobically into the bead matrix.

### 3.5.6 PEPTIDE SEQUENCING

Beads were submitted to the Protein Microanalysis Facility at the University of Texas at Austin for sequencing. A single bead is placed sandwiched between a Zytex membrane and a glass fiber support and inserted into an Applied Biosystems 477A pulsed liquid protein sequencer. The beads are washed with ethyl acetate, dried, and then five cycles of Edman degradation methods are performed.

# CHAPTER 4: DETECTION OF NERVE AGENT DEGRADATION PRODUCTS IN WATER BY A COMBINATORIAL ARRAY SENSOR SYSTEM

## 4.0 Introduction

As described previously, a multi-faceted approach was taken in order to develop a new signaling protocol that coupled a combinatorial library of receptors with a multi-component sensing device. These methods demonstrated proof of concept by using principal component analysis (PCA) to illustrate that a library of chemosensors (**3.1**) can differentiate between adenosine 5'-triphosphate (ATP) and guanosine 5'-triphosphate (GTP) in aqueous solutions. Herein, the capabilities of this combinatorial array sensor system are expanded to characterize other compounds such as hydrolysis products of nerve agents in order to illustrate the general utility of this novel sensing scheme and demonstrate the suitability for potential applications in verification analysis of chemical warfare agents (CWAs).

Of the different types of CWAs, the most lethal are the nerve agents which act on the nervous system by reacting irreversibly with the enzyme acetylcholinesterase.[116] Typically CWAs such as Soman and VX hydrolyze quickly under base; once they have been exposed to water, they decompose to form non-volatile alkyl phosphonic acids (Scheme 4.1). These degradation products are often used as an indirect way of monitoring the presence of CWAs.[117] However, detection of these compounds has proven to be difficult

because they do not contain chromophoric groups for optical monitoring by UV-Visible or fluorescence spectroscopy.

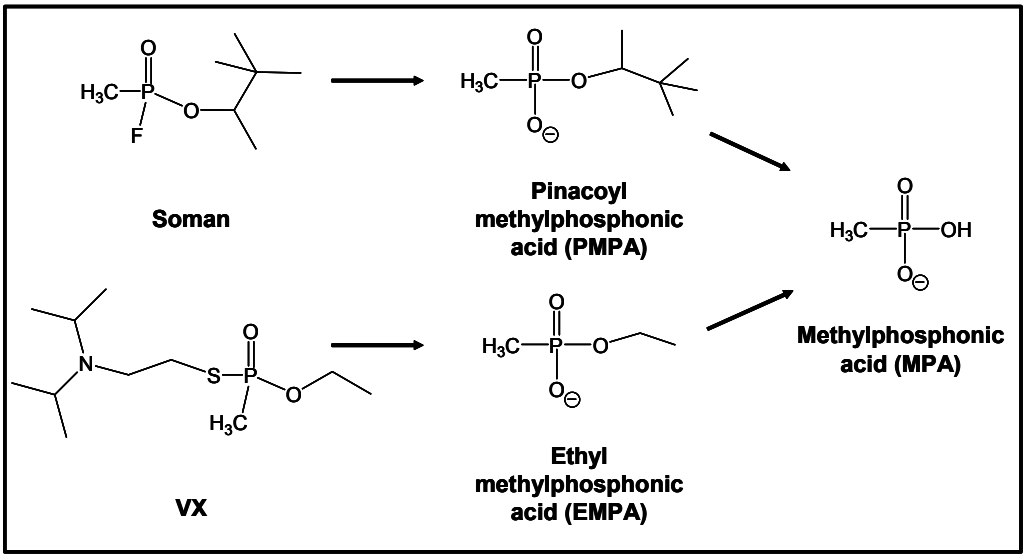


**Scheme 4.1:** Common hydrolysis pathways for some nerve agents in water.

The development of a chip-based multianalyte detection system for different nerve agent degradation products in solution is presented here. First, the synthesis of a new combinatorial library of receptors is described and the studies of these new chemosensors in the array platform are reported in order to help further understand the role of the first series of combinatorial receptors described earlier. A discussion contrasting the chemical diversity of the two different combinatorial receptor libraries will be presented next. Third, studies that lend to an understanding of the sensing protocol mechanism are discussed in the context of redesigning and optimizing the assay conditions toward the successful detection of various phosphonates in solution. Then a more scrutinous approach of analyzing the raw data is taken by applying a series of "filters" or data input

strategies to the raw data and observing how these filters affect the outcome in the PCA. To summarize, the improvements made to the combinatorial array sensing protocol and the data input strategies are implemented to detect nerve agent degradation products in solution within the array platform and used to demonstrate that this sensing scheme is robust.

## 4.1 Evaluating Chemosensor Microenvironments

### 4.1.1 Design and Synthesis of "Control" Resin-Bound Library

Following the successful development and demonstration of a library populated microbead array approach for discrimination of biologically cofactors (Chapter 3), the importance of the scaffolding present in the library of receptors **3.1** in producing such displacement assays was studied. Likewise, the necessity of the rationally designed scaffold in the receptors used in those studies for binding guests also needed to be investigated in order to achieve a more complete understanding of the details of the indicator-displacement assays. To this end, a new resin-bound combinatorial library solely composed of tripeptide chains was synthesized (**4.1**) to serve as a control within chip-based CWA detection system.

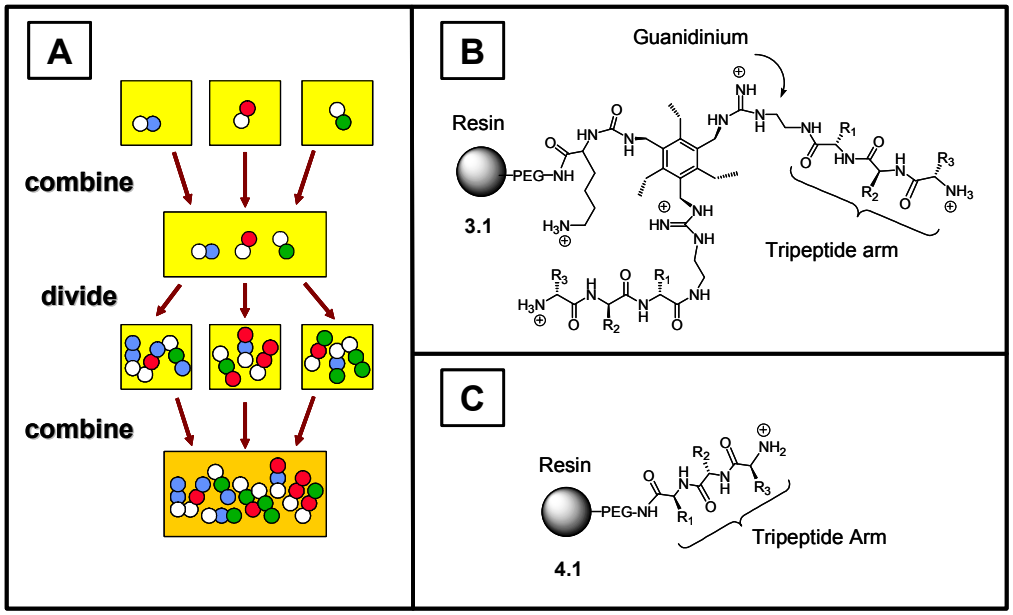


**Figure 4.1:** (A) Schematic summarizing the split and pool method used to generate each library of resin-bound receptors. (B) General molecular structure of receptor library series **3.1**. (C) General molecular structure of "control" resin-bound peptide library **4.1**.

For the preparation of **4.1**, the spit-and-pool method[27] used previously was employed (Figure 4.1A). It is an established method used to generate one-bead, one-compound combinatorial libraries that allows for incorporation of standard solid phase peptide 9-fluorenylmethoxycarbonyl chloroformate (Fmoc) chemistry.[118] With this popular method, oligomeric libraries are quickly generated by coupling aliquots of resin in separate reaction vessels with a single compound, recombining the resin and then dividing the resins again into aliquots for another reaction to another single compound (Figure 4.1A).

The same TentaGel-$NH_2$ resins used in the preparation of the **3.1** library of receptors (Figure 4.1B) were chosen for the synthesis of the **4.1** library. These

resin-bound receptors contained tripeptides consisting of 19 amino acids (cysteine was omitted to avoid the formation of intramolecular disulfide bonds). Solid phase synthesis techniques were used to build each trimer on TentaGel-$NH_2$ resins. A general scheme for the coupling of the amino acids to solid supports is depicted in Figure 4.2.

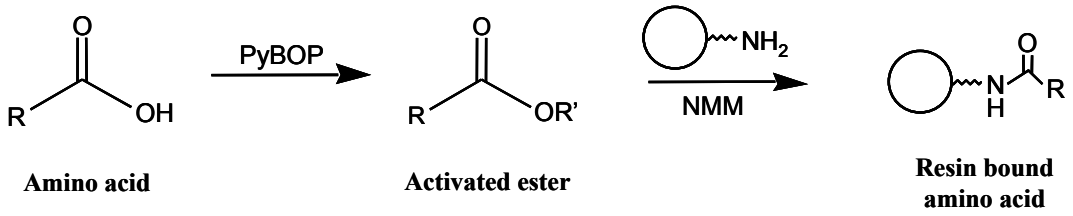


**Figure 4.2:** General synthetic scheme for solid phase synthesis of trimers on TentaGel-$NH_2$ resins.

The synthesis of each tripeptide on the resin began with the reaction of a coupling agent (benzotriazole-1-yl-oxy-tris-pyrrolidino-phophonium hexafluorophosphate, PyBOP) with an amino acid unit to form the activated ester. The α amino group is protected as its Fmoc and the ε amino group protected with an acid labile group (See Experimental). This ester was then reacted with a resin bound amine in the presence of 4-methylmorpholine (NMM) to form an amide linkage to the solid support. At this point a Kaiser test[119] would be performed. All tests were negative (no free amines present) indicating that each coupling had gone to completion. The α-protecting group, Fmoc, was then removed from the anchored amino acid with dilute base (20% piperidine in dimethylformamide). The resins would be recombined, washed, and separated into different reaction vessels where an additional amino acid monomer unit would be added in the same

manner as described above. This process of splitting, coupling, deprotection, and pooling of the resins was repeated twice more. The ε–Boc protecting groups were ultimately removed from the resin-bound trimers under acidic conditions (50% trifluoroacetic acid in dichloromethane). A combinatorial library of 6859 members (the theoretical maximum) was prepared and the general structure of library **4.1** is shown in Figure 4.1C.

### 4.1.2 ARRAY PLATFORM STUDIES

In order to gain a further understanding of how the presence of the receptors on the bead modify the microenvironment of the resin matrix and their effects on the displacement assays, studies were performed utilizing both series of receptor libraries within the array platform. The main components of this array platform are chemically derivatized beads, a silicon microchip, a flow cell, and a charged-coupled device (CCD) camera, all having been described earlier.[81,82]

Studies of the newly synthesized resin-bound receptor library (**4.1**) were conducted within the array platform to elucidate the role that the scaffold present in library **3.1** plays in binding target analytes. To this end, dye uptake studies were performed on an array containing fifteen microsensors from each type of library and the results of five random beads from each library are shown in Figure 4.3. As seen in Figure 4.3A, the ability of members in library series **4.1** to associate with fluorescein varies significantly from bead to bead. For instance, the percent standard deviation for the absorbance values of the beads shown in Figure 4.3A is 113%. Yet, the percent standard deviation is 1.8% for the sensing ensemble **3.1**:**3.2** population (Figure 4.3B.) These observations suggests that the

diversity among the members of library series **3.1** is not as pronounced as the chemistries associated with library series **4.1** due to the significant structural difference between the two types of chemosensors. It also appears that the presence of the scaffold is necessary for every member within a library series to become a viable chemosensor capable of sensing for the analyte of interest. However, it is also true that chemosensors can be derived from screened populations of libraries prepared without the scaffolding structure.

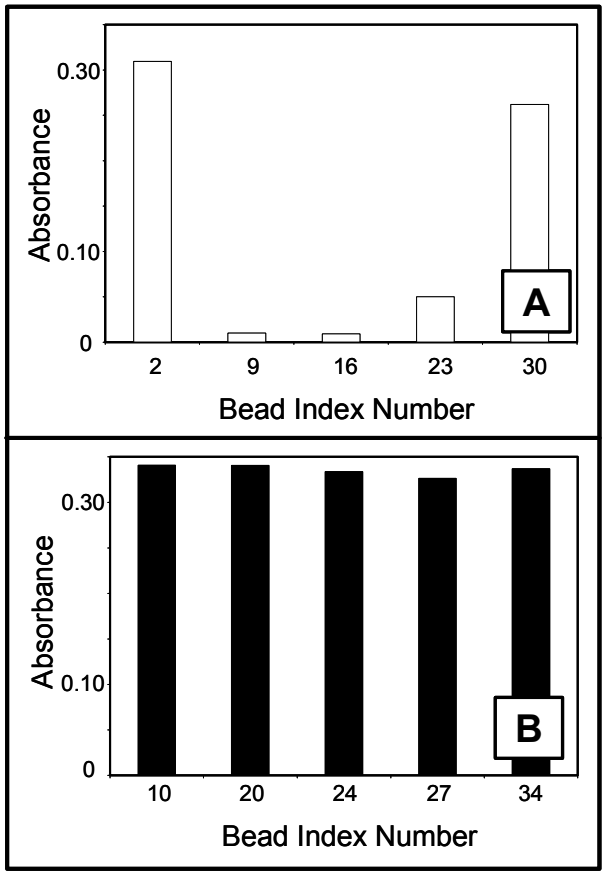


**Figure 4.3:** Dye uptake characteristics of the two different series of combinatorial receptor libraries subjected to identical experimental conditions. (A) Capacity of five random beads selected from library series 4.1 to uptake dye from a 0.30 mM solution of **3.2**. (B) Capacity of five random beads selected from library series **3.1** to uptake dye from a 0.30 mM solution of **3.2**.

### 4.1.3 SEQUENCING RESULTS

Only eight beads were analyzed due to the high cost of peptide microsequencing. These sequences are shown in Table 4.1. Even though statistical analysis of the sequencing results cannot be performed due to the small number of beads analyzed, some conclusions can be drawn for this discussion.

For library series **3.1,** where all members studied within the array possessed the ability to uptake dye, seven hydrophilic and five hydrophobic amino acid residues were present. Even though each member of library series **3.1** demonstrated the ability to associate with the dye to varying degrees, the differences are slight and it follows that the presence of the scaffold plays a dominant role in the binding properties of the receptor where the tripeptide chains incur differential binding characteristics to the receptor only to a lesser degree (Figure 4.3B).

| Binding Pocket | Tripeptide Sequence | Dye Uptake |
|---|---|---|
| Yes | Asp-Asn-Ser | High |
| Yes | Phe-Trp-Phe | High |
| Yes | Thr-Thr-Ser | High |
| Yes | Val-Asn-Tyr | High |
| No | Ala-Ala-Tyr | Low |
| No | Tyr-Phe-Ser | Low |
| No | Gln-Gln-Val | High |
| No | Lys-Gln-Trp | High |

**Table 4.1:** Sequencing results and contrast of the two different series of combinatorial receptor libraries as attributed to the library lacking the binding scaffolding moiety.

On the other hand, the difference in hydrophobic and hydrophilic residues in the library series **4.1** sequence results for members that took up dye readily versus members that exhibited low dye uptake is significant. As shown in Table 4.1, library **4.1** members that did not associate with fluorescein possessed five hydrophobic groups and only one hydrophilic group, serine. With only one

group capable of binding to the fluorescein, it follows that little or no dye was detected in these chemosensors. This is in stark contrast to library **4.1** members that readily took up dye. These members were found to have four hydrophilic residues capable of associating with the anionic dye and two hydrophobic residues. These preliminary conclusions suggest that the chemical diversity attributed to each library series is dependent on the presence of rationally designed scaffold or residues on the peptide chain possessing groups capable of binding a chromophore or analyte.

## 4.2 Nerve Agent Degradation Product Detection

### 4.2.1 ASSAY OPTIMIZATION

In Chapter 3, several experimental conditions were elucidated and tested in order to develop an assay that would reproducibly generate a **3.1:3.2** sensing ensemble that could potentially signal the presence of a nucleotide phosphate in solution within the array platform. The ability of **3.1:3.2** to detect the presence of a representative member of the hydrolysis products of CWAs (i.e. pinacoyl methylphosphonic acid, PMPA) is presented here. This allows for the investigation of whether or not this combinatorial sensor array system can be used for detecting multiple classes of analytes.

Ultimately, it was envisioned that the responses of one resin-bound member (**3.1**) could be compared to different hydrolysis products of CWAs. In Chapter 3, a "zero point" or baseline was established through a series of acidic and basic washes (Section 3.2.2). This procedure had to be altered here because when these washes were used in the assay with the phosphonates, the

chemosensors responded by forming a precipitate within each bead turning them a pinkish-brown color. It was found through a series of experiments that the introduction of strong base into the array was deteriorating the beads and rendering them unusable for subsequent bead-based assays.

This problem was overcome by redesigning the assay to include a different wash sequence. This was accomplished by flowing a 2 M sodium chloride solution over the array containing the dye-loaded beads so that charge-charge screening factors could be used to disrupt the charge pairing between the dye (or the analyte) and the receptor. Next, a small amount (three 2.0 mL pulses) of nanopure water was introduced to the array of beads with eluting buffer in an attempt to reduce the microenvironment's electrolyte concentration back to modest values. This established a stable signal in the presence of eluting buffer in repeated trials.

### 4.2.2 BINDING DATA

An array of beads containing thirty **3.1**, three **3.4**, and two **3.5** chemosensors was placed into the flow cell and studied. Dye uptake proceeded as described earlier (Section 3.2.2). At this time, the CCD data acquisition was initiated to begin taking time dependent images of the microarray with 25 mM HEPES buffer (pH 7.5) eluting through the flow cell. Then, a 20 mM PMPA sample (in 25 mM HEPES at pH 7.5) was introduced into the array. The array is exposed to this sample for 2 min while the CCD continued to record images of the microarray. Once the sample had exited the flow cell, buffer flow was continued so as to elute over the microarray for 5 min. The wash sequence is carried out to

bring the chemosensors to their original "zero point." Likewise, the total time for each assay was 30 min.

The assay was repeated three times, and the data extraction and RGB analysis of these trials yields the following plot. In Figure 4.4, A and B show a representative normalized absorbance trace for four of the beads in the array after an injection of 20 mM PMPA. Upon injection of PMPA, the absorbance values fall off at different rates. The disappearance of color from each bead was rationalized to be the result of the dye molecule, now free from the binding pocket, being washed out of the flow cell by the eluting buffer. Notably, the off rates, or absorbance trace slopes seen in Figure 4.4, for the dye molecule from each library bead are reproducibly different. The variability of signal for each bead from trial to trial is less than 10 %. The response of the control beads was the similar to that seen in previous experiments.

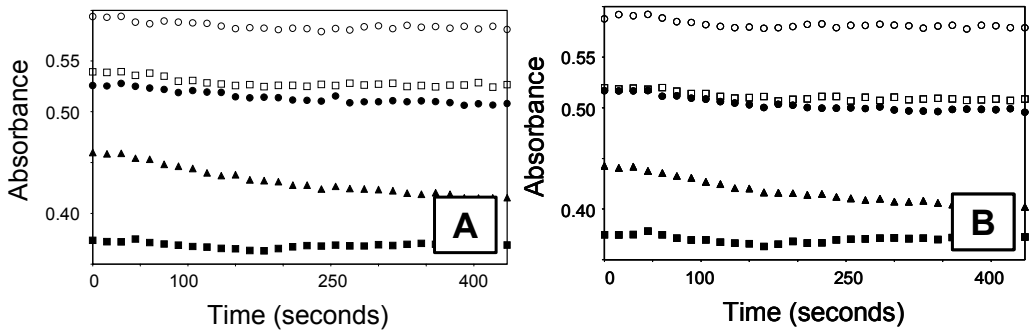


**Figure 4.4:** Absorbance values plotted over time for the **3.2**:**3.1** sensing ensemble in eluting 25 mM HEPES buffer at pH 7.5 upon addition (2.0 mL pulse) of two successive [(A) Trial #1 and (B) Trial #2] 20 mM PMPA solutions in 25 mM HEPES (pH 7.5). (●Bead 3, ○Bead 4, ▲Bead 20, ■Bead 22, □Bead 26)

As seen in Scheme 4.1, the three samples to be studied only vary slightly in structure (i.e. methylphosphonic acid, MPA vs. ethyl methylphosphonic acid, EMPA only vary in the presence of an ethyl ester group.) Here, experiments are described so that the optical responses from **3.1**:**3.2** sensing ensembles upon introduction of three different samples (MPA, EMPA, and PMPA) could be monitored and evaluated. In one experiment, thirty beads from the library were randomly chosen, given an index number, and placed in a micromachined chip-based array platform. The RGB intensity values for the thirty library beads in the array were recorded over time after a 2.0 mL injection of 20 mM samples of MPA, EMPA, or PMPA in 25 mM HEPES buffer (pH 7.5). Also, the array of chemosensors was exposed to the different CWA degradation products by cycling through each type of phosphonate and then repeating each cycle for a new trial to avoid any possible memory effects of the chemosensors. Three trials were performed for each sample for a total of nine trials, and absorbance values ($A_B$) were calculated by taking the negative log of the ratio of the blue channel intensity over the red channel intensity for each bead (See Experimental).

Comparison of the four beads in Figure 4.5 reveals a fingerprint response from the combinatorial sensor system to various CWA degradation products. The distributions of dye-displacement (absolute value of trendline slopes) for four of the beads in the array are shown below. For instance, the average trendline slope of bead 3 for MPA versus EMPA differs by 110 %. Whereas, the percent difference in trendline slope values for bead 20 between MPA and EMPA is only 11 %. As seen in Figure 4.5, each bead reproducibly responds with the same

displacement rate to the same type of sample. Some differences among the samples are visible to the naked eye, however, more subtle differences between samples for each chemosensors response can be extracted through data analysis and application of pattern recognition.

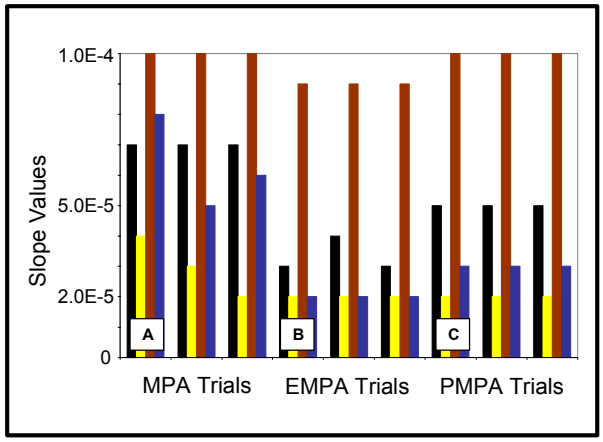


**Figure 4.5:** Graphical representation of multicomponent fingerprint responses yielded by the sensing ensemble ( library series **1**: dye molecule) upon the introduction of (A) 20 mM MPA, (B) 20 mM EMPA, and (C) 20 mM PMPA solution in 25 mM HEPES at pH 7.5. (■Bead 3, ■Bead 4, ■Bead 20, ■Bead 26).

### 4.2.3 DATA INPUT STRATEGIES FOR PRINCIPAL COMPONENT ANALYSIS

As before, the method of PCA was utilized to investigate the relationship between all nine data sets. The spectral data was analyzed using Statistica Factor Analysis software where each data set generates a score. The scores describe the relationship of the original data relative to the rotated principal component (PC) axes where each PC accounts for the variance among samples. Since the PCs characterize the variance among the samples, the scores fully characterize the

relationship between samples. Proximity in space on a loading plot directly correlates to similar spectral responses.

With the integration of PCA for extracting the fingerprint response of each compound analyzed within the array platform,[120] the importance of how the raw data is processed before implementation of PCA becomes significant. In Figure 4.6, input strategy #1 was used to generate the PCA plot presented. Input strategy #1 consisted of areas of interest (AOIs) with a radius of five pixels being drawn at the center of each chemosensor and the RGB signature extracted from each bead for each image taken by the CCD during analyte injection (See Experimental.) At this point, the data would be processed by calculating "effective absorbance" measurements for each image reported by the CCD. The slope of the absorbance values from 30-435 seconds was calculated for each bead in each sample and these values were used for analysis (the first two images taken at time 0-30 are not of the analyte injection). The resulting plot using the raw data (Figure 4.6) shows a two-dimensional score plot for the first two PCs (PC1 and PC2) that account for 93.25% of the variance, but do not demonstrate clearly defined clusters of each CWA degradation product.

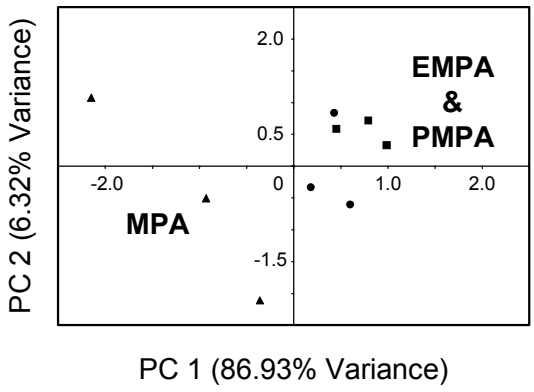


**Figure 4.6:** Principle component analysis plot of three trials for each CWA degradation sample (▲MPA, ■EMPA, ●PMPA) with the raw data inputted into Statistica (input strategy #1).

However, when the same data was treated using a series of preprocessing methods (input strategy #2), a different result is obtained from the PCA. These preprocessing methods applied here serve as a useful means to improve the quality of the data analysis. With this strategy, AOIs with a larger pixel size (10) are drawn at the center of each chemosensor and used to extract out RGB attenuations for "effective absorbance" calculations. The increase in AOI size allows for more information to be catalogued by the computer and reduce the influence of noise somewhat in the data set. Slope values from 30-435 seconds are also calculated using a trendline function and a Q-test is performed on each of the thirty microsensors where the criterion is dictated by the variance in the trendline slope value for each bead within each trial. The rational for applying these data preprocessing strategies is to help average out the errors that may result of localized experimental errors like tiny bubbles underneath the microsensors or slight movements of the microsensors within its cavity. Systematic errors of this

type are minimized with the application of a Q-test. For this case, only four beads of the thirty were removed from the data set due to implementation of the Q-test. Further improvements in experimental design will likely eliminate the need for such preprocessing methods of the raw data.

Figure 4.7 illustrates a two-dimensional score plot for the first two PCs with clustering of MPA, EMPA, and PMPA samples. It should be noted that PC2 explains only 6.01% of the variance; whereas, PC1 explains 88.71% of the variance in Figure 8B. Therefore, the variation along the y-axis is exaggerated by the PC plot. The PCA plot demonstrates visually that the array of library sensors differentiates among structurally similar molecules such as MPA, EMPA, and PMPA.

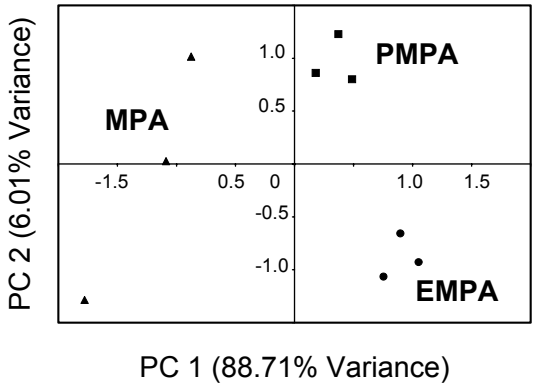


**Figure 4.7:** Principle component analysis plot of three trials for each CWA degradation sample (▲MPA, ■EMPA, ●PMPA) with data input strategy #2.

## 4.3 Summary

By combining a combinatorial library of resin-bound sensors with a multicomponent sensor array, it was demonstrated that an indicator-displacement

assay is suitable for the detection of multiple classes of analytes. Further, dye-uptake experiments allow for near real-time assessment of the efficacy of individual members within the library to successfully sense for different analytes. The ability to extract quickly out members responsive to diverse chemistries is readily accomplished with this methodology.

Specifically, the sensing strategy presented here yielded a CWA detection device capable of differentiating between the structurally similar compounds MPA and EMPA in aqueous solution. The synthesis of a "control" resin-bound peptide library (**4.1**) helped elucidate the role of the scaffold present in the library series **3.1** towards the binding of our target analytes. Improvements were made to this combinatorial array sensing protocol by incorporating new input strategies toward the raw data, resulting in clustering of three trials each of MPA, EMPA, and PMPA. With the technical challenges associated with sensing for CWAs and their degradation products, our CWA detection strategy possesses many characteristics that are favorable for incorporation into a field device.

At present, the CWA detection capacity reported here requires further efforts to improve sensitivity and to expand studies to include a variety of matrices as well as explore common interference effects. Screening of the libraries to define strategic beads having high sensitivity and high selectivity will likely yield dramatic improvements in performance. The development of targeted libraries towards other classes of analytes using resin-bound peptide-based receptors is also currently being investigated. Exciting areas of interest include incorporating library screening techniques to customize microchips for the

detection of arsenates and toxic metals. Other possible investigations could include the development of targeted libraries for other classes of analytes such as sugars using resin-bound peptide-based receptors.

## 4.4 Experimental

### 4.4.1 MATERIALS

The synthesis of **3.1** has been previously reported.[97] Methylphosphonic acid (MPA), ethyl methylphosphonic acid (EMPA), pinacoyl methylphosphonate (PMPA), and fluorescein were obtained from Aldrich and used without further purification. Sodium chloride was obtained from Mallinckrodt. The buffer 4-(2-Hydroxyethyl)piperazine ethanesulfonic acid-*N*-(2-Hydroxyethyl)piperazine-*N*'-(2-ethanesulfonic acid) (HEPES) was of reagent grade.

Solvents used in the synthesis of **4.1** were dichloromethane (DCM), methanol (MeOH), and dimethylformamide (DMF) obtained from Fisher Scientific. The TentaGel-$NH_2$ resins (loading of 0.29 mmol/g) and the coupling agents 1-hydroxybenzotriazole (HOBt) and 2-(1H-Benzotriazole-1-yl)-1,1,3,3-tetramethyluronium tetrafluoroborate (TBTU) were obtained from NovaBiochem. Sure sealed 4-methylmorpholine (NMM), piperidine, 1,2-ethanedithiol (EDT), and triisopropylsilane (TIPS) were obtained from Aldrich and used without further purification.

### 4.4.2 SYNTHESIS OF "CONTROL" RESIN-BOUND LIBRARY (4.1)

The library **4.1** was prepared by the split-and-pool method[118,121] using 19 of the 20 amino acids (cysteine was omitted). Fmoc-protected amino acids were purchased from NovaBiochem and Advanced Chemtech. Side chain protections were as follows: t-butyl ether (Tyr), trityl (Ser, Asn, Gln, Thr), tert butyl ester (Asp, Glu), 4-methyltrityl (His), tert butoxycarbonyl (Lys, Trp), and 2,2,4,6,7-pentamethyldihydro-benzofuran-5-sulfonyl (Arg). Amino acid couplings were carried out on an Argonaut Quest 210 Synthesizer.

The TentaGel-$NH_2$ resins (2.0 g, 0.60 mmol amine) were prepared for synthesis by shrinking the resins in methanol and dividing the resins into 19 equivalent portions. The resins were washed by the following sequence: 2xDMF, 1xMeOH, 2xDCM, and 3xDMF. To each portion 1.0 mL of DMF was added, Fmoc-amino acid (0.16 mmol), HOBt (10.3 mg, 0.76 mmol), TBTU (24.4 mg, 0.76 mmol), and NMN (12.5 μL, 0.76 mmol). The portions were agitated for 1 hr at room temperature. The resins were then washed by the following sequence: 3xDMF, 1xDCM, and 3xMeOH. At this point, Kaiser tests[119] would be preformed on each coupling reaction to validate if the reaction went to completion. All tests were negative (no free amines present) for each coupling indicating that each coupling had gone to completion. The portions of methanol and resins were recombined, filtered, and washed (1xMeOH, 3xDMF). The terminal Fmoc groups were removed with 20% piperidine in DMF for 30 min. This process of splitting, coupling, deprotection, and pooling of the resins was repeated twice more.

After the coupling step in the third cycle, the N-terminal Fmoc groups were removed as previously described. The resins were washed by the following sequence: 3xDCM, 1xMeOH, 1xDMF, and 2xDCM. Peptide side chain protecting groups were removed with TFA, $H_2O$, TIS, EDT, and DCM (94%, 1%, 2%, 2%, 1%) for 1 hr. The resins were then washed (3xDCM and 3xMeOH) dried *in vacuo* for 4 hr and stored at $4^oC$.

In order to verify that the couplings were successful, two members of the library were randomly chosen and submitted for peptide sequencing. The reported sequences were (1) Tyr-Phe-Ser and (2) Thr-Lys-Pro. As expected, each resin bead contained only three detectable amino acid residues.

### 4.4.3 ASSAY CONDITIONS

Each assay was performed at room temperature under continuous flow conditions. Indicator uptake proceeded with two cycles of 2 mL injections of a 0.3 mM fluorescein dye in a 25 mM HEPES buffer solution at pH 7.5 via the fluid delivery system. To remove excess dye within the beads, the buffered solution was allowed to pass through the flow cell at 1 mL/min for 5 min. Then a 2 mL pulse of 30 mM NaOH was introduced into the array and the buffered solution would resume at 1mL/min for a total time elapse of 5 min. At this time, the CCD captured an image sequence file and the data was recorded for later analysis. Next, a 2 mL phosphonate sample (20 mM) in a 25 mM HEPES buffer solution at pH 7.5 was injected into the array, and the CCD camera recorded the disappearance of the indicator by the analyte. Finally, the residual indicator within the library beads was rinsed out through a series of salt (2 M NaCl) and

nanopure solution washes. The typical standard deviation for regeneration of signal for each bead trial-to-trial ranged from 0.8 - 4.0%.

## Final Perspective

Toward the goal of understanding molecular recognition and chemical sensing of solution phase analytes, a novel sensing strategy was developed that coupled the principles of supramolecular chemistry and pattern recognition. Chapter 2 demonstrated this principle by utilizing a synthetic host with indicator displacement assays for the successful determination of citrate and calcium in commercially available beverages using artificial neural networks. The power behind this simple approach is that it creates multi-analyte sensing protocols in the absence of an array setting. In Chapter 3 and Chapter 4, indicator displacement assays were also shown to be useful in a combinatorial sensor array-based system. By incorporating differential sensors into a multicomponent sensor array, a universal approach was established that allowed for the discrimination of various members in two different classes of analytes, namely, nucleotide phosphates and phosphonates, through application of principal component analysis. With this sensing strategy, the potential for high sensitivity, low detection limits, reduction of false positives, short assay times, and minimal consumption of reagents exists as demonstrated in previous reports utilizing the "electronic tongue" detection platform. Overall, the principle studies in this dissertation have provided a foundation that may make the utility of the signaling strategies presented herein promising towards even greater achievements in differential sensing.

## References


1. Delaage, M. *Molecular Recognition Mechanisms*, (VCH Publishers, New York, 1993).

2. Dougherty, D.A. Cation-pi interactions in chemistry and biology: A new view of benzene, Phe, Tyr, and Trp. *Science* **271**, 163-168 (1996).

3. Tanford, C. *The Hydrophobic Effect: Formation of Micelles and Biological Membranes*, (Wiley and Sons, New York, 1980).

4. Adam, D.S., P.; Simmerer, J.; Haussling, L.; Siemensmeyer, K.; Etzbach, K. H.; Ringsdorf, H.; Haarer, D. Fast Photoconduction in the Highly Ordered Columnar Phase of a Discotic Liquid Crystal. *Nature* **371**, 141-143 (1994).

5. Sharp, K.A., Nicholls, A., Fine, R.F. & Honig, B. Reconciling the Magnitude of the Microscopic and Macroscopic Hydrophobic Effects. *Science* **252**, 106-109 (1991).

6. Williams, D.H.S., M. S.;. An Approach to Molecular Recognition Based on Partitioning of Free Energy Contributions. in *Molecular Recognition: Chemical and Biological Problems II* (ed. Roberts, S.M.) 20-29 (Royal Society of Chemistry, Cabridge, 1992).

7. Lehn, J.M. Supramolecular Chemistry Scope and Perspectives - Molecules Supermolecules Molecular Devices. *Journal of Inclusion Phenomena* **6**, 351-396 (1988).

8. Pedersen, C.J. The Discovery of Crown Ethers. *Science* **241**, 536-540 (1988).

9. Dietrich, B.L., J. M.; Sauvage, J. P. Diaza-Polyoxa-Macrocyclic and Macrobicyclic Compounds. *Tetrahedron Letters*, 2885-2888 (1969).

10. Sessler, J.L. & Allen, W.E. Anion carriers: New tools for crossing membranes. *Chemtech* **29**, 16-24 (1999).

11. Ikeda, A. & Shinkai, S. Novel cavity design using calix n arene skeletons: Toward molecular recognition and metal binding. *Chemical Reviews* **97**, 1713-1734 (1997).

12. Jasat, A. & Dolphin, D. Expanded porphyrins and their heterologs. *Chemical Reviews* **97**, 2267-2340 (1997).

13. Khan, A.R., Forgo, P., Stine, K.J. & D'Souza, V.T. Methods for selective modifications of cyclodextrins. *Chemical Reviews* **98**, 1977-1996 (1998).

14. D'Souza, V.T. & Lipkowitz, K.B. Cyclodextrins: Introduction. *Chemical Reviews* **98**, 1741-1742 (1998).

15. Buhlmann, P., Nishizawa, S., Xiao, K.P. & Umezawa, Y. Strong hydrogen bond-mediated complexation of H2PO4- by neutral bis-thiourea hosts. *Tetrahedron* **53**, 1647-1654 (1997).

16. Verboom, W., Rudkevich, D.M. & Reinhoudt, D.N. Molecular Recognition by Artificial Receptors. *Pure and Applied Chemistry* **66**, 679-686 (1994).

17. Spivak, D.S., Kenneth J. Molecular Imprinting of Carboxylic Acids Employing Novel Functional Macroporous Polymers. *Journal of Organic Chemistry* **64**, 4627-4634 (1999).

18. Turiel, E.M.-E., Antonio ; Fernandez, Pilar ; Perez-Conde, Concepcion ; Camara, Carmen. Molecular recognition in a propazine-imprinted polymer and its application to the determination of triazines in environmental samples. *Analytical Chemistry* **73**, 5133-5141 (2001).

19. Sreenivasan, K. Effect of the type of monomers of molecularly imprinted polymers on the interaction with steroids. *Journal of Applied Polymer Science* **68**, 1863-1866 (1998).

20. Mayes, A.G.A., Lars I. ; Mosbach, Klaus. Sugar binding polymers showing high anomeric and epimeric discrimination obtained by noncovalent molecular imprinting. *Analytical Biochemistry* **222**, 483-488 (1994).

21. Meng, Z.H. & Qin, L. Determination of degradation products of nerve agents human serum by solid phase extraction using molecularly imprinted polymer. *Analytica Chimica Acta* **435**, 121-127 (2001).

22. Toshifumi, T.D., F.; Matsui, J. Combinatorial Molecular Imprinting: An Approach to Synthetic Polymer Receptors. *Analaytical Chemistry* **71**, 285-290 (1999).

23. Ye, L. & Mosbach, K. Molecularly imprinted materials: towards the next generation. *Materials Research Society Symposium Proceedings 723*, 51-59 (2002).

24. Van Wageningen, A.M.A. & Liskamp, R.M.J. Solution phase combinatorial chemistry using cyclotriveratrylene-based tripodal scaffolds. in *Tetrahedron Letters 40* Vol. 52 9347-9351 (1999).

25. Furlan, R.L.E., Ng, Y.-F., Otto, S. & Sanders, J.K.M. A New Cyclic Pseudopeptide Receptor for Li+ from a Dynamic Combinatorial Library. *Journal of the American Chemical Society* **123**, 8876-8877 (2001).

26. Berkessel, A. & Herault, D.A. Discovery of peptide-zirconium complexes that mediate phosphate hydrolysis by batch screening of a combinatorial undecapeptide library. in *Angewandte Chemie, International Edition* Vol. 38 102-105 (1999).

27. Furka, A., Sebestyen, F., Asgedom, M. & Dibo, G. General-Method for Rapid Synthesis of Multicomponent Peptide Mixtures. *International Journal of Peptide and Protein Research* **37**, 487-493 (1991).

28. Cheng, Y.S., Toshiro; Still, W. Clark. Sequence-Selective Peptide Binding with a Peptido-A,B-trans-steroidal Receptor Selected from an Encoded Combinatorial Receptor Library. *Journal of the American Chemical Society* **118**(1996).

29. Boyce, R.L., Ge; Nestler, H. Peter; Suenaga, Toshiro; Still, W. Clark. Peptidosteroidal Receptors for Opioid Peptides. Sequence-Selective Binding Using a Synthetic Receptor Library. *Journal of the American Chemical Society* **116**, 7955-7956 (1994).

30. Arienzo, R.K., Jeremy D. Combinatorial libraries of diamidopyridine-derived 'tweezer' receptors and sequence selective binding of peptides. in *Tetrahedron* Vol. 58 711-719 (2002).

31. Davies, M.B., Murielle; Guillier, Fabrice; Kilburn, Jeremy D.; Bradley, Mark. Screening an Inverted Peptide Library in Water with a

Guanidinium-Based Tweezer Receptor. *Journal of Organic Chemistry* **63**, 8696-8703 (1998).

32. Winssinger, N.H., Jennifer L.; Backes, Bradley J.; Schultz, Peter G. From split-pool libraries to spatially addressable microarrays and its application to functional proteomic profiling. in *Angewandte Chemie, International Edition* Vol. 40 3152-3155 (2001).

33. Yoon, J. & Czarnik, A.W. Fluorescent Chemosensors of Carbohydrates - a Means of Chemically Communicating the Binding of Polyols in Water Based on Chelation-Enhanced Quenching. *Journal of the American Chemical Society* **114**, 5874-5875 (1992).

34. James, T.D., Linnane, P. & Shinkai, S. Fluorescent saccharide receptors: A sweet solution to the design, assembly and evaluation of boronic acid derived PET sensors. *Chemical Communications*, 281-288 (1996).

35. Sandanayake Sanmankumara, K.R.S., S. *Angewandte Chemie-International Edition* **35**, 1911-1922 (1996).

36. Hong, S.Y. & Czarnik, A.W. A Metal-Ion-Insensitive Polyanion Chemosensor. *Journal of the American Chemical Society* **115**, 3330-3331 (1993).

37. Ungaro, R., Arduini, A., Casnati, A., Pochini, A. & Ugozzoli, F. New synthetic receptors based on calix 4 arenes for the selective recognition of ions and neutral molecules. *Pure and Applied Chemistry* **68**, 1213-1218 (1996).

38. Pina, F., Bernardo, M.A. & Garcia-Espana, E. Fluorescent chemosensors containing polyamine receptors. *European Journal of Inorganic Chemistry*, 2143-2157 (2000).

39. Schmidtchen, F.P. & Berger, M. Artificial organic host molecules for anions. *Chemical Reviews* **97**, 1609-1646 (1997).

40. Green, D.P.B., Bruce J.; Lees, Thomas J. Sensor measurement and experimental control in nuclear magnetic resonance imaging. in *Review of Scientific Instruments* Vol. 67 102-107 (1996).

41. Fields, B.A.G., Fernando A.; Dall'Acqua, William; Malchiodi, Emilio L.; Cauerhff, Ana; Schwarz, Frederick P.; Ysern, Xavier; Poljak, Roberto J.;

Mariuzza, Roy A. Hydrogen Bonding and Solvent Structure in an Antigen-Antibody Interface. Crystal Structures and Thermodynamic Characterization of Three Fv Mutants Complexed with Lysozyme. in *Biochemistry* Vol. 35 15494-15503 (1996).

42. Shao, Y.M., Michael V. Preparation and characterization of NM-sized electrochemical sensors. *Proceedings - Electrochemical Society* **96-9**, 1-11 (1996).

43. Lavigne, J.J. Dissertation, University of Texas at Austin (2000).

44. Stryer, L. in *Biochemistry* 61 (W. H. Freeman, New York, 1995).

45. Connors, K.A. in *Binding Constants: The Measurement of Molecular Complex Stability* 161 (John Wiley and Sons, New York, 1987).

46. Delapena, A.M., Ndou, T., Zung, J.B. & Warner, I.M. Stoichiometry and Formation-Constants of Pyrene Inclusion Complexes with Beta-Cyclodextrin and Gamma-Cyclodextrin. *Journal of Physical Chemistry* **95**, 3330-3334 (1991).

47. Pendergast, D.D.C., K. A.;. *Journal of Pharmaceutical Science* **73**, 1779-1783 (1984).

48. Rossotti, F.J.R., H. S. in *The Determination of Stability Constants* 108 (McGraw-Hill, New York, 1961).

49. Lenkinski, R.E.E., G. A.; Reuben, J. *Journal of Magnetic Resonance* **32**, 367-376 (1978).

50. Feryforgues, S., Lebris, M.T., Guette, J.P. & Valeur, B. Ion-Responsive Fluorescent Compounds .1. Effect of Cation Binding on Photophysical Properties of a Benzoxazinone Derivative Linked to Monoaza-15-Crown-5. *Journal of Physical Chemistry* **92**, 6233-6237 (1988).

51. deSilva, A.P. et al. Signaling recognition events with fluorescent sensors and switches. *Chemical Reviews* **97**, 1515-1566 (1997).

52. Vance, D.H. & Czarnik, A.W. Real-Time Assay of Inorganic Pyrophosphatase Using a High- Affinity Chelation-Enhanced Fluorescence Chemosensor. *Journal of the American Chemical Society* **116**, 9397-9398 (1994).

53. Bourson, J., Pouget, J. & Valeur, B. Ion-Responsive Fluorescent Compounds .4. Effect of Cation Binding on the Photophysical Properties of a Coumarin Linked to Monoaza-Crown and Diaza-Crown Ethers. *Journal of Physical Chemistry* **97**, 4552-4557 (1993).

54. Bramhall, J.H., Jan; DeGuzman, Ron; Montestruque, Silvia; Schell, Richard. Temperature dependence of membrane ion conductance analyzed by using the amphiphilic anion 5(6)-carboxyfluorescein. in *Biochemistry* Vol. 26 6330-6340 (1987).

55. Graber, M.L.D., Douglas C.; Friedman, Bradford L.; Pastoriza-Munoz, Enrique. Characteristics of fluoroprobes for measuring intracellular pH. in *Analytical Biochemistry* Vol. 156 202-212 (1986).

56. Lakowicz, J.R. *Principles of Fluorescence Spectroscopy*, (Kluwer Academic, New York, 1999).

57. Hamasaki, K. et al. Fluorescent Sensors of Molecular Recognition - Modified Cyclodextrins Capable of Exhibiting Guest-Responsive Twisted Intramolecular Charge-Transfer Fluorescence. *Journal of the American Chemical Society* **115**, 5035-5040 (1993).

58. Ikeda, H. et al. Fluorescent cyclodextrins for molecule sensing: Fluorescent properties, NMR characterization, and inclusion phenomena of N- dansylleucine-modified cyclodextrins. *Journal of the American Chemical Society* **118**, 10980-10988 (1996).

59. Ueno, A., Ikeda, A., Ikeda, H., Ikeda, T. & Toda, F. Fluorescent cyclodextrins responsive to molecules and metal ions. Fluorescence properties and inclusion phenomena of N- alpha-dansyl-L-lysine-beta-cyclodextrin and monensin- incorporated N-alpha-dansyl-L-lysine-beta-cyclodextrin. *Journal of Organic Chemistry* **64**, 382-387 (1999).

60. Ueno, A., Suzuki, I. & Osa, T. Host Guest Sensory Systems for Detecting Organic-Compounds by Pyrene Excimer Fluorescence. *Analytical Chemistry* **62**, 2461-2466 (1990).

61. Minato, S. et al. Intramolecular Excimer Formation and Molecular Recognition of Modified Cyclodextrins Appended by 2 Naphthalene Rings. *Photochemistry and Photobiology* **54**, 593-597 (1991).

62. Ueno, A. Fluorescent Cyclodextrins for Detecting Organic Compounds with Molecular Recognition. in *Fluorescent Chemosensors for Ion and Molecule Recognition*, Vol. 538 (ed. Czarnik, A.W.) 74-84 (ACS Series Symposium, Washington, D. C., 1992).

63. Wieb Van Der Meer, B.C.I., G.; and Chen, S. Y. *Resonance Energy Transfer: Theory and Data.*, (VCH, New York, 1994).

64. Engeser, M.F., Luigi; Licchelli, Maurizio; Sacchi, Donatella. A fluorescent molecular thermometer based on the nickel(II) high-spin/low-spin interconversion. in *Chemical Communications* Vol. 13 1191-1192 (1999).

65. Prasanna de Silva, A.S., K.; Samankumara, R. A. Fluorescent PET (photoinduced electron transfer) sensing reagent for alkali cations: optimization of sensor action by variation of structure and solvent. in *Tetrahedron Letters* Vol. 32 421-424 (1991).

66. Lavigne, J.J. & Anslyn, E.V. Sensing a paradigm shift in the field of molecular recognition: From selective to differential receptors. *Angewandte Chemie-International Edition* **40**, 3119-3130 (2001).

67. Krantz-Rulcker, C., Stenberg, M., Winquist, F. & Lundstrom, I. Electronic tongues for environmental monitoring based on sensor arrays and pattern recognition: a review. *Analytica Chimica Acta* **426**, 217-226 (2001).

68. Jurs, P.C., Bakken, G.A. & McClelland, H.E. Computational methods for the analysis of chemical sensor array data from volatile analytes. *Chemical Reviews* **100**, 2649-2678 (2000).

69. Grate, J.W. Acoustic wave microsensor arrays for vapor sensing. *Chemical Reviews* **100**, 2627-2647 (2000).

70. Ballantine, D.S., Rose, S.L., Grate, J.W. & Wohltjen, H. Correlation of Surface Acoustic-Wave Device Coating Responses with Solubility Properties and Chemical-Structure Using Pattern-Recognition. *Analytical Chemistry* **58**, 3058-3066 (1986).

71. Grate, J.W., Rosepehrsson, S.L., Venezky, D.L., Klusty, M. & Wohltjen, H. Smart Sensor System for Trace Organophosphorus and Organosulfur Vapor Detection Employing a Temperature-Controlled Array of Surface-

Acoustic-Wave Sensors, Automated Sample Preconcentration, and Pattern-Recognition. *Analytical Chemistry* **65**, 1868-1881 (1993).

72. Lonergan, M.C. et al. Array-based vapor sensing using chemically sensitive, carbon black-polymer resistors. *Chemistry of Materials* **8**, 2298-2312 (1996).

73. Patel, S.V., Jenkins, M.W., Hughes, R.C., Yelton, W.G. & Ricco, A.J. Differentiation of chemical components in a binary solvent vapor mixture using carbon/polymer composite-based chemiresistors. *Analytical Chemistry* **72**, 1532-1542 (2000).

74. Pearce, T.C., Gardner, J.W., Friel, S., Bartlett, P.N. & Blair, N. Electronic Nose for Monitoring the Flavor of Beers. *Analyst* **118**, 371-377 (1993).

75. Albert, K.J. et al. Cross-reactive chemical sensor arrays. *Chemical Reviews* **100**, 2595-2626 (2000).

76. Lauks, I.R. Microfabricated biosensors and microanalytical systems for blood analysis. *Accounts of Chemical Research* **31**, 317-324 (1998).

77. Sangodkar, H., Sukeerthi, S., Srinivasa, R.S., Lal, R. & Contractor, A.Q. A biosensor array based on polyaniline. *Analytical Chemistry* **68**, 779-783 (1996).

78. Takagi, S., Toko, K., Wada, K., Yamada, H. & Toyoshima, K. Detection of suppression of bitterness by sweet substance using a multichannel taste sensor. *Journal of Pharmaceutical Sciences* **87**, 552-555 (1998).

79. Takagi, S., Toko, K., Wada, K. & Ohki, T. Quantification of suppression of bitterness using an electronic tongue. *Journal of Pharmaceutical Sciences* **90**, 2042-2048 (2001).

80. Walt, D.R. Fiber optic imaging sensors. *Accounts of Chemical Research* **31**, 267-278 (1998).

81. Goodey, A. et al. Development of multianalyte sensor arrays composed of chemically derivatized polymeric microspheres localized in micromachined cavities. *Journal of the American Chemical Society* **123**, 2559-2570 (2001).

82. Lavigne, J.J. et al. Solution-based analysis of multiple analytes by a sensor array: Toward the development of an "electronic tongue". *Journal of the American Chemical Society* **120**, 6429-6430 (1998).

83. Goodey, A.P. & McDevitt, J.T. Multishell microspheres with integrated chromatographic and detection layers for use in array sensors. *Journal of the American Chemical Society* **125**, 2870-2871 (2003).

84. Christodoulides, N. et al. A microchip-based multianalyte assay system for the assessment of cardiac risk. *Analytical Chemistry* **74**, 3030-3036 (2002).

85. Curey, T.E. et al. Characterization of multicomponent monosaccharide solutions using an enzyme-based sensor array. *Analytical Biochemistry* **293**, 178-184 (2001).

86. Lavine, B.K. Chemometrics. *Analytical Chemistry* **72**, 91R-97R (2000).

87. Otto, M. *Chemometrics: Statistics and Computer Application in Analytical Chemistry*, (Wiley-VCH, Weinheim, 1999).

88. Beebe, K.R.P., R. J.; Seasholtz, M. B. *Chemometrics*, (John Wiley and Sons, New York, 1998).

89. Gardiner, W.P. *Statistical Analysis Methods for Chemists*, (The Royal Society of Chemistry, Glasgow, UK, 1997).

90. Burns, J.A. & Whitesides, G.M. Feedforward Neural Networks in Chemistry - Mathematical Systems for Classification and Pattern-Recognition. *Chemical Reviews* **93**, 2583-2601 (1993).

91. Metzger, A. & Anslyn, E.V. A chemosensor for citrate in beverages. *Angewandte Chemie-International Edition* **37**, 649-652 (1998).

92. Metzger, A., Lynch, V.M. & Anslyn, E.V. A synthetic receptor selective for citrate. *Angewandte Chemie-International Edition in English* **36**, 862-865 (1997).

93. Niikura, K., Metzger, A. & Anslyn, E.V. Chemosensor ensemble with selectivity for inositol- trisphosphate. *Journal of the American Chemical Society* **120**, 8533-8534 (1998).

94. Cabell, L.A. et al. Metal triggered fluorescence sensing of citrate using a synthetic receptor. *Journal of the Chemical Society-Perkin Transactions 2*, 315-323 (2001).

95. Lavigne, J.J. & Anslyn, E.V. Teaching old indicators new tricks: A colorimetric chemosensing ensemble for tartrate/malate in beverages. *Angewandte Chemie-International Edition* **38**, 3666-3669 (1999).

96. Kilway, K.V.S., J. S. *Journal of the American Chemical Society* **114**, 255-261 (1995).

97. Schneider, S.E., O'Neil, S.N. & Anslyn, E.V. Coupling rational design with libraries leads to the production of an ATP selective chemosensor. *Journal of the American Chemical Society* **122**, 542-543 (2000).

98. Chin, J. et al. A rational approach to selective recognition of NH4+ over K+. *Angewandte Chemie-International Edition* **38**, 2756-2759 (1999).

99. Szabo, T., O'Leary, B.M. & Rebek, J. Self-assembling sieves. *Angewandte Chemie-International Edition* **37**, 3410-3413 (1998).

100. Echavarren, A., Galan, A., Lehn, J.M. & Demendoza, J. Chiral Recognition of Aromatic Carboxylate Anions by an Optically-Active Abiotic Receptor Containing a Rigid Guanidinium Binding Subunit. *Journal of the American Chemical Society* **111**, 4994-4995 (1989).

101. Muller, G.R., J.; Schmidtchen, F. P. *Angewandte Chemie-International Edition* **27**, 1516-1518 (1988).

102. Benesi, H.A.H., J. H. *Journal of the American Chemical Society* **71**(1949).

103. Bremer, C. & Grell, E. Protolysis and Mg2+ binding of methylthymol blue. *Inorganica Chimica Acta* **241**, 13-19 (1996).

104. Hulanicki, A., Glab, S. & Ackermann, G. Complexiметric Indicators - Characteristics and Applications. *Pure and Applied Chemistry* **55**, 1137-1230 (1983).

105. Green, F.J. in *The Sigma-Aldrich Handbook of Stains, Dyes and Indicators* 468 and 740 (Aldrich Chemical Company, Milwaukee, 1990).

106. Wardi, A.H.A., W. S.; Varma, R. *Analytical Chemistry* **46**, 919-920 (1974).

107. Kneeland, D.M., Ariga, K., Lynch, V.M., Huang, C.Y. & Anslyn, E.V. Bis(Alkylguanidinium) Receptors for Phosphodiesters - Effect of Counterions, Solvent Mixtures, and Cavity Flexibility on Complexation. *Journal of the American Chemical Society* **115**, 10042-10055 (1993).

108. Wiskur, S.L.F., P.N.; Anslyn, E.V.; McDevitt, J.T. A Multicomponet Sensing Ensemble in Solution: Differentiation between Structurally Similar Structures. *Angewandte Chemie-International Edition* **42**, 2070-2072 (2003).

109. McCleskey, S.C., Metzger, A., Simmons, C.S. & Anslyn, E.V. Competitive indicator methods for the analysis of citrate using colorimetric assays. *Tetrahedron* **58**, 621-628 (2002).

110. Toko, K. A taste sensor. *Measurement Science & Technology* **9**, 1919-1936 (1998).

111. Hayashi, K., Yamanaka, M., Toko, K. & Yamafuji, K. Multichannel Taste Sensor Using Lipid-Membranes. *Sensors and Actuators B-Chemical* **2**, 205-213 (1990).

112. Iverson, D.J., Hunter, G., Blount, J.F., Damewood, J.R. & Mislow, K. Static and Dynamic Stereochemistry of Hexaethylbenzene and of Its Tricarbonylchromium, Tricarbonylmolybdenum, and Dicarbonyl(Triphenylphosphine)Chromium Complexes. *Journal of the American Chemical Society* **103**, 6073-6083 (1981).

113. Lakowicz, J.R. in *Principle of Fluorescence Spectroscopy* 546-551 (Plenum Publishers, New York, 1999).

114. Romanovicz, D. (ed. McCleksey, S.) (Austin, 2002).

115. Schneider, S.E. Dissertation, University of Texas at Austin (1999).

116. Elhanany, E. et al. Resolving pathways of interaction of covalent inhibitors with the active site of acetylcholinesterases: MALDI-TOF/MS analysis of various nerve agent phosphyl adducts. *Chemical Research in Toxicology* **14**, 912-918 (2001).

117. Kientz, C.E. Chromatography and mass spectrometry of chemical warfare agents, toxins and related compounds: state of the art and future prospects. *Journal of Chromatography A* **814**, 1-23 (1998).

118. Lebl, M. & Krchnak, V. Synthetic peptide libraries. in *Solid-Phase Peptide Synthesis*, Vol. 289 336-392 (1997).

119. Wellings, D.A. & Atherton, E. Standard Fmoc protocols. in *Solid-Phase Peptide Synthesis*, Vol. 289 44-67 (1997).

120. McCleskey, S.C., Griffin, M.J., Schneider, S.E., McDevitt, J.T. & Anslyn, E.V. Differential receptors create patterns diagnostic for ATP and GTP. *Journal of the American Chemical Society* **125**, 1114-1115 (2003).

121. Furka, A.S., F.; Asgedom, M.; Dibo, G. *International Journal of Peptide and Protein Research* **37**, 487-493 (1991).

# Vita

Shawn Catherine McCleskey was born in Spring, Texas on May 19th, 1976, the daughter of Marilu and Michael McCleskey. She spent her preteen years in Texas and California, and finished high school in Oklahoma after her parent's divorce. Shawn put herself through undergraduate school at the University of Central Oklahoma by working several jobs and taking out student loans. She completed her B. S. in chemistry in May 1998 with honors. In August 1998, she entered the University of Texas at Austin chemistry graduate program. She is a member of the American Chemical Society and Alpha Chi Sigma.

Permanent address: 11717 N. Douglas Blvd, Jones, OK 73049

Shawn Catherine McCleskey typed this dissertation.